2007

Synthesis of Transition Metal - Carbon Nanotube Hybrid Materials

Jamie E. Ellis

Synthesis of Transition Metal – Carbon Nanotube Hybrid Materials

Jamie E. Ellis

May 2007

Thesis

Submitted in Partial Fulfillment of the Requirements for the Degree of Master of Science

Approved:

Thomas Gennett

Thesis Advisor, Thomas Gennett

Terrence Morrill

Department Head, Terrence C. Morrill

Department of Chemistry

Rochester Institute of Technology

Rochester, New York 14623

Synthesis of Transition Metal – Carbon Nanotube Hybrid Materials

Jamie E. Ellis _____

Jamie E. Ellis

_____

Date

Table Of Contents

List Of Figures ii
List Of Tables vi
Acknowledgements vii
Abstract viii

1.0 Introduction 1
1.1 Historical Overview 2
1.2 Properties of Single-Walled Carbon Nanotubes 4
1.3 Synthesis of Single Walled Carbon Nanotubes 9
1.3.1 Synthesis of SWNTs via Arc Discharge 12
Synthesis of SWNTs via Laser Vaporization 14
1.3.2 Synthesis of SWNTs via Chemical Vapor Deposition 19
1.4 Purification and Characterization of SWNTs 23
1.4.1 Purification 23
1.4.2 Characterization of the Purified SWNTs 25
1.5 SWNTs as Catalyst Supports in Fischer - Tropsch Synthesis 28
1.5.1 Fischer – Tropsch Synthesis: A Historical Overview 29
1.5.2 Fischer – Tropsch Reaction Mechanism 32
1.5.3 Fischer – Tropsch Reactor Beds 35
1.5.4 Catalyst Preparation for Fischer – Tropsch Synthesis 39
1.5.5 Synthesis of Transition Metal – Carbon Nanotube Hybrid Materials 44
2.0 Experimental 50
2.1 Synthesis of Single Wall Carbon Nanotubes via Laser Vaporization 50
2.2 Purification of Single Wall Carbon Nanotubes 51
2.3 Deposition of Various Transition Metals onto the Surface of the SWNTs 53
2.3.1 Adsorption Followed by Sodium Borohydride Reduction 54
2.3.2 Direct Reduction of the SWNTs with Alkali Metals Followed by Metal Deposition 55
2.4 Characterization of the Transition Metal – Carbon Nanotube Hybrid Materials 57
2.4.1 Transmission Electron Microscopy 57
2.4.2 Temperature Programmed Desorption Experiments Used to Analyze for Hydrogen Storage and Fischer-Tropsch Synthesis 58
3.0 Results and Discussion 61
3.1 Characterization of Purified SWNTs 61
3.2 Characterization of the Transition Metal – Carbon Nanotube Hybrid Material 63
3.2.1 Metal Deposition via the Adsorption Technique 63
3.2.2 Metal Deposition via the Direct Reduction Technique 67
3.2.3 Metal Deposition via Pre-reduction of the SWNT Surface 72
3.3 Hydrogen Storage in the Transition Metal – Carbon Nanotube Hybrid Materials 76
3.4 Heterogeneous Catalysis Reactions Using the Newly Synthesized Hybrid Materials 91
4.0 Conclusions and Future Work 102
4.1 Conclusions 102
4.2 Future Work 104
5.0 List of Terms 106
6.0 References 108

Appendix A A-1

List Of Figures

Figure 1: Various allotropes of carbon, including diamond, graphite, buckminsterfullerene, and carbon nanotube.[34] 3
Figure 2: Transmission electron micrographs of (A) various diameter multi-walled carbon nanotubes[1] and (B) an individual single-walled carbon nanotube[2]. As is seen, MWNTs can range from the smallest double-walled tubes (DWNTs) upwards. The images to the left and right of the DWNT provides examples of five- and seven-shell MWNTs. 5
Figure 3: Graphene sheet with (*n,m*) integers designated. The chiral angle, θ, is measured from the zigzag axis. All SWNTs are semiconducting, unless the quantity (n-m)/3 is an integer in which case the SWNTs will be metallic.[35] 7
Figure 4: Three main types of SWNTs, including armchair, zigzag, and chiral tubes, which are determined based on their chirality vector. Also shown are the corresponding hemispherical end caps derived from various sized fullerenes.[36] 8
Figure 5: Transmission electron micrograph of SWNT bundle. Inset shows a close-up schematic of how the bundle is held together through Van der Waals interactions.[14] 10
Figure 6: Schematic of a typical arc discharge apparatus used in the synthesis of SWNTs. 13
Figure 7: High-resolution transmission electron micrograph of SWNTs synthesized by the arc discharge method over a Ni/Co primary catalyst. 15
Figure 8: Schematic of a laser vaporization apparatus used in the synthesis of SWNTs. 16
Figure 9: Transmission electron micrograph of SWNTs synthesized by the laser vaporization method over a Ni/Co catalyst. 17
Figure 10: Schematic for the sequence of events in the growth mechanism of SWNTs by laser vaporization.[51] 18
Figure 11: Schematic of CVD apparatus used in the synthesis of SWNTs.[55] 21
Figure 12: Transmission electron micrograph of SWNTs synthesized by the CVD method over a $Fe(NO_3)_3/Al_2O_3$ catalyst. Methane was used as the carbon source.[55] 22
Figure 13: TGA of a 1 – 2 mg sample of crude, acid refluxed, and purified SWNT material. Samples were ramped from 25 – 875°C at 5°C per minute under 100 sccm flowing air.[10] 26
Figure 14: Reaction schemes for various competitive heterogeneous catalysis reactions. 30
Figure 15: Proposed C + CR FT synthesis mechanism. (1) CO and H_2 dissociation. (2) C + H → CH reaction and CH diffuses to step site. (3) At steps C + CH → CCH. (4) CCH formation. (5) CCH + H → CCH_2 and CCH_2 + H → CCH_3. CCH_3 then diffuses to another step to start C + CCH_3 → $CCCH_3$. Alternatively, CCH_3 may rearrange to ethylene, C_2H_4, which desorbs readily from the Ru catalyst surface.[17] 34
Figure 16: Fluidized bed FT reactors: (A) CFB reactor, (B) FFB reactor, and (C) slurry phase bubbling bed reactor.[18] 37
Figure 17: Schematic of a multitubular fixed bed FT reactor.[18] 38

Figure 18: Schematic showing the hydrogenation of CO over a transition metal – carbon nanotube catalyst, and the production of various hydrocarbons. 42
Figure 19: Schematic of common functionalization routes used to derivatize SWNTs at end and defect sites.[59] 43
Figure 20: Schematic showing the reduction of oxidative on the surface of SWNTs. Functional groups such as –COOH, -CO, and –OH are generally introduced during purification processing, creating defect sites. Upon removal of these groups, pristine SWNTs are obtained. 49
Figure 21: Close-up schematic of the target in the synthesis of SWNTs using the laser vaporization method, and the resulting raw soot that is produced. 52
Figure 22: Schematic of the TPD apparatus used in the examination of the transition metal – carbon nanotube hybrid materials for H_2 storage and FT synthesis. 59
Figure 23: Transmission electron micrographs of: (A) as produced raw SWNT material, (B) SWNT material after HNO_3 reflux and 500°C air oxidation, and (C) purified SWNT material achieved through subsequent HCl washes and air oxidations. Carbonaceous and metal catalyst impurities are seen as small, dark spots among the SWNT bundles. 62
Figure 24: Schematic of an individual SWNT, which shows that the carbonaceous and metal catalyst impurities have been removed, but various defects and kinks remain. In this case carboxylic acid groups are prevalent at the defect sites, however, carbonyl and hydroxyl groups may be present as well. It is at these oxidized defect sites, and possibly kinked sites, that the transition metal adsorption appears to takes place.[59] 65
Figure 25: Transmission electron micrographs of a Cr-SWNT sample prepared from Chromium(III) Nitrate just that the final mass of metal would be 15% of the final sample mass. Images are provided in increasing resolution from (A) 100 nm, (B) 50 nm, (C) 20 nm, and (D) 10 nm. As is seen the Cr particle size varies on average between 10 – 50 nm. 66
Figure 26: Transmission electron micrographs of Cr-SWNTs prepared from (A) Na-reduced SWNTs and (B) Li-reduced SWNTs. Both images are scaled to 0.2μm. As can be seen, both samples show significant metal deposition with relatively the same particle size distribution. 69
Figure 27: Rh-SWNTs prepared by the direct reduction of Chlorotris(triphenylphosphine)rhodium(I) onto Na-reduced SWNTs. The diameter of the metal particles ranges from approximately 20 nm to 200 nm. 70
Figure 28: Transmission electron micrographs of Rh-SWNTs prepared by the direct reduction of Chlorotris(triphenylphosphine)rhodium(I) onto Na-reduced SWNTs for (A) 1 hour, (B) 16 hours, and (C) 144 hours. 71
Figure 30: Transmission electron micrograph of Rh-SWNTs prepared by prereducing the purified SWNTs with $NaBH_4$ to yield pristine SWNTs, followed by the direct reduction of the metal onto Na-reduced SWNTs from a Rhodium(III) 2,4-Pentanedionate salt solution. (A) is scaled to 20nm whereas (B) is a higher resolution images scaled to 10nm. 74
Figure 31: Various models for 50% H_2 coverage on SWNTs, including lines, rings, and spiral.[72] 75

Figure 32: Degas spectrum of the K-reduced SWNTs obtained by TPD. The sample was loaded onto the TPD apparatus under inert He atmosphere, and degassed from 25 – 700°C over the course of 20 min..... 78
Figure 33: Degas spectrum of the Li-reduced SWNTs obtained by TPD. The sample was loaded onto the TPD apparatus under inert He atmosphere, and degassed from 25 – 700°C over the course of 20 min..... 79
Figure 34: Degas spectrum of the Na-reduced, pristine-like SWNTs obtained by TPD. The sample was loaded onto the TPD apparatus under inert He atmosphere, and degassed from 25 – 700°C over the course of 20 min. Removal of the oxygen-containing defects prior to the Na-reduction of the SWNTs, causes a non-traditional H_2 peak around 300°C, as well as the traditional H_2 peak at approximately 400 – 500°C. This sample demonstrated the desorption of an irreversible 4 wt.% H_2..... 82
Figure 35: Degas spectrum of the Na-reduced SWNTs obtained by TPD. The sample was loaded onto the TPD apparatus under inert He atmosphere, and degassed from 25 – 700°C over the course of 20 min. In comparison Na-reduced, pristine-like SWNTs, it was demonstrated that the non-traditional H_2 peak disappeared. 83
Figure 36: TPD degas spectrum for Na-reduced activated carbon, prepared after removing oxygen-containing defects by heat treatment. The non-traditional H_2 peak at 200°C, as well as the traditional H_2 peak at 350°C confirm the unique character observed with the Na-reduced, pristine-like SWNTs. 84
Figure 37: TPD degas spectrum for Na-reduced activated carbon. The non-traditional H_2 peak at 200°C is not observed when the oxygen-containing defects are not removed. The presence of only the traditional H_2 peak exemplifies the results obtained for the Na-reduced SWNTs..... 85
Figure 38: (A) Representative degas spectrum of the H_2 signal on Na-SWNTs. Typically, approximately 4% w/w H_2 is desorbed. (B) Representative degas spectra of the mass signal for H_2, HD, and D_2, respectively. This data was obtained after preparing the Na-SWNTs using naphthalene-d_8 and THF-d_8. As is seen the hydrogenation of the Na-SWNTs is caused by reaction with THF. 86
Figure 39:Proposed mechanism by which hydrogenation of Na-SWNTs occurs. In Scheme [I], the SWNT-Na radical system reacts with THF to undergo hydrogenation, forming SWNT-H.[73] Ethylene is formed as a byproduct, which reacts in Scheme [II] with the adjacent arene rings of the nanotubes to form Na-SWNT-$(H)_{n-1}(CH2CH2)_{n-1}$.[75] 87
Figure 40: Mass spectrum of the Na-reduced SWNTs after dosing for 10 min with H_2. An initial physisorbed H_2 peak is observed immediately after quenching the reaction and removing the N_2 (l). The spetra for both the K- and Li-reduced SWNTs is very similar to the data obtained for the Na-SWNTs..... 89
Figure 41: Degas spectra for Co-SWNTs prepared via the direct reduction technique on K- and Li-reduced SWNTs, respectively, from a solution of Cobalt(II) 2,4-Pentanedionate. H_2 desorption from these samples resembles either the reduced SWNTs or purified SWNTs, and does not show increased H_2 desorption. The Fe-, Ni-, and Cr-SWNT samples had similar degas spectra..... 90
Figure 42: Mass spectrum of Rh-SWNTs produced by the pre-reduction of the nanotubes followed by the direct reduction of the metal particles onto Na-reduced SWNTs from a Rhodium(III) 2,4-Pentanedioante solution. The spectrum shows the

potential for this sample to act as a Kubas complex as seen by the H2 peak at 100°C. 92
Figure 43: Mass spectrum of Rh-SWNTs produced by the adsorption technique from a Rhodium(III) 2,4-Pentanedioante solution. The spectrum demonstrates the conversion of CO2 and H2 to CO as well as CH4. This indicates that both the RWGS and Sabatier reactions have occurred. 95
Figure 44: Mass spectrum of Rh-SWNTs produced by the pre-reduction of the nanotubes followed by the direct reduction of the metal particles onto Na-reduced SWNTs from a Rhodium(III) 2,4-Pentanedioante solution. As can be seen from the mass spectrum, the Sabatier reaction has taken place, which is evident by the production of CO and H2O. 96
Figure 45: Mass spectrum of Co-SWNTs after dosing with CO to 100 torr and H_2 to 500 torr. Upon heating, methane and water are observed desorbing from the sample, indicating that the FT reaction has occurred. 97
Figure 46: Mass spectrum of Cr-SWNTs after dosing with CO to 100 torr and H_2 to 500 torr. Upon heating, methane and water are observed desorbing from the sample, indicating that the FT reaction has occurred. 98
Figure 47: Mass spectrum of Fe-SWNTs after dosing with CO to 100 torr and H_2 to 500 torr. Upon heating, methane and water are observed desorbing from the sample, indicating that the FT reaction has occurred. 99
Figure 48: Representative data for Co-SWNT hybrid materials. The TPD data shows the presence of methane, ethane and propane at increasing degas temperatures (A: -50°C, B: -15°C, C: 0°C) in the mass spectrum. 100

List Of Tables

Table 1: Calculated reaction barriers (Ea) for various C/C coupling reactions on Ru catalyst (step or flat surface) as determined by DFT experiments.[17] 33
Table 2: Various electrochemical reduction half reactions. The reactions is [1] represent the transition metals that were spontaneously deposited on the surface of SWNTs by Dia et al[61], [2] represents various other transition metals that could potentially be deposited spontaneously on the surface of SWNTs, and [3] represents the metals that were studied in this thesis research. As can be seen, Co, Cr, Fe, and Ni will not be spontaneously deposited unless the E_{red} of the SWNTs is modified by as described in the direct reduction technique. Rh is the only metal to be studied in this reaction that could potentially be deposited spontaneously onto the surface of the SWNTs..... 47
Table 3: Synthesis parameters for the deposition of various transition metals onto the surface of SWNTs via adsorption followed by $NaBH_4$ reduction. 54
Table 4: Synthesis parameters for the deposition of various transition metals onto the surface via direct reduction of the SWNTs with alkali metal followed by metal deposition..... 56
Table 5: Project summary. 101

Acknowledgements

I gratefully acknowledge the funding for this project from both the Chemistry Department at RIT as well as the DOE Office of Energy Efficiency and Renewable Energy and Office of Science, Basic Energy Sciences, Division of Material Science.

I would like to thank my advisor, Dr. Tom Gennett, for his enthusiasm and expertise, which were instrumental in successfully completing this project. I am truly grateful for the many opportunities I have been afforded through working under the direction of Dr. Gennett, especially for the opportunity to work at the National Renewable Energy Laboratory (NREL) in Golden, CO. I would like to acknowledge the contributions from Drs. Michael Heben, Calvin Curtis, Jeffery Blackburn, Lin Simpson, and Kim Jones at NREL for their time and support of this project. I am appreciative of the fruitful discussions, encouragement, participation, and friendships that transpired during my time at NREL. I would also like to thank my committee members at RIT, including Drs. Christina Collison, Andreas Langner, and Paul Rosenberg for their input and suggestions that helped to define this project and my research experience.

Lastly, I would like to recognize and thank my parents and my sister for their unwavering support and always believing that I can achieve anything I set my mind to. I would also like to thank Adam for his patience, motivation, and loving support throughout this endeavor.

Abstract

In this thesis research, three novel methodologies have been examined for their use in the synthesis of transition metal – carbon nanotube hybrid materials. These newly synthesized materials were assessed as catalysts in various heterogeneous catalysis reactions, including Fischer Tropsch synthesis, the Sabatier reaction, and the Reverse Water Gas Shift reaction. Specifically, this research was aimed at evaluating the relationship between particle size, support material, and activity of the metal-centered-nanotube hybrid catalysts as compared to more traditional heterogeneous catalysts. Efforts were centered on establishing the conditions needed to obtain the optimum metal crystallite size deposited on the nanotube support, as required for achieving the best catalytic activity for a particular reaction scheme. This was done by modifying various synthesis parameters such as the reaction temperature and time, as well as reviewing the metals used for the catalyst deposition.

In Fischer Tropsch synthesis, carbon monoxide is hydrogenated over a transition metal catalyst to produce varying length hydrocarbons and olefins. Traditionally, iron, nickel, and cobalt catalysts have been used, and were supported on various oxides and activated carbon. In this thesis research, a series of transition metals, including iron, nickel, cobalt, chromium, and rhodium were deposited on purified single walled carbon nanotubes (SWNTs). SWNTs have recently gained considerable attention do to their unique physical and chemical properties, which can be tailored for the use in numerous applications. In this thesis research, the use of SWNTs as catalyst supports is explored. The large surface area, chemical inertness, mechanical strength, and meso-porous structure, make SWNTs an excellent candidate for a catalyst support material.

Catalyst deposition was achieved in this project through an adsorption technique, a direct reduction technique, and through the pre-reduction of the SWNT surface. In typical catalyst synthesis, the metal particles are reduced onto the catalyst support using flowing H_2, however, through the use of the proposed adsorption technique, the transition metal is nucleated onto the surface of the SWNTs at the position of a defect site, and is subsequently reduced with the aid of a reducing agent thus causing the growth of the particle. On the other hand, the direct reduction technique involves the modification of the nanotube reduction potential by pre-reducing the SWNTs with alkali metals, such that the metal catalyst particle will be spontaneously reduced and deposited onto the surface of the SWNTs at the position of a defect site. Lastly, the third technique proposed for the synthesis of the hybrid materials involves the pre-reduction of the SWNT surface with a reducing agent, followed by the direct reduction of the metal catalyst particles. This technique yields pristine-like SWNTs, free of most oxidative defects, and causes the transition metals to be reduced and precipitated evenly over the entire surface of the SWNT material. Of these three techniques, the latter was found to produce hybrid materials with well dispersed metal nanoparticles having <2 nm diameters. This was confirmed by transmission electron microscopy (TEM). Additionally, these materials were examined for their use as efficient catalysts in the heterogeneous catalysis reactions named previously. Temperature programmed desorption (TPD) data demonstrated the ability of these materials to catalyze the Fischer Tropsch reaction. Additionally, the Rh-SWNT samples have shown evidence that they can be used as catalysts in the Sabatier and Reverse Water Gas Shift reactions when doped with the appropriate reagents as well.

1.0 Introduction

Since their discovery[1], carbon nanotubes (CNTs) have gained considerable attention due to their unique physical and chemical properties. Numerous studies have focused on the synthesis[2-5], purification[6-11], and characterization[10,12-14] of these new materials. CNTs can be tailored via a variety of methodologies to meet the needs of a particular application. Consequently, significant efforts are being made to exploit the physio-chemical properties of CNTs for their use in energy storage, molecular electronics, sensors, and composite materials, to name just a few.[15] The focus of this thesis research was the application of single-walled carbon nanotubes (SWNTs) as a transition metal catalyst support material for heterogeneous catalysis reactions, namely Fischer – Tropsch synthesis, the Sabatier reaction, and the Reverse Water Gas Shift Reaction. Fischer – Tropsch synthesis, which involves the hydrogenation of carbon monoxide over a transition metal catalyst to form varying length hydrocarbons, was of particular interest.[16-19]

In the past, the transition metal catalyst was supported on an oxide substrate such as Al_2O_3, SiO_2, and TiO_2, and eventually on activated carbon supports.[18,20-21] More recently, Fisher – Tropsch catalysts have been prepared on Multi-Walled Carbon Nanotubes (MWNTs), and proposed for SWNTs, but very little has been reported in the literature regarding the preparation of transition metal – carbon nanotube hybrid materials for this purpose.[22-27] As such, the focus of this thesis research was on possible synthetic methodologies for the deposition of various transition metals, including iron, nickel, cobalt, chromium, and rhodium, onto the surface of the SWNTs. Three novel incipient wetness impregnation techniques were developed for the metal deposition, including an

adsorption technique and a direct reduction technique. The third synthetic technique is based on pre-reducing the SWNT surface followed by the direct reduction of the transition metal onto the nanotube matrix. These three techniques have provided a means to synthesize transition metal – carbon nanotube hybrid materials, which have proven to act as efficient Fischer – Tropsch catalysts as demonstrated by their ability to facilitate the hydrogenation of carbon monoxide to produce varying length hydrocarbons.

1.1 Historical Overview

In 1985, the discovery of the C_{60} buckminsterfullerene, or *buckyball*, by Kroto and Smalley generated renewed interest in nanostructured carbon materials. The fullerene was observed coincidentally during experiments to study long-chain carbon molecules. Synthesis of the fullerene was achieved by the vaporization of a carbon source by laser irradiation, followed by the expansion and photoionization of the carbon clusters. The resulting buckyball was detected by mass spectrometry.[28] Up until this point, the only other known allotropic forms of carbon were the diamond and graphite.[29]

In 1991, shortly after the discovery of fullerenes, the first form of tubular carbon was reported by Iijima, which was referred to as multi-walled carbon nanotubes (MWNTs) (Figure 1). The MWNTs were first synthesized using an arc-discharge method, which at the time was being employed for the mass production of C_{60} fullerenes. MWNTs consist of concentric layers or shells of graphene rolled in cylindrical fashion one inside the other.[30] Though MWNTs presented scientists with an opportunity to advance the field of nanotechnology, not much was known about the properties of these unique new materials. Most theoretical predictions regarding the electronic structure and

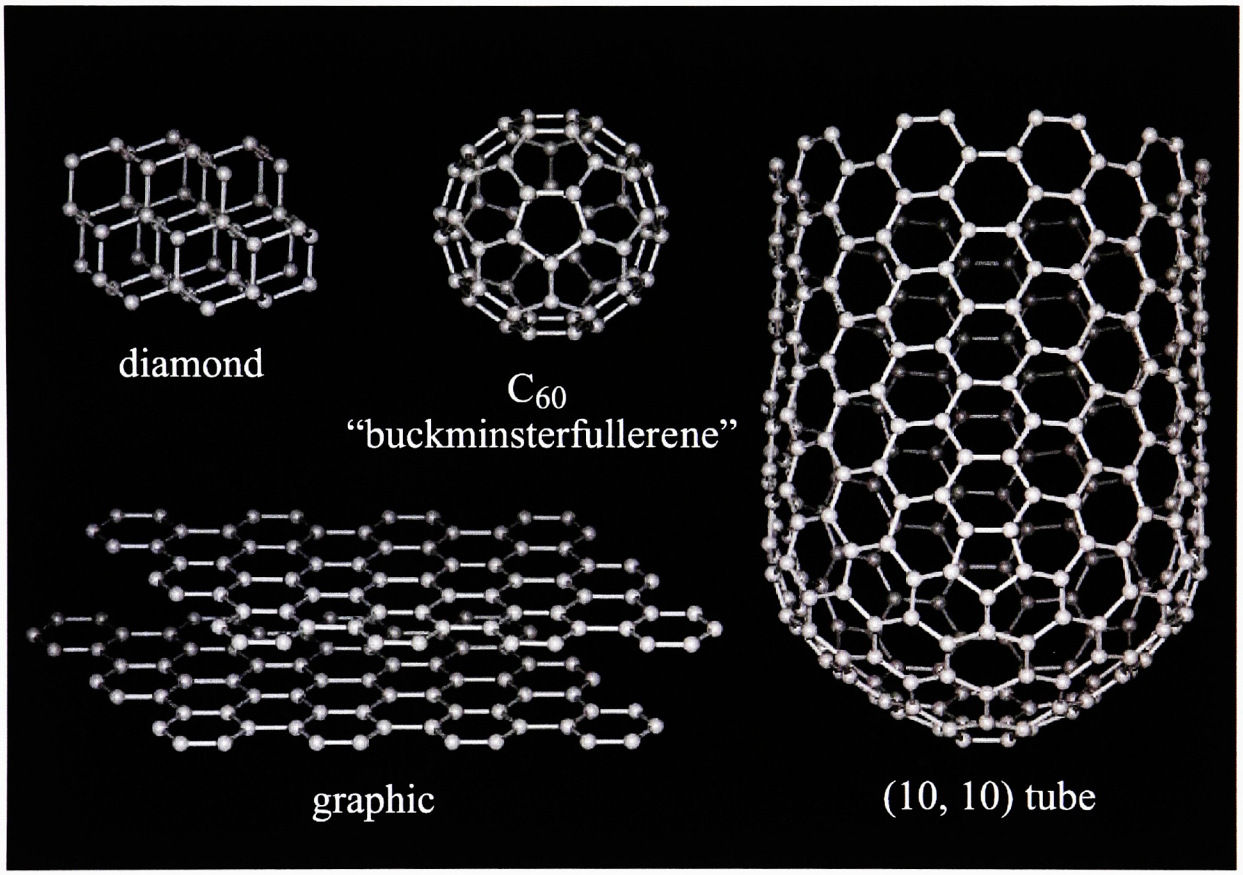

Figure 1: Various allotropes of carbon, including diamond, graphite, buckminsterfullerene, and carbon nanotube.[34]

mechanical strength of MWNTs were carried out using single-shell tubes as a model, yet these materials did not exist at the time.[30-33]

In 1993, single-walled carbon nanotubes (SWNTs) were discovered independently by both Iijima[2] and Bethune[3]. Again these novel materials were first synthesized using an arc-discharge method, similar to the one employed for both fullerene and MWNT synthesis. Unlike MWNTs, SWNTs consist of only a single, cylindrical graphene sheet (Figure 2). Until 1995, arc-discharge was the exclusive technique used for the synthesis of SWNTs until Guo discovered a technique that involved synthesis via laser vaporization.[4] Shortly thereafter, in 1996, Dai et al reported the chemical vapor deposition (CVD) synthesis of SWNTs.[5] Since then, all three methods continue to be studied and improved in an effort to perfect the synthesis of SWNTs in a manner that allows for high yield and high purity batches of material to be produced.

1.2 Properties of Single-Walled Carbon Nanotubes

Since they were first reported by Iijima in 1993, SWNTs have been the focus of much attention due to their unique physical and chemical properties, which is evident by the overwhelming numbers of studies reported in the literature in this regard over the last 15 years. The properties of SWNTs arise mostly from their aromaticity and relatively long length and small diameter. With an aspect ratio upwards of 10^6, SWNTs are considered to be nearly one-dimensional structures. There are two main regions that comprise a SWNT, the sidewall and the end cap. The sidewall is made up of a single graphene sheet rolled seamlessly into an elongated cylinder. This structure is terminated with a hemispherical end cap resembling the structure of a half fullerene. SWNTs ideally have strong sp^2 bonding and a perfect hexagonal network. The shape and size of the end

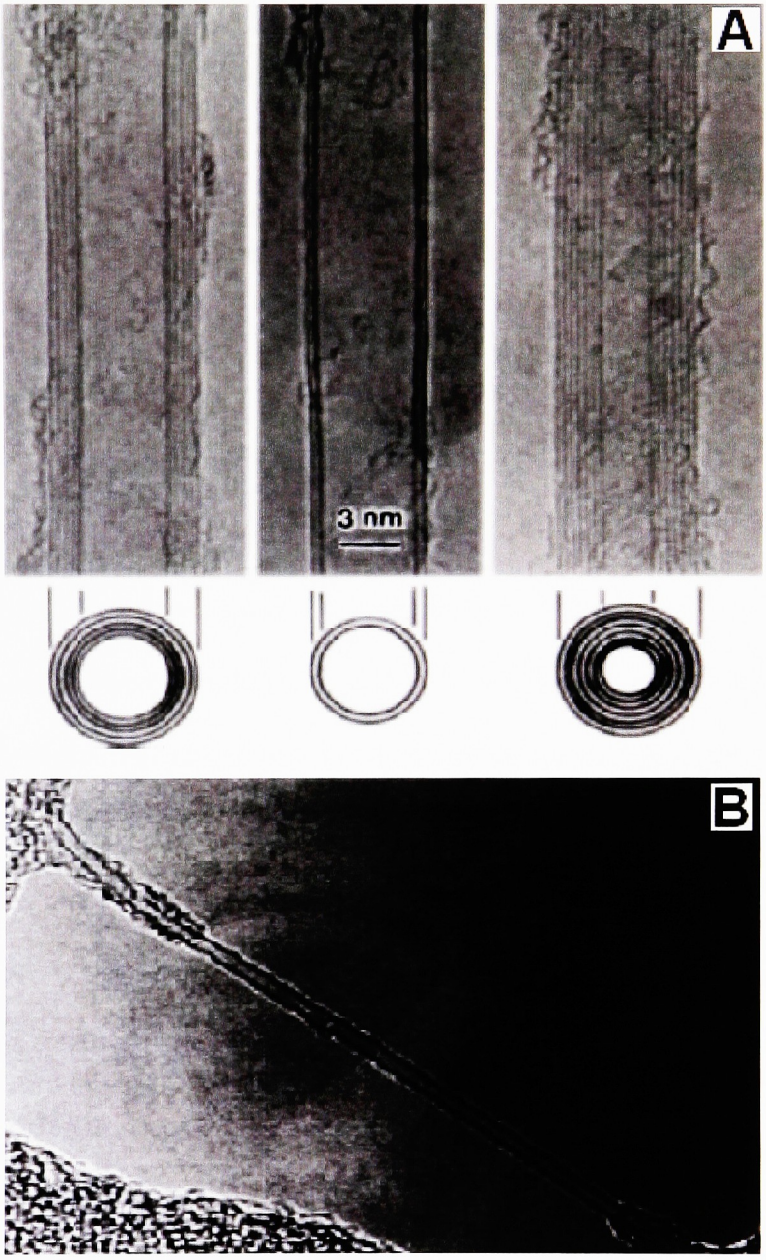

Figure 2: Transmission electron micrographs of (A) various diameter multi-walled carbon nanotubes[1] and (B) an individual single-walled carbon nanotube[2]. As is seen, MWNTs can range from the smallest double-walled tubes (DWNTs) upwards. The images to the left and right of the DWNT provides examples of five- and seven-shell MWNTs.

cap are dictated by both Euler's Theorem and the Isolated Pentagon Rule. Euler's Theorem states that there must be twelve pentagons in a hexagonal network in order to obtain a closed cage structure, such as the end cap or a fullerene. The Isolated Pentagon Rule states that the amount of local surface stress induced by curvature must be minimized. This is done by maximizing the distance between the twelve pentagons in the end cap by surrounding each with five hexagons.[29,35,36]

While this generally describes the structure of a SWNT, it is important to note that there are three main types of SWNTs that are defined based on their roll-up vector, C_h. This is sometimes referred to as the chiral vector as well. Essentially, C_h is determined by choosing two atoms on the graphene sheet, where one is designated as the origin. The graphene sheet is rolled into a cylindrical tube until the second atom is imposed on the origin. The chiral vector is then defined as the vector pointing from the origin to the second atom of choice (Figure 3).[29,35,36]

The chiral vector is determined based on the following formula, but is more commonly referred to by the (n,m) designation:

$$C_h = na_1 + ma_2$$

where a_1 and a_2 are lattice vectors. The ability to determine the chiral vector is what allows for the distinction between the three types of SWNTs, which include the (n,n) armchair, $(n,0)$ zigzag, and (n,m) chiral tubes (Figure 4). When referring to chiral (n,m) SWNTs, the chiral angle, θ, is defined as the angle between C_h and the $(n,0)$ zigzag axis. Additionally, these SWNTs can be either metallic or semiconducting. The extent to which a given type of SWNT is either metallic or semiconducting is dependent on the

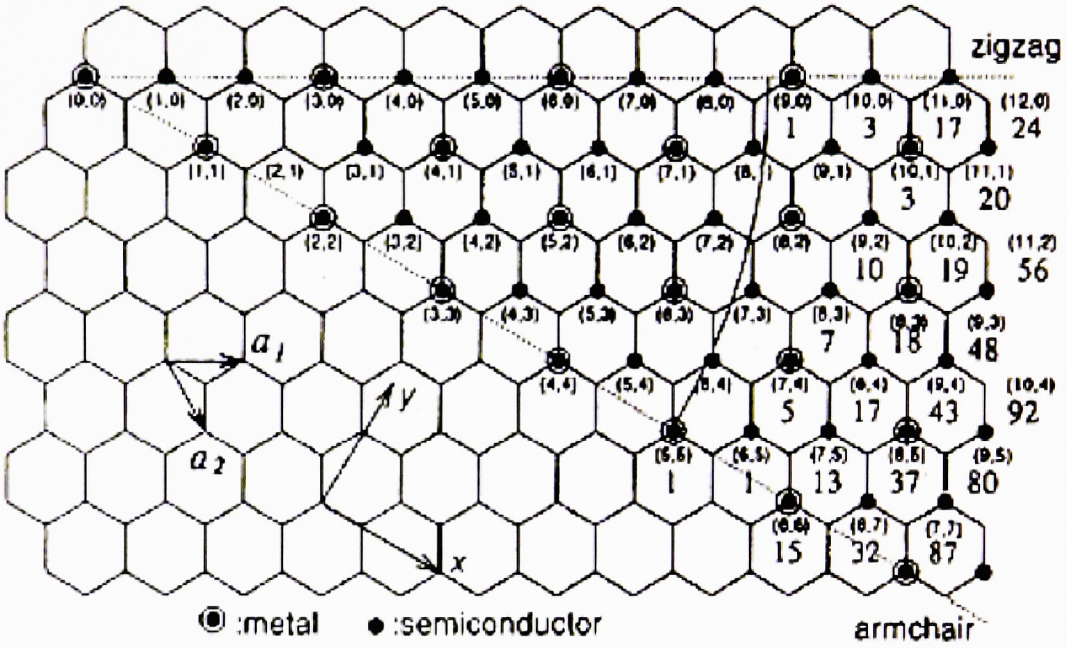

Figure 3: Graphene sheet with (*n,m*) integers designated. The chiral angle, θ, is measured from the zigzag axis. All SWNTs are semiconducting, unless the quantity (n-m)/3 is an integer in which case the SWNTs will be metallic.[35]

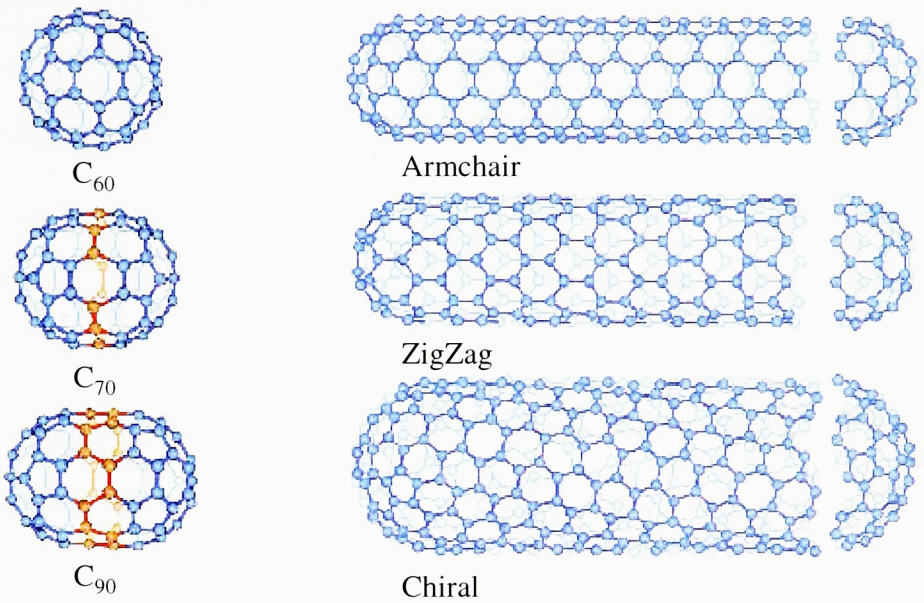

Figure 4: Three main types of SWNTs, including armchair, zigzag, and chiral tubes, which are determined based on their chirality vector. Also shown are the corresponding hemispherical end caps derived from various sized fullerenes.[36]

quantity $(n - m)/3$. When this quantity is an integer or zero, the SWNT is metallic, otherwise the SWNT is semiconducting.[29,35,36]

Aside, from their unique electronic properties, SWNTs are also known to possess a high degree of mechanical strength. This is evident in the average carbon-carbon bond strength of 152 kcal/mol within the sp^2 hybridized, hexagonal carbon network of the SWNTs. In 2000, Li et al reported the theoretical tensile strength of SWNT bundles to be between 2.3 ± 0.2 to 14.2 ± 1.4 GPa, and a tensile strength of an individual SWNT as high as 22.22 ± 2.2 GPa.[37] These values were extrapolated from the experimental tensile strength determined for SWNT ropes. In addition to their large tensile strength, Salvetat reported that SWNTs with relatively large length and small diameter have a Young's Modulus of approximately 1 TPa, and approximately 1 GPa for larger diameter tubes.[38,39] These predictions suggest SWNTs have a strength 10 to 100 times greater than that of steel.[40] It is clear that SWNTs possess exceptional mechanical strength, which causes them to be resilient to strain in the axial direction, however, due to their long length, they remain relatively flexible.[35] These properties combined are what make SWNTs attractive for use in a variety of applications.

1.3 Synthesis of Single Walled Carbon Nanotubes

SWNTs are generally synthesized using one of three methods: 1) arc discharge, 2) laser vaporization, or 3) chemical vapor deposition. Independent of the method employed, the raw material that is produced contains impurities, including amorphous carbon, metal catalyst particles, and smaller-sized fullerenes. In addition, these synthesis techniques yield SWNTs with various chiralities, lengths, and tube diameters, as well as a mixture of metallic and semiconducting tubes. It is important to note that each synthesis

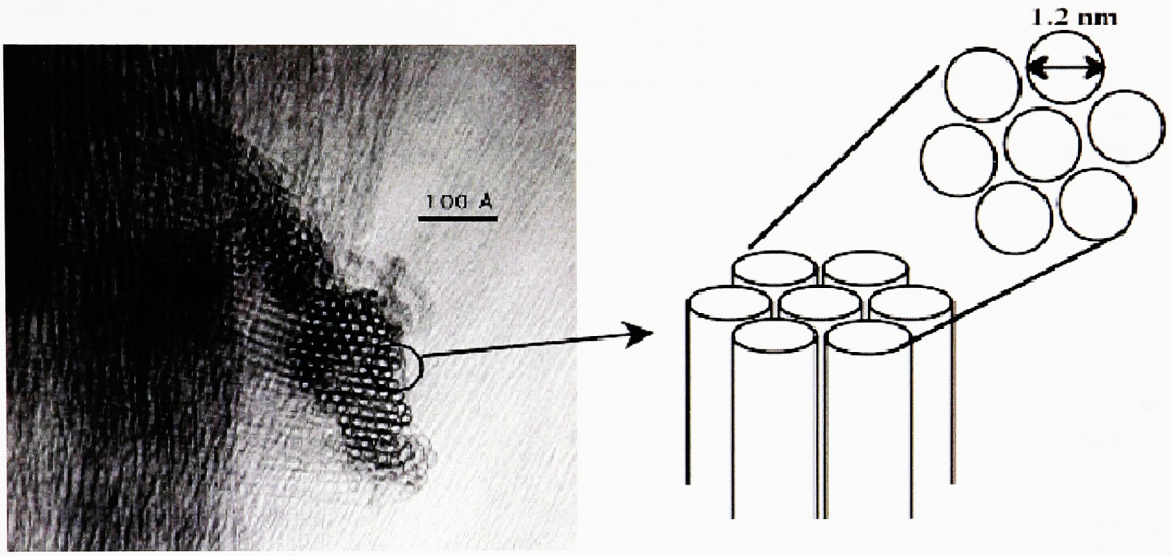

Figure 5: Transmission electron micrograph of SWNT bundle. Inset shows a close-up schematic of how the bundle is held together through Van der Waals interactions.[14]

technique has associated advantages and disadvantages in producing various types of SWNTs. There is no single technique that can be used to synthesize pure, monodisperse SWNTs, but research efforts are focused on improving the current technology with the goal of producing more material in each synthesis batch with fewer contaminants, defects, and impurities.

Aside from the inherent disadvantages in the current technology used to synthesize SWNTs, there are two universal properties that are observed in the synthesis process that are independent of the technique used, *bundling* and *defects*. When synthesized, intermolecular forces cause an attraction between individual SWNTs, and bundles, held together by Van der Waals interactions, are formed (Figure 5). This is unlike the behavior of MWNTs, which do not bundle together. Each bundle of SWNTs is different in the sense that it is composed of varying numbers of individual tubes, each with potentially different diameters, lengths, and chiralities.[41] As with an individual SWNT, a bundle can be either metallic or semiconducting. This is dictated by the individual SWNTs that make up the bundle; if a single metallic tube is present in the bundle and its dielectric constant is large enough, then the entire bundle behaves as a metallic tube.[42,43]

In addition to bundling, SWNTs are also known to contain defects. A defect is created when either a carbon atom is missing or by Stone Wales defects. When a carbon atom is missing from the hexagonal carbon network, the resulting defect is referred to as a *dangling bond*. On the other hand, Stone Wales defects occur when there is a disruption in the ordering of the carbon atoms. In this case, the atoms are arranged in an adjacent heptagon-pentagon pair rather than the two hexagons as would otherwise be

expected.[44] SWNT bundling and surface defects are characteristic of the material and are to be expected no matter what synthesis technique is employed.

1.3.1 Synthesis of SWNTs via Arc Discharge

The first SWNTs were synthesized by an arc discharge method.[2,3] This synthesis was carried out in a reaction vessel under inert atmosphere (He, Ar, etc.) between 100 - 500 torr. Within the reaction vessel, two graphitic carbon rods serve as the anode and cathode, respectively (Figure 6). A hole is drilled in the anode and is filled with a mixture of graphite powder, metal catalyst (typically Co, Fe, or Ni), and a promoter (typically Y, Bi, or Pb). The promoter is generally used to enhance the functionality of the primary catalyst, especially when synthesizing high-yield, large-diameter SWNTs. An electric current, either ac or dc, is generated between the two electrodes (60 – 100 A), while the voltage remains constant (15 – 30 V). As the discharge occurs, the two electrodes are brought together so as to maintain a constant distance of approximately 1 mm between them. This is necessary due to the fact that the anode is consumed during processing. A plasma is formed and the carbonaceous material is deposited at the cathode allowing for the growth of the SWNTs.[41,45,46] A high resolution transmission electron micrograph (TEM) of the raw soot produced by arc discharge is given in Figure 7. To date, the smallest recorded stable SWNT produced by arc discharge had a diameter of 0.4 nm, however typical tube diameters range from 1 - 2 nm for this type of synthesis.[46,47] Although the arc discharge method of synthesis is relatively inexpensive and can produce gram quantities of raw nanotube soot in a matter of minutes, the main disadvantage is that the soot only yields approximately 30% w/w SWNTs.[41]

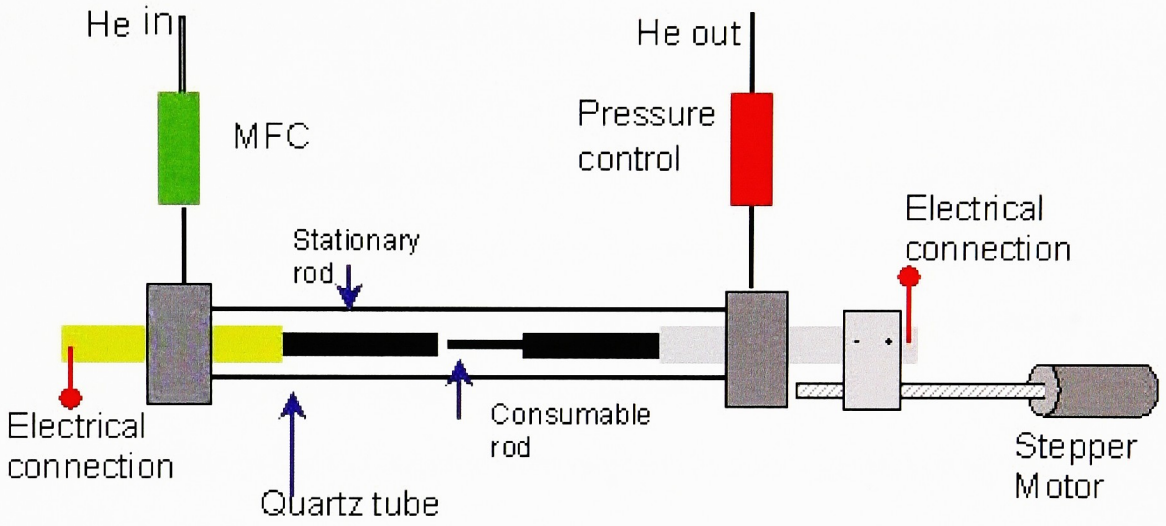

Figure 6: Schematic of a typical arc discharge apparatus used in the synthesis of SWNTs.

Synthesis of SWNTs via Laser Vaporization

The synthesis of SWNTs by laser vaporization was first reported in 1995 by Guo et al.[4] With this technique, the synthesis is carried out in a quartz tube reaction chamber, which is able to be heated with an external furnace. A compressed graphitic target, containing a mono- or bi-metallic catalyst (usually composed of varying amounts of Fe, Ni, or Co), is placed in the center of the heated portion of the reaction chamber (Figure 8). The chamber is filled with inert gas (typically Ar at 500 torr), and is heated to a constant temperature between 800 -1200°C. A laser beam is then scanned uniformly across the face of the target causing the material to be vaporized. A plume is formed in front of the target and is then carried out of the heated portion of the reaction chamber in flowing Ar at 100 sccm where it condenses on to the walls of the quartz tube.[4,48-51] A TEM of the as produced SWNTs obtained from synthesis by laser vaporization is provided (Figure 9). In an effort to understand the growth mechanism of SWNTs produced by laser vaporization, *in-situ* imaging and spectroscopic diagnostics of the plume were carried out by Geohegan et al. From this study, the time needed for the growth of SWNTs inside the hot furnace was elucidated (Figure 10). It was determined that after the first 100 μs of vaporization, the plume consists only of excited atoms and molecules. The excited carbon atoms return to the ground state after approximately 200 μs due to condensation, and begin to form carbon clusters. At that time, the metal catalyst still remains in the excited state. At approximately 0.8 ms, the metal catalyst atoms return to the ground state, and at 2 ms begin to form carbon – metal clusters. The growth of short SWNTs (<240 nm in length) is achieved approximately 25 ms after

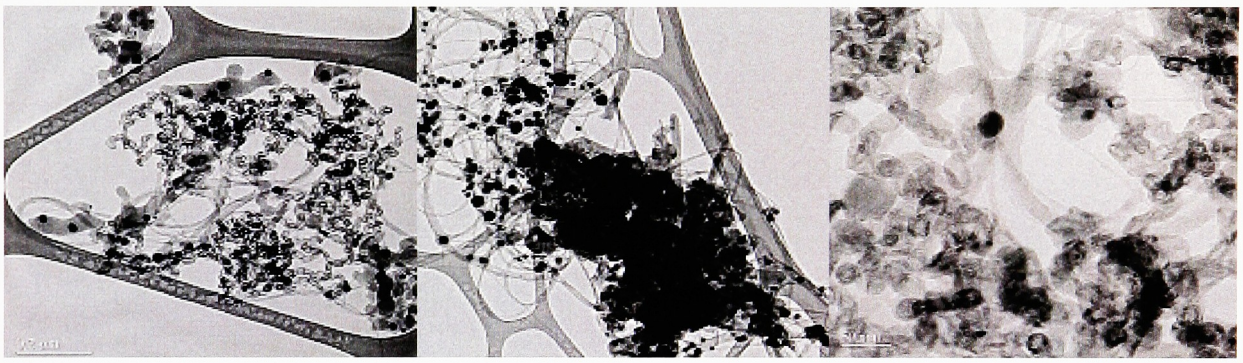

Figure 7: High-resolution transmission electron micrograph of SWNTs synthesized by the arc discharge method over a Ni/Co primary catalyst.

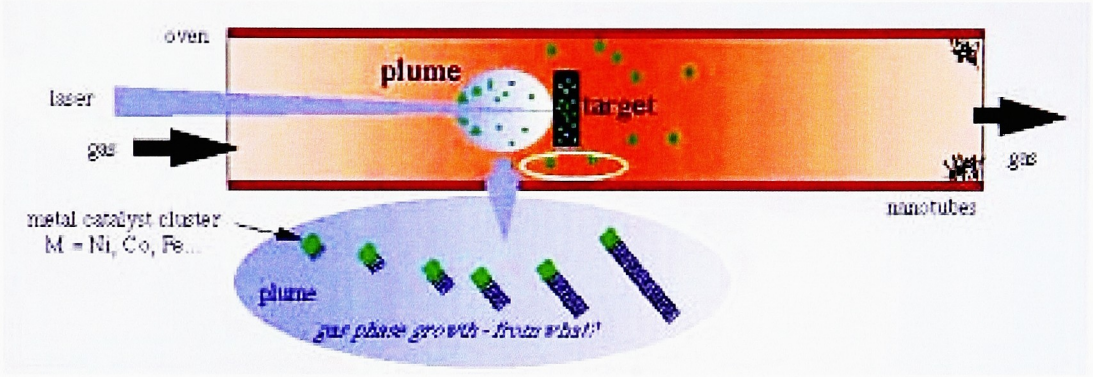

Figure 8: Schematic of a laser vaporization apparatus used in the synthesis of SWNTs.

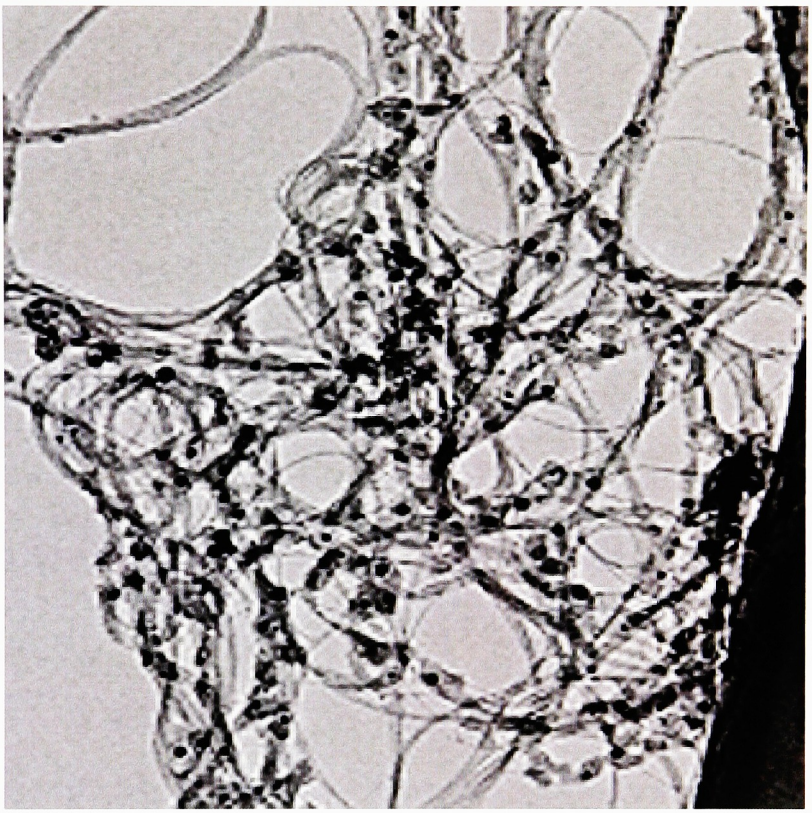

Figure 9: Transmission electron micrograph of SWNTs synthesized by the laser vaporization method over a Ni/Co catalyst.

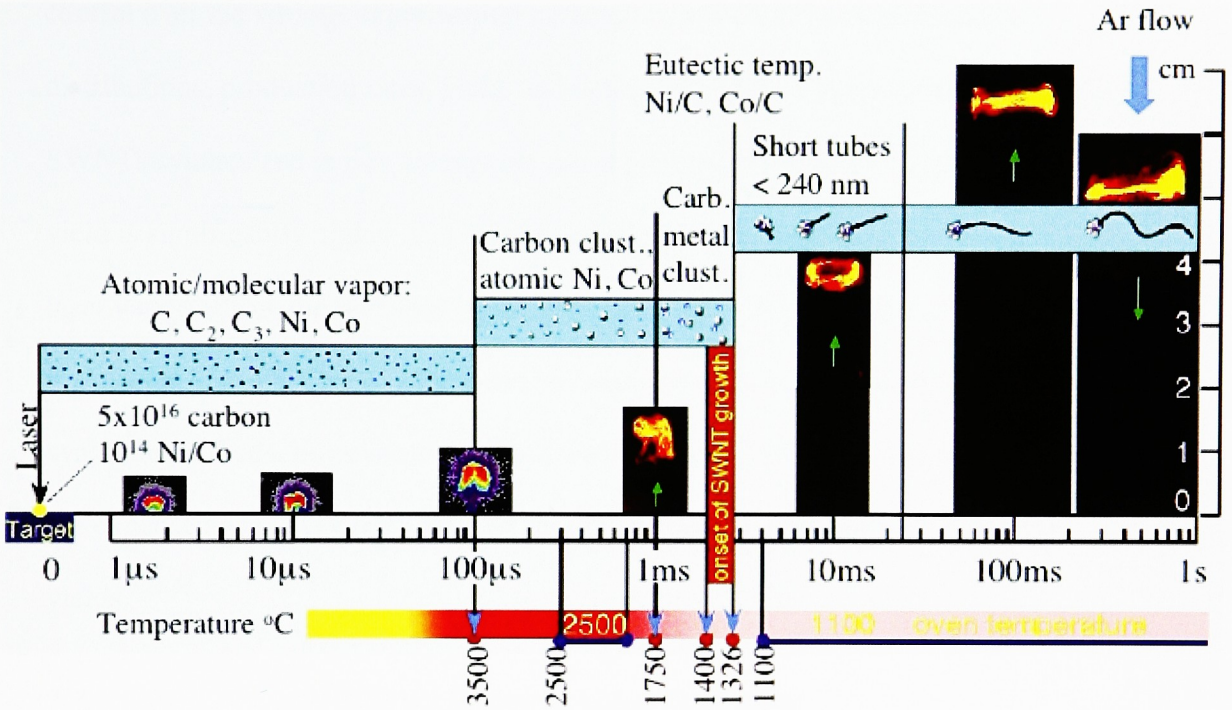

Figure 10: Schematic for the sequence of events in the growth mechanism of SWNTs by laser vaporization.[51]

vaporization, indicating that much longer times are needed for complete growth of the SWNTs.[51]

It is important to note that the SWNTs used in the present study were all synthesized using the laser vaporization method. This method provides considerable control over the various experimental parameters, which influences diameter distributions, production rates, yield, and defect densities. Typical tube diameters for SWNTs synthesized in this manner are again generally between 1 - 2 nm, however the yield is significantly higher than was observed for synthesis by arc discharge. Using laser vaporization, the raw soot typically contains 90% w/w SWNTs. It is obvious that the quality of the SWNTs synthesized by laser vaporization far exceeds that of most other synthetic methods, however the major drawbacks associated with this technique include the expense and energy required, and the relatively long synthesis times and low yields.[3,35,51]

1.3.2 Synthesis of SWNTs via Chemical Vapor Deposition

Chemical vapor deposition (CVD) synthesis of SWNTs is currently the most scalable technique available, and is commonly used to produce industrial quantities of material. This synthetic technique involves the growth of SWNTs from a gaseous carbon feedstock onto a pre-prepared substrate containing a metal catalyst (typically Fe, Ni, or Co). The catalyst is deposited onto a substrate (either alumina or silica) by chemical deposition. The substrate is placed into the reaction chamber after the appropriate catalyst preparation (Figure 11), and the gaseous carbon feedstock is then passed over or through the material. Typically the carbon feedstock comes from methane, carbon monoxide, or acetylene, however a wide range of carbon sources have been reported in

the literaure. Energy is applied to the carbon feedstock, generally by thermal heating, such that it *cracks* the carbon source and generates the reactive atomic carbon atoms required for the nanotube synthesis. The synthesis is carried out at elevated temperatures between 650 – 900°C. As the carbon atoms migrate over the catalyst substrate, they bind and form a hemispherical cap on the metal catalyst particle. As more carbon is introduced, it can either continue to chemisorb to the metal particle, which causes deactivation of the catalyst, or it can insert into the cylindrical portion of the cap causing the growth of the SWNTs. The growth is terminated when the strain of curvature becomes too great.[5,52-54] Figure 12 provides a TEM of the raw soot obtained from CVD synthesis.

This technique provides good control over the diameter distribution and growth rate of the SWNTs, however the tubes often have a significant number of defects. A typical CVD synthesis will yield approximately 30 - 50% w/w SWNTs.[35] Additionally, the as produced material contains a significant amount of amorphous carbon that coats the SWNTs due to the fact that the hydrocarbons used in the carbon feedstock may pyrolize at the required synthesis temperatures. In an effort to improve SWNT yields by CVD synthesis, Smalley proposed a high pressure carbon monoxide disproportionation process (HiPco) with the intention that it could be used for the mass production of SWNTs. The synthesis of SWNTs with an average diameter of 0.7 nm was achieved by flowing the CO feedstock with a small amount of gaseous iron pentacarbonyl ($Fe(CO)_5$), which functions as the catalyst, in a heated reaction chamber. This process was shown to not only increase the yield of SWNTs, but it also significantly increases their purity as well. Since the discovery of the HiPco process in 1999, many efforts have been made to

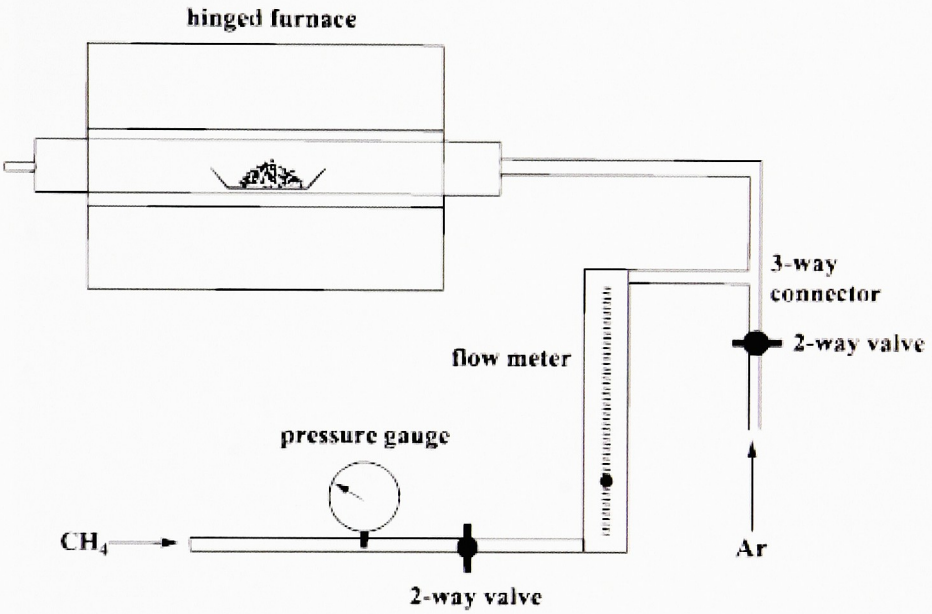

Figure 11: Schematic of CVD apparatus used in the synthesis of SWNTs.[55]

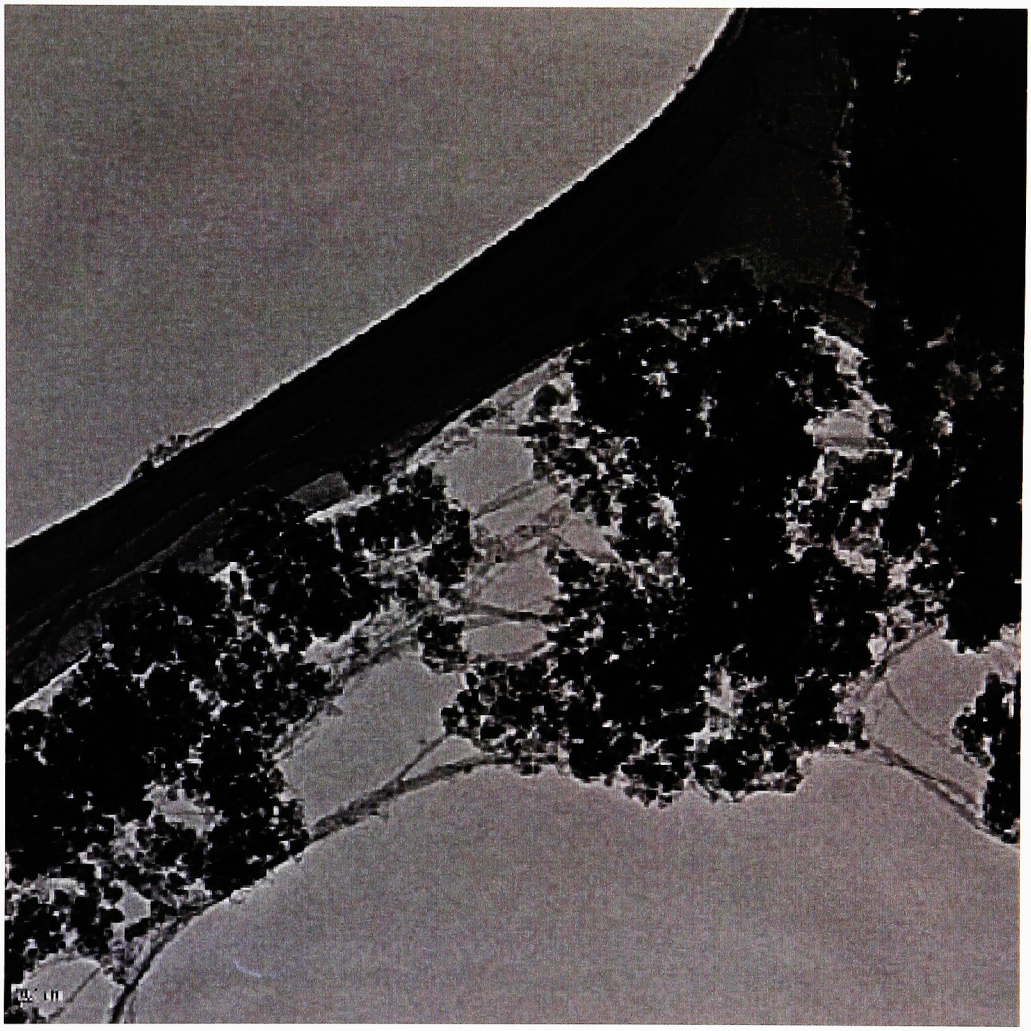

Figure 12: Transmission electron micrograph of SWNTs synthesized by the CVD method over a $Fe(NO_3)_3/Al_2O_3$ catalyst. Methane was used as the carbon source.[55]

improve upon this synthesis technique by varying the experimental parameters. The intention of such studies is to increase the yield and quality of the SWNT materials produced.[56]

1.4 Purification and Characterization of SWNTs

1.4.1 Purification

The as-produced materials obtained from the arc discharge, laser vaporization, and CVD synthesis methods are generally contaminated with amorphous carbon, metal catalyst particles, and smaller fullerenes. For many applications, these impurities must be removed because they interfere with most nanotube properties, however the difficulty remains that no single purification technique is widely applicable to the purification of raw nanotube soot obtained from the three synthesis methods. The raw soot obtained from the arc discharge method is known to have a significant amount of graphite encapsulated metal catalyst particles, which are generally difficult to remove. The first successful method of purification for arc produced SWNTs was reported by Roth in 1999. This method involved purification through the use of size exclusion chromatography (SEC), however one major disadvantage was the limited solubility of the SWNTs.[6] Another, more widely utilized technique was reported in 2002 by Eklund, who demonstrated that the raw soot generated by arc discharge could be purified by microwave heating of the metal catalyst particles within the as produced materials. Microwave treatment (2.45 GHz, 150W) was employed to cause either the carbonaceous coating over the metal particles to burst by thermal expansion, or oxidize. In both cases the coating was weakened and the metal particles were then removed via hydrochloric acid, HCl, reflux. In this case, it was necessary to optimize the experimental parameters,

otherwise if heated too quickly the SWNT material would be consumed during the exothermic oxidation of the metals, and if heated too slowly this type of purification would be inefficient. However, when performed at optimal conditions, this technique yielded SWNT materials with 99.8% w/w purity.[7] A more conventional method, also reported in 2002 by Huang, involved a three step process by which the raw soot was soft oxidized by dilute nitric acid reflux, air oxidized by heating to 550°C, and finally exposed to high temperature vacuum treatment at1600°C and 10^{-3} Pa.[8] The first step was carried out to form an oxide layer on the surface of the metal catalyst particles to avoid any of the SWNT material from undergoing metal-assisted dissociation upon further processing. Steps two and three were used to remove any remaining carbonaceous impurities, and to consume any defects by rearrangement of the SWNTs using the high temperature anneal.

Although the HiPco process provided much more pure yields of material over traditional CVD synthesis methods, the as produced materials still need to be purified before they can be used in subsequent applications. The main impurity in HiPco synthesized raw soot is encapsulated metal catalyst particles. In 2001, Hauge et al reported a purification technique that allowed for the metal catalyst particles to be exposed after low temperature wet Ar/O_2 air oxidation. Upon breaking the carbonaceous coating around the metal catalyst particles, the metal was removed in HCl. The sample was then dried and annealed at 800°C. It was noted that when compared to laser produced raw soot purified in the same manner, the HiPco tubes were less stable in air than the laser produced tubes. It is believed that this is due to the smaller tube diameter of the HiPco tubes, respectively, which tend to be more reactive than the larger diameter tubes synthesized by laser vaporization.[9]

The oxidative purification methods described for the arc discharge and HiPco raw soot mainly stem from processes developed for materials synthesized by laser vaporization. In 1999, Dillon et al reported a simple technique for the purification of materials synthesized by laser vaporization.[10] The raw soot was first refluxed in dilute nitric acid, and then filtered and washed with deionized water. The reflux allowed for the carbonaceous impurities to be digested and redistributed uniformly over the surface of the SWNTs, and allowed for the exposure of the metal catalyst particles. A subsequent air oxidation served to remove many of these impurities, leaving behind approximately 20% of the initial sample mass in the form of SWNTs with >98% purity. The purification process was completed with a brief anneal, however, in 2001 Hauge et al noted that complete removal of the metal catalyst particles was necessary prior to exposing the material to high temperatures in order to avoid any metal catalyzed oxidation of the SWNTs. Therefore, after completing the nitric acid reflux, filtration, and air oxidation, the sample is washed several times with an HCl solution, each time followed by subsequent air oxidations.[11]

1.4.2 Characterization of the Purified SWNTs

The purity of the SWNT material, which was synthesized by laser vaporization and purified using the acid/air oxidation methods described previously, can be assessed using a variety of methods, including Thermogravimetric Analysis (TGA), microscopy, and spectroscopy. TGA is a widely accepted method used for semi-quantitative purity determination of SWNT materials.

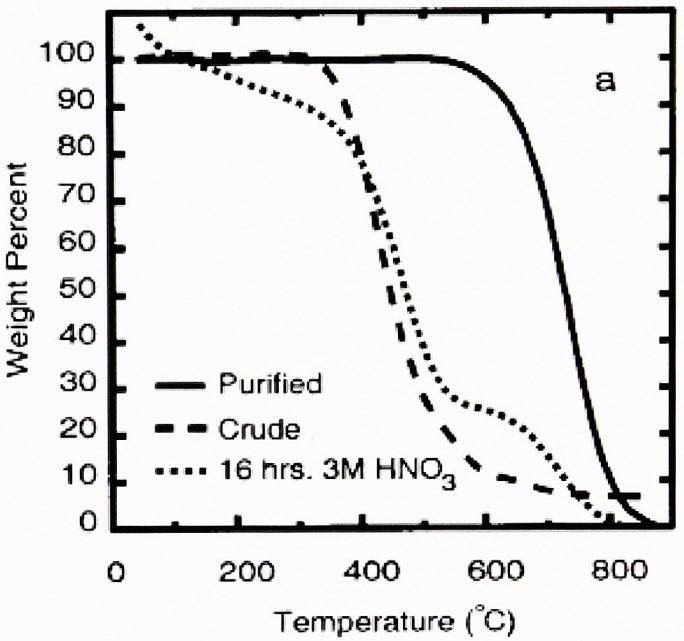

Figure 13: TGA of a 1 – 2 mg sample of crude, acid refluxed, and purified SWNT material. Samples were ramped from 25 – 875°C at 5°C per minute under 100 sccm flowing air.[10]

TGA is generally used to evaluate the stability of a material by monitoring the change in mass of a sample while uniformly increasing the temperature in flowing gas (typically air).[12] Dillon et al showed that TGA provided a means of comparing raw soot and purified materials.[10] This technique allows for the purity of the SWNT material and the percentage of residual metal catalyst to be determined on a weight percent basis, as compared to as - produced and acid refluxed materials (Figure 13). Analysis showed that the purified SWNTs were quite stable. In the heated region up to 550°C, amorphous carbon impurities are combusted. As illustrated by the plateau in the spectra, there is no significant loss in mass in the purified sample up to 550°C, indicating efficient removal of any carbonaceous impurities. When the temperature of the sample reaches 850°C, all carbonaceous materials, including the SWNTs, are consumed and any remaining mass is due to residual metal catalyst particles. Recently two concerns have been raised with the TGA method of analysis. First, it has been determined through inductively coupled plasma (ICP) spectroscopy and energy dispersive X-ray (EDX) analysis that in addition to metal catalyst particles, other impurities such as SiO_2, which can withstand the SWNT decomposition temperatures, may be present in the sample as well. A second concern with the TGA method is that it does not take into account that thermal oxidation of the metal catalyst particles may cause premature combustion of the SWNTs if the material contains a high degree of defects. In an effort to combat these concerns, Landi et al devised a protocol for a thermal oxidative profile (TOP) of the SWNT material, which would essentially allow for the creation of purification calibration curves by subjecting a SWNT sample to a systematic series of thermal treatments. This technique offers an

advantage over TGA due to the fact that it would allow for the efficiency of purification to be enhanced and the amount of material retained after purification to be maximized.[13]

In addition to TGA and TOP analyses, various microscopy techniques are used as a means of confirming the purity of the material. In this study Transmission Electron Microscopy (TEM) is used to assess the purity of the SWNT materials. TEM, as well as Scanning Electron Microscopy (SEM), provide information regarding the number of individual SWNTs in a bundle, diameter distributions, length distributions, and defect densities. TEM and SEM can also be used to assess the purity of a sample because amorphous carbon, large graphite particles, and metal catalyst particles can all be visualized in the images. Examination of the SWNT surface would expose any residual carbonaceous or metal catalyst impurities. In addition to electron microscopies, scanning probe microscopies, such as Scanning Tunneling Microscopy (STM) and Atomic Force Microscopy (AFM), can provide much of the same information.[14]

1.5 SWNTs as Catalyst Supports in Fischer - Tropsch Synthesis

The unique physical and chemical properties of SWNTs make them an attractive material to be used in a variety of applications including energy storage, molecular electronics, sensors, and composite materials.[15] In the present study, the use of SWNTs as a catalyst support in heterogeneous catalysis reactions. In heterogeneous catalysis reactions, the catalyst is present in a well defined state, where as the reactants are in a separate phase. Typically, the catalyst is a solid, which provides a surface for the desired reaction to occur, and can ultimately be removed upon completion of the reaction. This is in contrast to homogenous catalysis reactions where the catalyst and reactants are present in the same phase.[57]

In FT synthesis carbon monoxide is hydrogenated over a transition metal catalyst to form varying length, linear and bent hydrocarbons, as well as oxygenates (alcohols, aldehydes, acids and ketones), olefins, and paraffins. Two other heterogeneous catalysis reactions may compete with the FT synthesis, the Sabatier reaction and the Water-Gas Shift (WGS) reaction (Figure 14). The Sabatier reaction is similar to FT synthesis in that it is a hydrogenation reaction that takes place in the presence of a transition metal catalyst, however the Sabatier reaction utilizes carbon dioxide in place of carbon monoxide, and the only product formed is methane. As with the Sabatier reaction, the WGS reaction involves the reduction of carbon dioxide. In this case, there is no formation of methane or any other hydrocarbons. The main product in the WGS reaction is carbon monoxide. It is obvious that all three heterogeneous catalysis reactions are very similar, and careful attention is needed in monitoring the products of all experiments performed to determine which type of heterogeneous catalysis reaction is dominant.[16-19]

1.5.1 Fischer – Tropsch Synthesis: A Historical Overview

Prior to the discovery of FT synthesis, many efforts were being made to perform catalytic carbon monoxide hydrogenation reactions. In 1902, Sabatier and Senderens attempted a methanation reaction over a nickel catalyst. Later, in 1913, BASF attempted a high pressure synthesis of hydrocarbons and oxygenates over a cobalt catalyst. Finally, in the early part of the 1920's Frans Fischer and Hans Tropsch discovered that hydrocarbons could be synthesized at atmospheric pressure over iron, cobalt, or nickel

$$4H_2 + CO_2 \rightarrow CH_4 + 2H_2O$$ Sabatier Reaction

$$(2n+1)H_2 + nCO \rightarrow C_nH_{2n+2} + nH_2O$$ Fischer-Tropsch Reaction

$$CO + H_2O \rightarrow CO_2 + H_2$$ Water-Gas Shift Reaction

$$H_2 + CO_2 \rightarrow CO + H_2O$$ Reverse Water-Gas Shift Reaction

Figure 14: Reaction schemes for various competitive heterogeneous catalysis reactions.

catalysts. This was done by flowing synthesis gas (syngas), which consists of a mixture of H_2 and CO, over the transition metal catalyst. Syngas can be produced in one of two ways. Historically, syngas was produced by the gasification of coal, which was efficient due to the low cost of production and the ease of coal transportation. More recently, syngas has been produced by the reformation of natural gas. This process is favorable due to the fact that the process is more efficient than coal gasification. The process by which syngas is produced by the reformation of natural gas allows for a 70% carbon conversion to CO, whereas coal gasification has an associated 50% loss in carbon due to the formation of CO_2.[16-19]

The discovery of FT synthesis was a major break through in the field, and it had significant implications in the political and economic realm, especially for countries that had an abundant supply of coal but limited access to oil. In the 1930's the process was commercialized by Germany, and an attempt was made during WWII to achieve self sufficiency using FT synthesis for the production of fuel. After the war, the oil reserves in the Middle East began to be exploited and it was no longer economic for Germany to maintain the production of fuels using FT synthesis. It was not until the 1970's that FT synthesis again became popular when the South African Synthetic Oil Limited (SASOL), who in the face of rising oil costs, realized the potential to make fuels by exploiting their abundant natural coal resources. FT synthesis remains a highly attractive method for producing synthetic fuels due to the fact that these fuels are known to be more environmentally sound relative to petroleum based fuels. This is due in part to the lower amounts of sulfur, nitrogen, and aromatic compounds in the synthetic fuels.[16]

1.5.2 Fischer – Tropsch Reaction Mechanism

While it is generally believed that the dissociation of the syngas is the first step in FT synthesis, there is still significant uncertainty in regards to the mechanism by which the hydrocarbon chains are grown, and elucidating that mechanism has proved to be a difficult task. In 2002, Hu carried out an extensive set of density functional theory (DFT) experiments to determine the most probably route toward FT synthesis. In this study, the relative stability of several intermediates was determined, and various C/C coupling mechanisms examined (Table 1). Although, Fe, Ni, and Co are traditionally the metal catalysts utilized in FT synthesis, Ru was used in the DFT experiments as a model due to the fact that it is expected to possesses the highest known FT reactivity. It was determined that *steps* or defects are generally the more active sites for FT synthesis rather than flat surfaces. In addition, it was determined that of all the C/C coupling mechanisms studied, the C + CR reaction was the most probable due to the fact that it requires the lowest activation energy. Additionally, this C/C reaction seemed to be favored because CH or CR is more kinetically stable on the Ru catalyst support than the CH_2 species produced in other coupling reactions. The CH_2 species was found to decompose quickly to form CH due to its relatively small energy barrier (0.17 eV). Lastly, various hydrogenation reactions were studied on hydrocarbon chains synthesized by the C + CR coupling reaction. It has been considered that the formation of CH_4 is a side product of FT synthesis due to the fact that the reaction is terminated prior to the growth of a longer hydrocarbon chain. The most favorable hydrogenation reaction in hydrocarbon chain growth is the CCH + H reaction (Figure 15).[16,17]

Table 1: Calculated reaction barriers (Ea) for various C/C coupling reactions on Ru catalyst (step or flat surface) as determined by DFT experiments.[17]

	Ru-step	Ru-flat		Ru-step	Ru-flat
C+C	1.05	1.51	$CH+CH_2$	1.20	0.97
C+CH	**0.43**	1.01	CH_2+CH_2	0.59	1.23
$C+CH_2$	0.56	1.08	CH_2+CH_3	1.40	1.80
CH+CH	0.95	0.87			

[a] The unit of *Ea* is eV

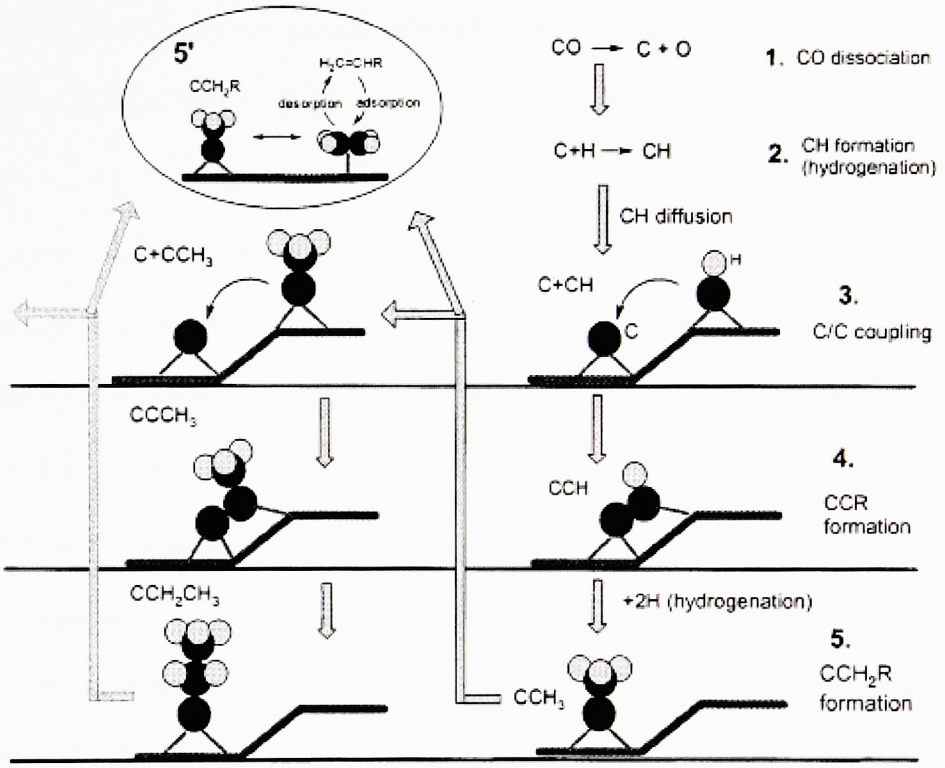

Figure 15: Proposed C + CR FT synthesis mechanism. (1) CO and H_2 dissociation. (2) C + H → CH reaction and CH diffuses to step site. (3) At steps C + CH → CCH. (4) CCH formation. (5) CCH + H → CCH_2 and CCH_2 + H → CCH_3. CCH_3 then diffuses to another step to start C + CCH_3 → $CCCH_3$. Alternatively, CCH_3 may rearrange to ethylene, C_2H_4, which desorbs readily from the Ru catalyst surface.[17]

1.5.3 Fischer – Tropsch Reactor Beds

Although the FT mechanism is not well understood, there are mainly two practical operating routes toward achieving FT synthesis, high temperature (300 – 350°C) and low temperature (200 – 240°C). The high temperature route is used in the production of gasoline and linear, low molecular weight olefins, whereas the low temperature route is used in the production of high molecular weight, linear waxes. Independent of the route used, the FT synthesis is a highly exothermic process and it is important to remove the heat from the reaction quickly. If the catalyst is overheated, the risk of deactivating the catalyst is increased. The temperature is typically maintained within standard operating conditions by either: (1) flowing the syngas at high linear velocity through long narrow tubes packed with the metal catalyst particles (Figure 16 (A) and (B)), or (2) using a fluidized catalyst bed reactor (Figure 16 (C), and Figure 17).

The first high temperature FT (HTFT) reactors were the fixed fluidized beds (FFB) designed in the mid 1950's (Figure 16B). The FFBs are considered HTFT reactors because they operated at 2 MPa and 300°C. The second generation of HTFT reactors are called the circulating fluidized beds (CFB), which operate at 2 MPa and 340°C (Figure 16A). CFBs contain two phases of fluidized catalyst. A dense phase is located in the standpipe. Here the catalyst moves down the standpipe while it is transported up to the lean zone where the reaction actually takes place. In order for this to occur, the differential pressure over the standpipe must always exceed that of the reaction zone. In either case, the FT synthesis occurs when the carbon is deposited onto the surface of the metal catalyst, which is typically Fe in HTFT reactor beds. There are several advantages to using an FFB reactor for FT synthesis. The cost associated with producing the reactor

is approximately 40% less for the FFB than that of the CFB. FFB reactors are smaller overall compared to the CFB reactor, and the reaction zone is larger allowing for more cooling coils to be installed and thus longer preservation of the catalyst. Additionally, the syngas can be provided to the FFB reactor at lower linear velocities than in the CFB reactor, which creates less of a need for routine maintenance. Most importantly, the entire catalyst is involved in the reaction at all times during the FT synthesis, whereas only portions of the catalyst are involved in the reaction at any given moment in the CFB reactor.[18,19,58]

Unlike HTFT reactors, the operation of low temperature FT (LTFT) reactors creates a significant amount of wax. In top-fed multitubular reactors (Figure 17) the wax trickles down and out of the reactor, however in slurry reactors the wax accumulates and continuously needs to be removed. Failure to remove the wax from a slurry reactor causes decreased activity of the catalyst until eventually it leads to pore plugging. The multitubular reactors operate at 2.7 MPa between 200 – 240^{o}C, and can contain between 2,000 to 10,000 tubes. Initially, the slurry reactor bed was not employed due to the fact that there was no efficient way to remove the wax from the catalyst. However, in 1990 a scalable filtration system was developed to remove the wax, and since that time the slurry reactor has been the focus of much attention. The technology has been advanced in recent years to the point where an on-line removal of the wax allows for longer reaction times. The ability to efficiently remove the wax from the catalyst has made the slurry reactor much more advantageous than the multitubular reactor. This is due largely to the fact that the slurry reactor costs 75% less than a multitubular apparatus, and it requires a much lower processing pressure. This in turn lowers the cost for the compression of the

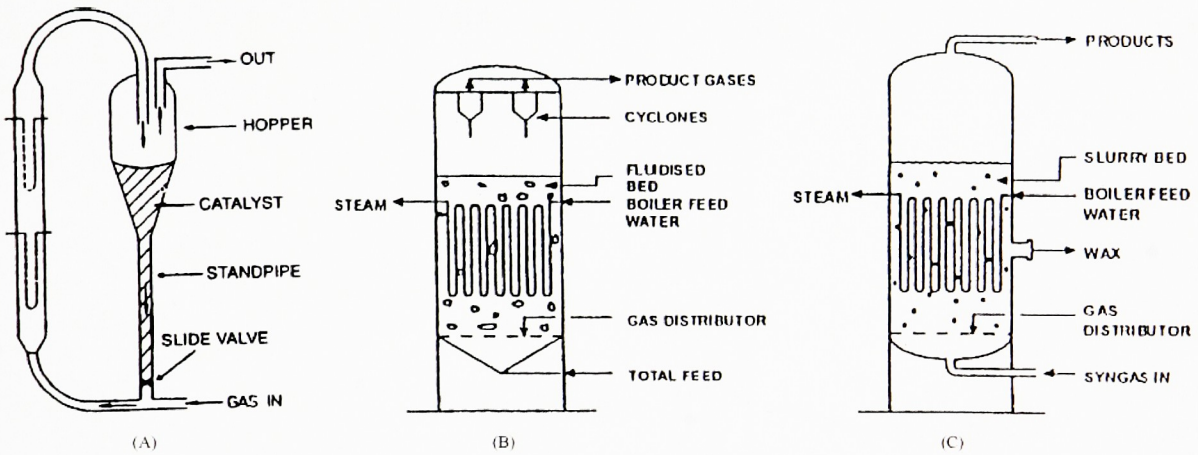

Figure 16: Fluidized bed FT reactors: (A) CFB reactor, (B) FFB reactor, and (C) slurry phase bubbling bed reactor.[18]

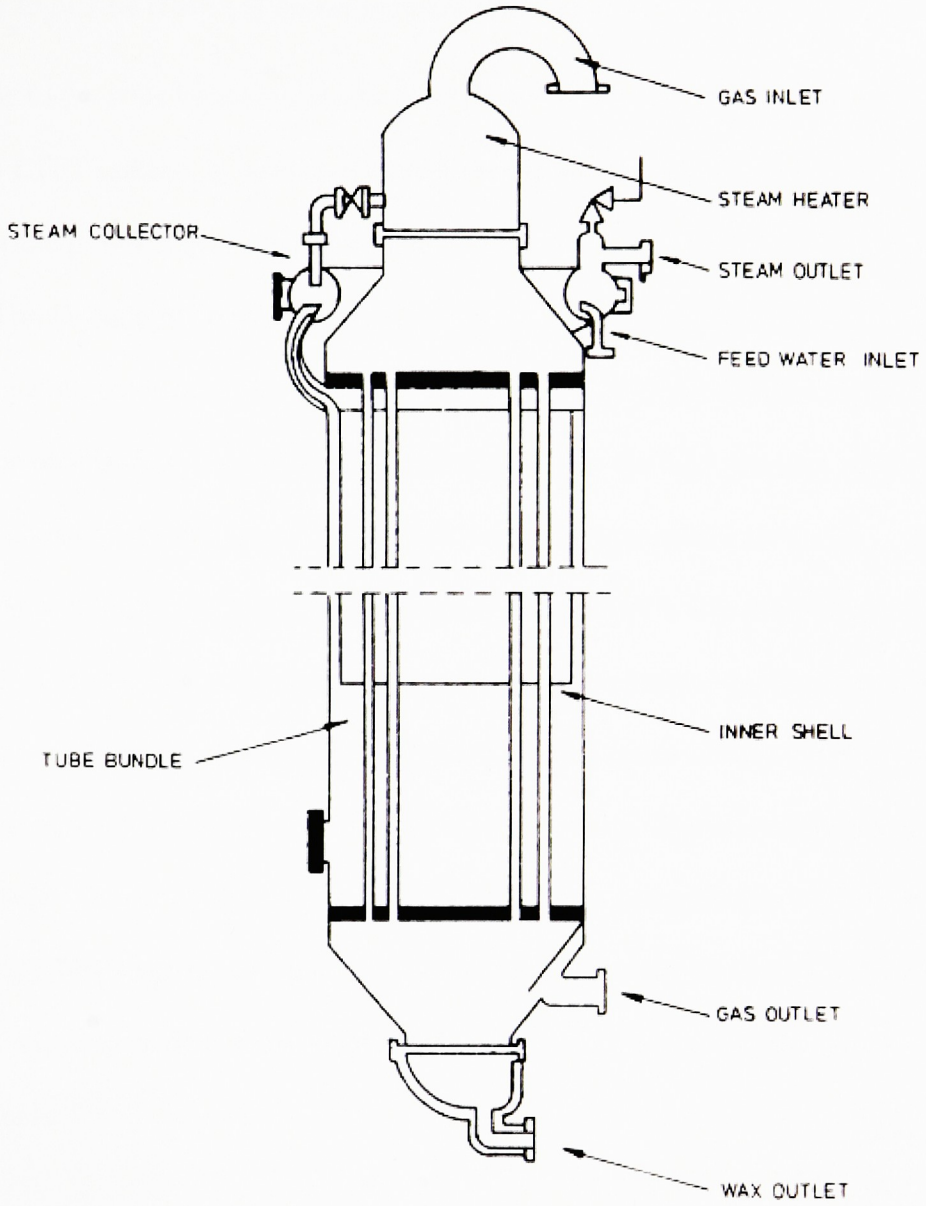

Figure 17: Schematic of a multitubular fixed bed FT reactor.[18]

syngas and allows for less consumption of the metal catalyst. The major advantage of the slurry reactor is the fact that it is more isothermal compared to the multitubular reactor. The ability to run the reactor at higher temperatures allows for a larger product yield.[18]

Due to the wide variety of products formed, the various synthetic parameters of HTFT and LTFT reactors have been studied to determine the best way to tailor the process for the production of either gasoline or diesel fuels. Using a FFB reactor at 340°C and an Fe catalyst, 20% of the crude product obtained is propene and 20% butene, which can be oligomerized to form high octane gasoline. Straight run gasoline obtained by the same process has low octane content mainly due to the high linearity and low aromatic content of the products formed. However, these properties are good characteristics of high quality cetane diesel fuels. Diesel fuel is best obtained from the crude product produced in a slurry bed reactor using a Co catalyst. In this case, 20% of the product is cetane that only needs to be hydrotreated in order to form usable diesel fuel, and 40-50% of the products are heavier diesel products. The heavier products can be converted to high quality diesel fuel by hydrocracking. Interestingly, both the HTFT reactors and LTFT reactors are capable of producing 10^3 tons of crude product per year, making FT synthesis a potentially viable method for sustaining the production of synthetic fuels.[18]

1.5.4 Catalyst Preparation for Fischer – Tropsch Synthesis

There is a significant expense for the catalyst used in FT synthesis, therefore it is ideal to use as little metal as possible, while at the same time increasing the surface area of the catalyst to achieve maximum catalytic activity. It has been demonstrated that the smaller the metal catalyst particles, the greater their activity in FT synthesis. In the past,

metal catalysts were typically supported on Al_2O_3, SiO_2, or TiO_2, and prepared by the precipitation of the transition metal followed by a partial reduction using H_2. It has been demonstrated that a major drawback in using oxide materials as supports for FT catalysts, is that during their preparation, the support may react with the transition metal causing a variety of compounds to be formed. This is especially true of Co catalysts. In any case, the results of producing transition metal catalysts in this manner are not reproducible except at significantly high reduction temperatures. More recently, activated carbon has been explored as a support for the metal catalyst support used in FT synthesis due to its increased surface area, stability at high temperatures under non-oxidising conditions, and its porous structure. Activated carbon provides significant improvements in FT catalysis relative to oxide supported catalysts, however, activated carbon is also flawed in that it has an ill-defined structure and it is typically impure.[18,20,21]

A good support for FT catalysts should have high purity, high mechanical strength, and high chemical inertness in order to combat the problems associated with traditional support materials. These properties are all characteristics of SWNTs, and as a result nanotubes are the most recent material to be explored as transition metal supports for FT catalysts. In the current literature, only the preparation of Fe and Co supported on MWNTs has been reported to date.[18,20,21] These materials were prepared by incipient wetness impregnation followed by either drying or by the precipitation of the metal on to the tube. As with more traditional catalysts, these metals are again partially reduced using H_2. In these studies, emphasis was placed mainly on the deposition of the metal catalyst on the MWNTs and demonstrating that they can be utilized as FT catalysts.

However, preliminary data has showen that the transition metal – MWNT materials had increased catalytic activity over catalysts prepared on more traditional catalyst supports.

As mentioned above, SWNTs provide distinct advantages in the synthesis of transition metal – carbon nanotube hybrid materials for FT catalysts. In addition to their purity, mechanical strength, and chemical inertness, SWNTs are also known to have an increased surface area over activated carbon. This is advantageous in that it allows for an increased number of metal particles to be deposited on the surface of the SWNTs, thus potentially resulting in increased catalytic activity. The increase in the number of active sites on the catalyst will allow for more reagent gases to be adsorbed, thereby increasing the kinetics of the FT synthesis. In addition to their large surface area, the curved nature of the SWNTs will introduce distortions on the various facets of the attached metal nanoparticles, which are predicted to assist in the creation of additional active sites.

The sub-nanometer pore structure and the capillary action inside the tubes and in interstitial sites within bundles, make SWNTs an attractive catalyst support as well (Figure 18). SWNTs are known to be meso-porous structures. In comparison to the micro-porous structure of the activated carbon, it is believed that this attribute will allow for facile mass transport of reactant gases along the solid nanotube surface to the active sites on the catalyst during FT synthesis. Additionally, the intrinsic capillary action of the SWNTs is believed to help carry reactant gases to the active sites and carry desorbed products away. This feature would leave sites available for further reaction, and would allow for increased catalytic activity in the FT synthesis.[18,20,22-27,59]

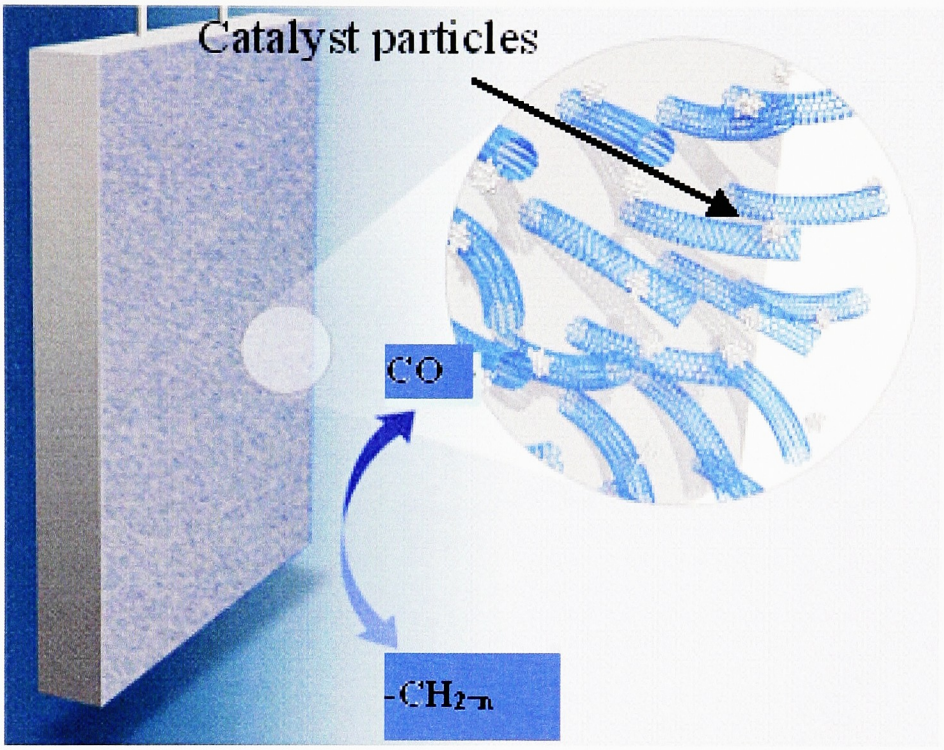

Figure 18: Schematic showing the hydrogenation of CO over a transition metal – carbon nanotube catalyst, and the production of various hydrocarbons.

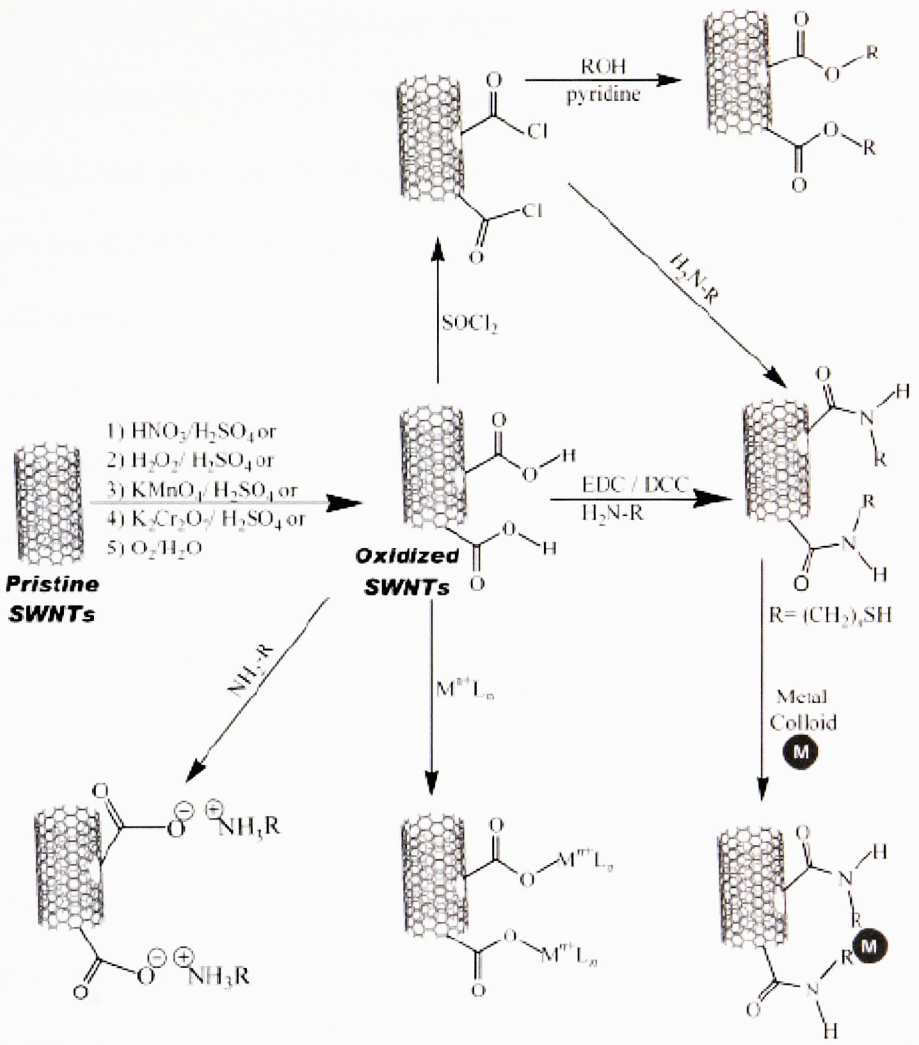

Figure 19: Schematic of common functionalization routes used to derivatize SWNTs at end and defect sites.[59]

1.5.5 Synthesis of Transition Metal – Carbon Nanotube Hybrid Materials

SWNTs have been functionalized through a variety of covalent and non-covalent pathways (Figure 19).[60,61] As described previously, the transition metal – carbon nanotube hybrid materials synthesized specifically for their use in FT synthesis were prepared through various precipitation reactions from metal salt solutions. However, the functionalization of SWNTs with transition metals has been extensively examined for a variety of different uses other than FT synthesis. In these instances, various transition metals have been deposited onto the surface of SWNTs via physical evaporation[62], spontaneous deposition[63], attachment after nanotube oxidation[64], electrdeposition[65,66], and electroless deposition with the aid of a reducing agent.[67] In the present study transition metal – carbon nanotube hybrid materials were synthesized with Fe, Ni, Co, Cr, and Rh using one of three novel incipient wetness techniques including: 1) the adsorption of metal from a metal salt solution onto the surface of the SWNTs followed by reduction with sodium borohydride, 2) the direct reduction of the SWNTs with Na-, K-, or Li-naphthalate followed by reaction with the metal salt solution, and 3) the pre-reduction of the SWNTs with sodium borohydride followed by the direct reduction technique. The interaction between the various transition metals with SWNTs is not yet well understood, however DFT studies and an examination of MWNTs decorated with transition metals provides some insight.

The adsorption of a transition metal onto the SWNTs followed by reduction of the metal via the aid of a reducing agent is the most common method for synthesizing transition metal – carbon nanotube hybrid materials. Synthesis of these hybrid materials has been typically studied using MWNTs, where it has been reported that metals tend to

attach to the ends or at kinks on the tube where defects and edge-plane-sites exist. As such, it is believed that the functionalization of the SWNT sidewalls is possible through defect chemistry as well.[61,66,68-70] Defects are created on the surface of the SWNTs during the purification process from the HNO_3 reflux. During this process, oxidative groups such as hydroxyl (-OH), carboxyl (-COOH), and carbonyl (-C=O) groups are introduced. Through the presence of these functional groups on the surface of the SWNTs, the directed deposition of various transition metals can be achieved. The transition metal is adsorbed onto the ends and surface defects of the SWNT, where it is partially reduced by the tube itself. In the present study, the complete reduction of the transition metal onto the SWNT was accomplished through the addition of $NaBH_4$. In previous studies, the transition metal – carbon nanotube hybrid material was dried, and then the metal was fully reduced in flowing H_2. The reduction of the transition metal using $NaBH_4$ simplifies the procedure by maintaining an all solution based chemistry, and only after the synthesis of the hybrid material is accomplished is the sample dried and ready for use in practical applications.

Synthesis of the hybrid materials via the direct reduction technique described previously eliminates the need for a reducing agent altogether. In 2002, Dai et al reported a method by which various noble metals could be spontaneously deposited onto the surface of the SWNTs by direct redox reaction between the metal ions and the SWNTs.[63] More specifically, it was determined that the reduction potential, E_{red}, of the SWNTs was -0.5 V relative to a standard hydrogen electrode (SHE). Therefore, both Au and Pt could be spontaneously reduced onto the surface of the nanotubes by a simple immersion of the SWNTs into a metal salt solution. This is possible because the

reduction potential, E_{red}, of both Au^{3+} and Pt^{2+} are greater than that of the SWNTs, 1.42 V and 1.2 V, respectively. The spontaneity of these reactions are governed by the simple equation given below:

$$E^{o} = E_{red} - E_{ox}$$

A positive standard potential, E_0, is indicative of a spontaneous reaction, and the opposite is true for a negative E_0. Although Dai et al only reported the spontaneous deposition of Au and Pt, other transition metals, such as Ag and Pd, could theoretically be deposited in similar fashion. In the direct reduction technique used in the present study, a spontaneous reaction between the SWNTs would only be achieved with Rh based on E_{red} values (Table 2). As such a spontaneous reaction between the SWNTs and the transition metal was only possible by modifying the E_{red} of the SWNTs prior to immersing them in the metal salt solution. The E_{red} of the SWNTs was modified by pre-reducing the nanotubes with alkali metals, in this case, Na, K, and Li. This causes the E_{red} of the reduced SWNTs to be close that of the alkali metals they were produced from.[71] As can be seen, an E_{red} of approximately -2.71 V, -2.93 V, and -3.04 V for the Na-, K-, and Li-SWNTs, respectively, should theoretically cause the spontaneous deposition of most transition metals onto the surface of the SWNTs. As with the adsorption technique, the direct reduction technique provides a purely solution based method for the synthesis of the hybrid materials.

Table 2: Various electrochemical reduction half reactions. The reactions is [1] represent the transition metals that were spontaneously deposited on the surface of SWNTs by Dia et al[61], [2] represents various other transition metals that could potentially be deposited spontaneously on the surface of SWNTs, and [3] represents the metals that were studied in this thesis research. As can be seen, Co, Cr, Fe, and Ni will not be spontaneously deposited unless the E_{red} of the SWNTs is modified by as described in the direct reduction technique. Rh is the only metal to be studied in this reaction that could potentially be deposited spontaneously onto the surface of the SWNTs.

Electrochemical Reduction Reactions

Reaction	Potential, Volts	
$Au^{3+} + 3e^- \rightarrow Au^0$	1.42	[1]
$Pt^{2+} + 2e^- \rightarrow Pt^0$	~1.2	

Reaction	Potential, Volts	
$Ag^+ + 1e^- \rightarrow Ag^0$	0.7996	[2]
$Pd^{2+} + 2e^- \rightarrow Pd^0$	0.83	

Reaction	Potential, Volts	
$Co^{2+} + 2e^- \rightarrow Co^0$	-0.28	
$Cr^{3+} + 3e^- \rightarrow Cr^0$	-0.424	
$Fe^{3+} + 3e^- \rightarrow Fe^0$	-0.04	[3]
$Ni^{2+} + 2e^- \rightarrow Ni^0$	-0.257	
$Rh^{3+} + 3e^- \rightarrow Rh^0$	0.76	

In the third synthetic technique explored in this thesis research, both the adsorption and direct reduction techniques were combined. Purified SWNTs were treated with $NaBH_4$ in the absence of a transition metal. In doing so, the oxidative groups (-COOH, -CO, and –OH) generated during the purification of the nanotubes were removed, and oxygen-free, pristine-like SWNTs were obtained (Figure 20). After achieving complete SWNT purity, the direct reduction technique was employed in the same manner as described previously. The efficiency of deposition was then compared based on defect chemistry, which involves the nucleation and growth of transition metal nanoparticles on the surface of the SWNTs, and the precipitation of the transition metal directly onto pristine nanotubes. Independent of the synthetic technique employed, the hybrid materials produced using all three methods were examined by TEM to determine that the metals had indeed been deposited and to determine that size of the metal particles. Additionally, these hybrid materials were analyzed for their use as catalysts in FT synthesis in comparison to more traditional catalysts.

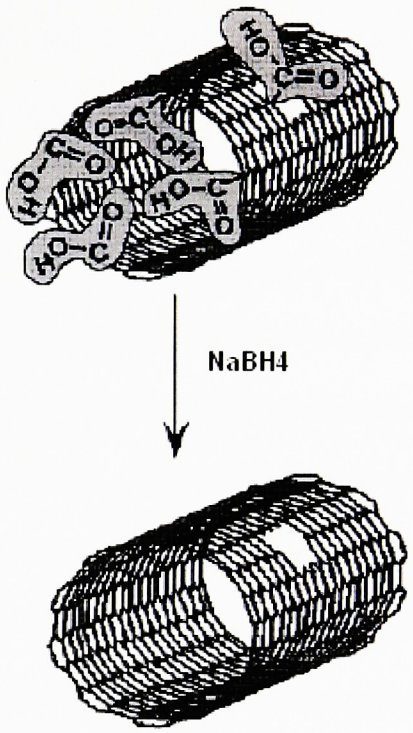

Figure 20: Schematic showing the reduction of oxidative on the surface of SWNTs. Functional groups such as –COOH, -CO, and –OH are generally introduced during purification processing, creating defect sites. Upon removal of these groups, pristine SWNTs are obtained.

2.0 Experimental

2.1 Synthesis of Single Wall Carbon Nanotubes via Laser Vaporization

The SWNT material used in the present study was synthesized at the National Renewable Energy Laboratory (NREL) by laser vaporization. A target was prepared by mixing 4 g of graphite (7-10 μm, 99%, Alfa Aesar) with 0.6 at.% cobalt (2.2-3 μm, 99.9%, Alfa Aesar) and 0.6 at.% nickel (1.6 μm, 99.8%, Alfa Aesar). The mixture was sealed in a rotating mixing apparatus and stirred for 48 - 96 hours to ensure homogeneity. The sample was then pressed using a Carver hydraulic pellet press (Model #3925) at 20,000 psi for 4 min. This yielded a disk with a 30 mm diameter and 5 mm thickness. The target was then loaded into a 1.48 m quartz reactor chamber tube with an inner diameter of 4.5 cm. Under normal conditions, the synthesis is carried out at 1200°C, and therefore an 80 cm region of the reactor chamber was placed within a furnace. Within the heated region of the reactor chamber, the target was held in place in the center using a quartz target holder. This ensured that one face of the pellet was facing the laser beam. With the target in place, the reactor chamber was then sealed and evacuated using a Welch vacuum pump (Model #8920) to a pressure of approximately 0.1 torr. This process was repeated a total of three times, and the subsequent backfill cycles were carried out using argon gas to minimize the amount of oxygen and moisture in the reactor chamber. The pressure was then filled to 500 torr with argon at a flow rate of 100 sccm using a mass flow controller. Through the aid of a series of computer controlled mirrors (GSI Lumonics SC 2000 scan controller), which were able to move at a rate of up to 20 Hz, the pulsed laser beam was directed across the surface of the target. A Pulsed Alexandrite laser (Single crystal $BeAl_2O_4$ doped with Cr^{3+}) produced 100 μs pulses with

a repetition rate of 10 Hz. Each pulse of the laser vaporized a small amount of material from the surface of the target creating a plume of vaporized material in front of the target. The vaporized material was then carried down the length of the quartz reactor tube by the flowing of argon gas. Eventually, the vaporized material exited the heated portion of the reactor chamber, and was deposited in the cold region of reactor chamber. The SWNT material was collected in the form of raw soot and is ready for further processing (Figure 21).

2.2 Purification of Single Wall Carbon Nanotubes

The following published procedure was used to purify all as produced materials. First, approximately 60 mg of raw soot and 120 mL of 2M nitric acid was placed into a flat bottom flask. The resultant was refluxed for 16.5 hr. at 230°C with stirring at 150 rpm. After cooling, the mixture was filtered in three 40 mL portions, such that each portion contained approximately 20 mg of SWNT material. Filtration was carried out using a filter disk filtration apparatus. The Zylon™ PTFE Membrane filters (47 mm, 5.0 μm, Pall Life Sciences) were impermeable to water, therefore they were first wetted with an appropriate organic solvent. Acetone was used in this case. Next, a 40 mL portion of the refluxed sample was poured over the filter. The sample was then washed with distilled water and 1M KOH, which serves to neutralize the nitric acid. Subsequently, the sample was washed with water and then acetone. This process was repeated twice before removing the filter and remaining sample and placing it in a 75°C oven (Single Wall Lab Oven, Blue M Electric Co.) for drying. Filtering the sample in this manner creates a SWNT *paper*. Once dry, the paper can easily be removed from the filter. Any remaining carbonaceous material was removed by burning the paper in air at 500°C in a Thermolyne

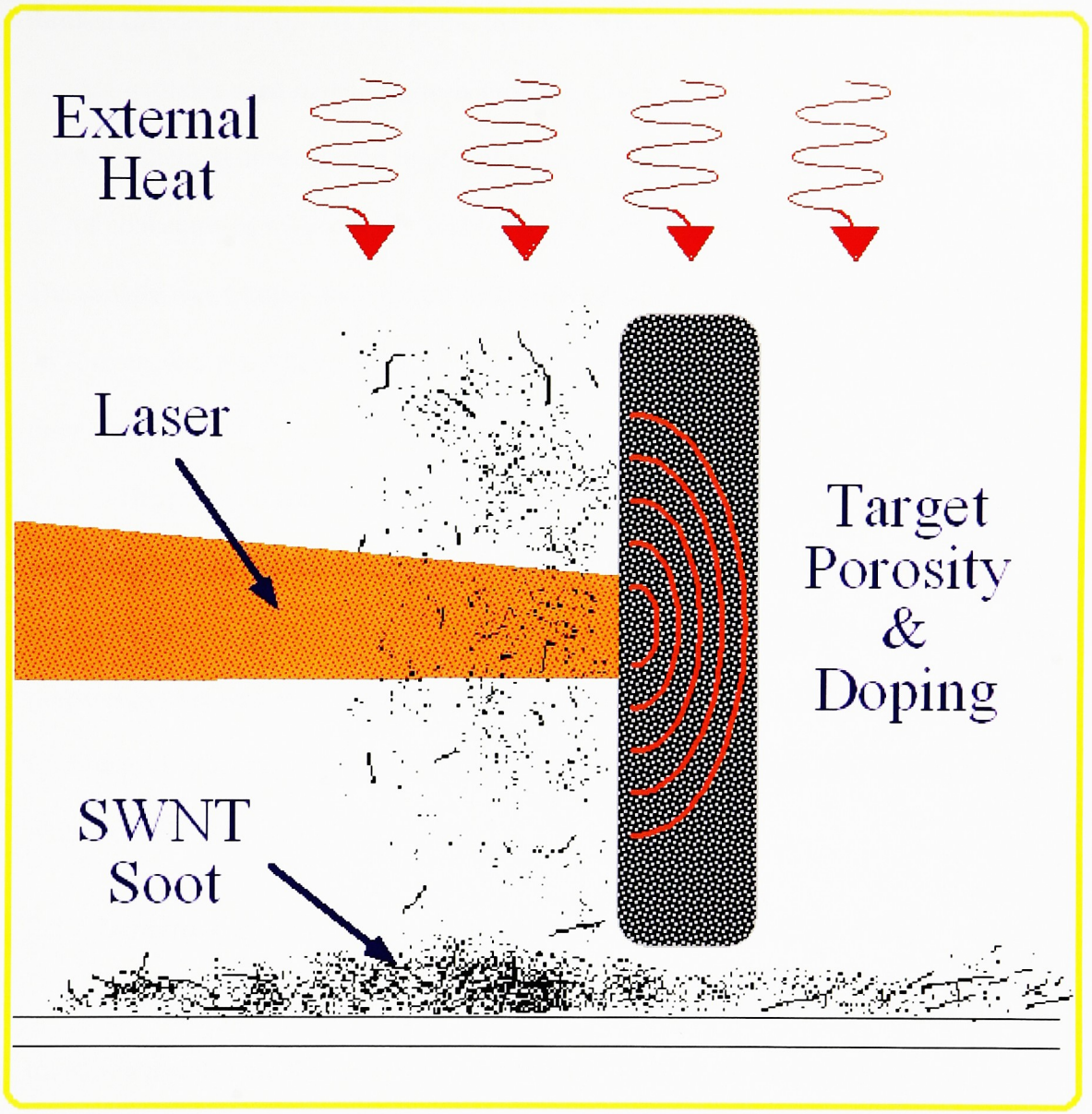

Figure 21: Close-up schematic of the target in the synthesis of SWNTs using the laser vaporization method, and the resulting raw soot that is produced.

furnace (Model #1300). At this point, the only persisting impurity was from the metal catalyst particles used in the synthesis process. The metal particles were removed by solvating them in concentrated hydrochloric acid. The SWNT paper was sonicated in 5 mL of concentrated hydrochloric acid for 5 min, and then diluted with distilled water. The sample was filtered and washed with copious amounts of distilled water, dried in a 75°C oven, and placed in a 500°C furnace for 1 min. This process was then repeated three times.

The purity of the resultant SWNT material was assessed using TEM. Analysis was performed by Mr. Kim Jones at NREL. A Philips 6M30 microscope with a 2.3 Å resolution was operated at 200 kV to obtain the images of the SWNT samples that were prepared by dry mounting approximately 0.2 mg of material on a 300 mesh Lacey Carbon grid. An energy dispersive X-ray spectrometer (EDS) was used in conjunction with the TEM for qualitative analysis.

2.3 Deposition of Various Transition Metals onto the Surface of the SWNTs

Three main incipient wetness techniques were examined for depositing various transition metals onto the surface of the SWNTs. These methods include: 1) the adsorption of metal from a metal salt solution onto the surface of the SWNTs followed by reduction with sodium borohydride, 2) the direct reduction of the SWNTs with Na-, K-, or Li-naphthalate followed by reaction with the metal salt solution, and 3) the pre-reduction of the SWNTs with sodium borohydride followed by the direct reduction technique described above. The transition metals to be studied are iron, nickel, cobalt, chromium, and rhodium.

2.3.1 Adsorption Followed by Sodium Borohydride Reduction

A 5 mg sample of purified SWNTs was first dispersed in 10 mL of ethanol (ACS Reagent Grade, ≥99.99%, 200 proof, absolute, Aldrich) via sonication for 30 min. An equal volume of DI water was then added and sonication continued for an additional 30 min. In the meantime, the amount of metal desired for deposition was determined such that the final mass of metal will be 15% of the total sample mass. The metal salt was then dissolved in a 1:1 ethanol:water solution. Upon complete dispersion of the SWNTs, the metal salt solution was added to the reaction flask containing the SWNTs, and the mixture was degassed with N_2 (g). Subsequently, 10 mL of a previously degassed 0.03M $NaBH_4$ (98%, Alfa Aesar) solution in ethanol was added. The mixture was allowed to stir at 150 rpm for 1 hr at temperatures ranging from 0, 25, and 50°C. A complete listing of reaction parameters and metals deposited can be found in Table (3). To isolate the final product, the sample was filtered using the same filter disk filtration apparatus as described for purification. The sample was washed using three alternating washes with ethanol and water and then allowed to dry at 25°C.

Table 3: Synthesis parameters for the deposition of various transition metals onto the surface of SWNTs via adsorption followed by $NaBH_4$ reduction.

Parameter	Specification
Temperature	0, 25, 50°C
Rxn. Time	1hr.
Rate of Stirring	150 rpm
Metal Salt Used for Deposition	Chromium(III) Nitrate Nonahydrate, 98.5%, Alfa Aesar
	Chromium(III) 2,4-Pentanedionate, 98%, Alfa Aesar
	Iron(III) 2,4-Pentanedionate, Alfa Aesar
	Rhodium(III) 2,4-Pentanedionate, Premion®, 99.99%, Alfa Aesar

2.3.2 *Direct Reduction of the SWNTs with Alkali Metals Followed by Metal Deposition*

Under inert atmosphere in a glovebox/bag filled with either He (g) or Ar (g), 5 mg of pristine SWNTs, 100 mg of naphthalene (98%, Aldrich), and alkali metal (Na, K, or Li) were added to a round bottom flask with a magnetic stir bar. The reaction flask was removed from the glovebox/bag and evacuated on a Schlenk line. The reaction flask was then backfilled with N_2 (house line, >99.99%). To the reaction flask, 100 mL of distilled THF (≥99.9%, Aldrich) was added. The mixture was sonicated for 30 min and then allowed to stir at 150 rpm for 12 hr. in order to ensure the reduction of the SWNTs. Upon completion of the reaction, the solution turned a green color indicating that no moisture was present and the SWNTs have been successfully reduced. The reduced SWNTs (Na-SWNTs) were transferred into a clean, evacuated 40 mL centrifuge tube using a cannula in order to remove the sample from any unreacted alkali metal. The reduced SWNTs were isolated by washing the sample repeatedly with additional aliquots of distilled THF. This was achieved by centrifuging the sample for 20 min at 2,500 rpm using a Marathon 8k Centrifuge (Fischer Scientific). The supernatant was removed using a cannula and an additional 40 mL of distilled THF was added. The sample was sonicated for 5 min to redisperse the Na-SWNTs. The entire process was repeated as many times as necessary to remove the naphthalate and the supernatant remains colorless.

In a separate centrifuge tube, the amount of metal desired for deposition was added. Again, enough metal salt was added such that the final mass of metal will be 15% of the total sample mass. The reaction flask was then degassed with N_2 and the metal dissolved in approximately 5 mL of distilled THF. The metal salt solution was added to the reaction flask containing the Na-SWNTs using a cannula. The metals examined using

Table 4: Synthesis parameters for the deposition of various transition metals onto the surface via direct reduction of the SWNTs with alkali metal followed by metal deposition.

Parameter	Specification
Alkali Metal Used for SWNT Reduction	Na, K, Li
Temperature	25°C
Rxn. Time	12hr.
Rate of Stirring	150 rpm
Inert Atmosphere	N_2 (g)
Metal Salt Used for Deposition	Chromium(III) 2,4-Pentanedionate, 98%, Alfa Aesar
	Chromium(III) Chloride, Anhydrous, Sublimed, 99%, Alfa Aesar
	Chromium(III) Nitrate Nonahydrate, 98.5%, Alfa Aesar
	Cobalt(II) 2,4-Pentanedionate, Alfa Aesar
	Iron(III) 2,4-Pentanedionate, Alfa Aesar
	Nickel(II) Bromide, Anhydrous, 99%
	Rhodium(I) Tris(triphenylphosphine) Chloride, 99.99%, Aldrich
	Rhodium(III) 2,4-Pentanedionate, Premion®, 99.99%, Alfa Aesar

this direct reduction technique can be found in Table (4). The mixture was sonicated for 30 min and then allowed to stir at 150 rpm for 24 hr at 25°C. To isolate the final product, the sample was spun down via centrifugation at 1,500 rpm, the supernatant removed, and the sample dried in flowing N_2 (g).

2.3.3 Deposition of Transition Metals onto the Surface of $NaBH_4$ Reduced SWNTs Followed by Direct Reduction with Alkali Metal

This technique is very much like the one described in section 2.3.2 with the exception that the purified SWNTs were first treated with $NaBH_4$. This was done by first dispersing a sample of purified SWNTs in a 1:1 ethanol:water mix via sonication, and then degassing the sample with N_2. To this sample, 10 mL of a 0.03M $NaBH_4$ solution was added. The sample was stirred at 150 rpm at 25°C for 1hr, was filtered and washed with ethanol and water, and was then air dried at 25°C.

Sodium metal and naphthalene were then added to the sample of SWNTs in a glovebag under Ar atmosphere. To that, approximately 100 mL of distilled THF was added and the sample was sonicated for 30 min to redisperse the SWNTs. The sample was allowed to stir at 150 rpm for 12 hr, and the Na-SWNTs were washed and isolated in the same manner as described in section 2.3.2. The metal salt solution was then prepared such that 15% of the final sample mass would be from the transition metal added. The transition metals used were the same as those used in the synthesis via the adsorption technique (Table 2). The transition metal of choice was dissolved in distilled THF and degassed with N_2. This metal salt solution was then transferred into the reaction flask containing the reduced SWNTs. The sample was stirred at 150 rpm for 12 hr at 25°C. To isolate the final product, the sample was spun down via centrifugation at 1,500 rpm, the supernatant removed, and the sample dried in flowing N_2 (g).

2.4 Characterization of the Transition Metal – Carbon Nanotube Hybrid Materials

2.4.1 Transmission Electron Microscopy

Transmission Electron Microscopy (TEM) was used to analyze the transition metal – carbon nanotube hybrid materials, much in the same manner as described previously for the examination of the purified SWNTs. Again, the assistance of Mr. Kim Jones at NREL was enlisted for the analysis. The resulting TEM images allowed for the visualization that the transition metal had been deposited, and also provided a means of determining the particle size and distribution.

2.4.2 *Temperature Programmed Desorption Experiments Used to Analyze for Hydrogen Storage and Fischer-Tropsch Synthesis*

Several Temperature Programmed Desorption (TPD) experiments were carried out to test the newly synthesized transition metal-carbon nanotube composite materials for both hydrogen storage and for Fischer-Tropsch (FT) synthesis. The sample was heated slowly over a given period of time and the headspace gas containing any desorbed molecules were monitored via mass spectrometry. Analysis was performed using a TPD apparatus like the one found in Figure 22.

The H_2 storage and FT experiments required only approximately 1 mg of sample to be loaded into a platinum foil packet and sealed. The Pt packet is then loaded into a thin quartz tube and tightened in place on the external port of the TPD apparatus. Due to the isolation valve and VCR connections, use of the external TPD port made sample analysis simple and rapid. All samples were analyzed twice for H_2 storage, once by loading the sample into the Pt package in a glovebox under inert He atmosphere, and the other by exposing the sample to air. The samples for the Fischer-Tropsch experiments were only loaded in air. Once affixed to the TPD apparatus, the chamber was evacuated down to 0.4 torr by using a GE 60 Hz roughing pump (Model #5KL36LN83X). A Pfelzer turbo pump was used to further evacuate the chamber down to 0.01 torr.

Upon complete evacuation of the chamber, the sample was heated to degas any adsorbed gaseous molecules on the transition metal-carbon nanotube hybrid material. The quartz tube containing the sample was fitted with a thermal couple and placed inside a programmable furnace. The sample was heated from 25°C to 250, 500, or 700°C over a 20 min period, and the headspace gas was monitored via mass spectrometry and displayed real-time on a computer. A HAL mass spectrometer was used for the analysis,

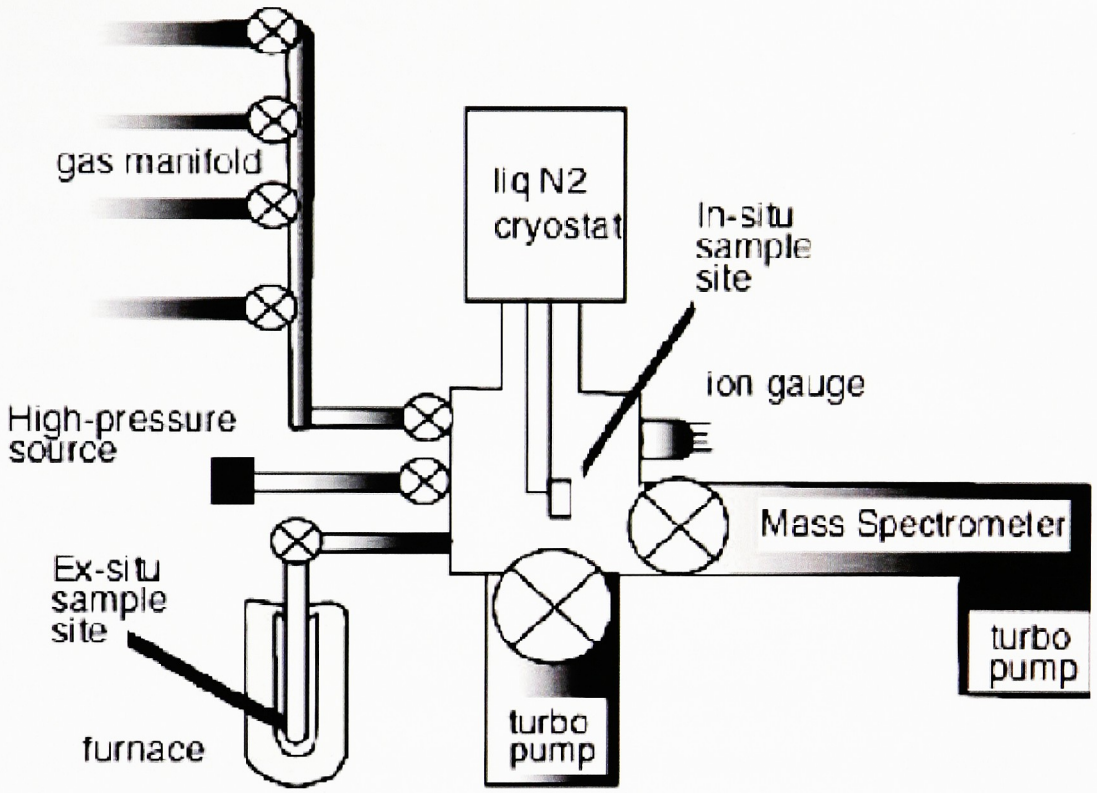

Figure 22: Schematic of the TPD apparatus used in the examination of the transition metal – carbon nanotube hybrid materials for H_2 storage and FT synthesis.

with a 3 sec time between scan. After degassing the sample, it was ready to be doped with the appropriate reagents for either H_2 storage or FT synthesis.

2.4.2.1 H_2 Storage

In order to test for H_2 storage, the degassed sample was dosed to 550 torr with H_2 for 10 min at 25°C. The reaction was quenched by submerging the quartz tube in liquid N_2 until the temperature reaches -196°C. The liquid N_2 was removed and the sample was allowed to warm to 25°C, all the while the headspace gas was being monitored by mass spectrometry. The furnace was again applied around the outside of the quartz tube and the sample was heated from 25°C to 500°C over a 10 min period while again monitoring headspace gas by mass spectrometry.

2.4.2.2 Fischer-Tropsch Synthesis

FT synthesis involves the hydrogenation of carbon monoxide to various hydrocarbons over a transition metal catalyst. In order to perform the synthesis over the transition metal-carbon nanotube hybrid material, the degassed sample was dosed with ^{13}CO to 100 torr and then H_2 to 500 torr. The reaction continued for 1 hr at 25°C. Again the reaction was quenched with liquid N_2 until the temperature reached -196°C. The sample was warmed to 25°C and was then heated with a furnace to 500°C while monitoring the headspace gas via mass spectrometry for the conversion to hydrocarbons.

3.0 Results and Discussion

3.1 Characterization of Purified SWNTs

The SWNTs used in this thesis research were synthesized at NREL via laser vaporization. Upon receipt of the as-produced SWNT raw soot, the material was purified according the aforementioned published procedure.[10,11] TEM analysis was utilized to qualitatively ascertain the purity of the nanotube material at various stages in the purification process. Although only a small portion of the overall sample can be viewed at a given time, TEM analysis provides valid information as to the morphology of the sample. A TEM image of the raw soot demonstrates the presence of the Ni/Co impurities in the SWNT bundles, as well as the carbonaceous impurities such as amorphous carbon and smaller-sized fullerenes. These impurities are seen in the TEM as small, dark spots intermittently scattered throughout the SWNT material (Figure 23A). It is necessary to remove these impurities prior to catalyst deposition. This is essential because the carbonaceous and metal catalyst impurities may interfere with many SWNT properties that are desired for various applications. In the present study impurities would make distinguishing a Ni/Co catalyst particle from an intentionally deposited transition metal difficult. Additionally, Ni and Co were both metals that were used in the three proposed synthetic techniques for the production of FT catalysts, which would complicate matters further. If these Ni/Co particles remain from the laser synthesis, it will be difficult to determine the extent of their contribution to any catalytic activity of interest.

The as produced SWNT sample was first treated by HNO_3 reflux, which oxidizes and redistributes the carbonaceous impurities evenly over the entire sample and

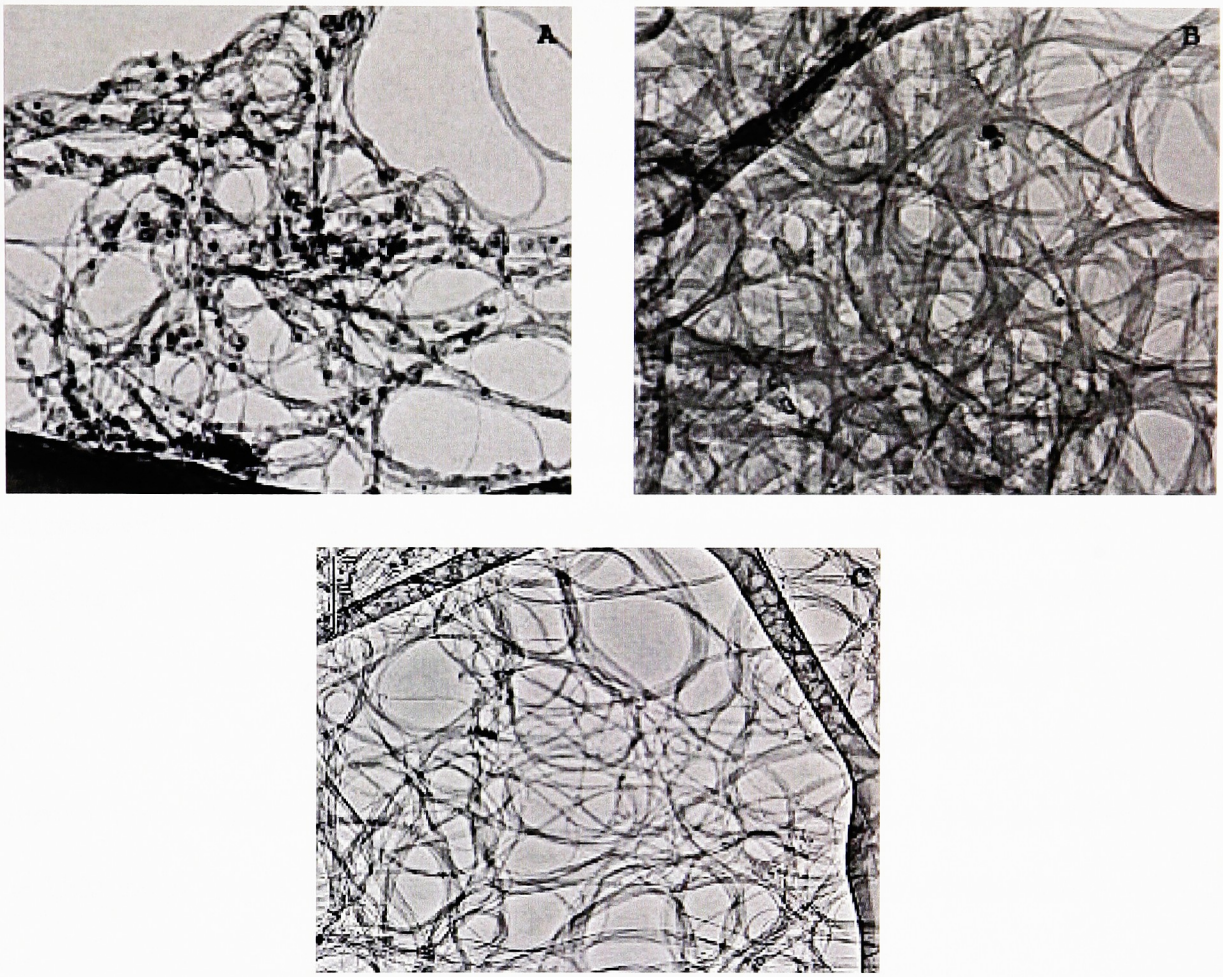

Figure 23: Transmission electron micrographs of: (A) as produced raw SWNT material, (B) SWNT material after HNO_3 reflux and 500°C air oxidation, and (C) purified SWNT material achieved through subsequent HCl washes and air oxidations. Carbonaceous and metal catalyst impurities are seen as small, dark spots among the SWNT bundles.

exposes/dissolves the majority of the metal catalyst particles. The 500°C air oxidation then removes the majority of the carbonaceous particles (Figure 23B). The most dramatic change in the morphology of the SWNT sample is seen at this point in a comparison of the raw soot to the refluxed material. This is mostly because >98% w/w impurities are removed during the initial purification steps as reported by Dillon et al.[10] Complete removal of the residual metal catalyst particles is achieved only after the sample has been repeatedly washed with concentrated hydrochloric acid, HCl, followed by base neutralization and subsequent 500°C air oxidations (Figure 23C). According to Hauge et al, the HNO_3 reflux combined with air oxidation and washes with HCl yields materials with >99% w/w SWNTs.[11] Although TEM analysis provides an image of only a portion of the SWNT sample from which inferences can be made as to the purity of the overall sample, TGA was also employed to confirm the purity of the sample. Using this analytical tool, it was determined that the only remaining impurities were from residual silicon introduced from the quartz tube during the SWNT synthesis. As can be seen from the TEM images provided, the samples used in this thesis research were of high purity.

3.2 Characterization of the Transition Metal – Carbon Nanotube Hybrid Material

3.2.1 Metal Deposition via the Adsorption Technique

Through the use of the adsorption technique, the isolation of the transition metal – carbon nanotube hybrid material was possible. This was achieved by immersing the purified SWNTs in a metal salt solution and fully reducing the transition metal with the aid of a $NaBH_4$ reducing solution. Upon introducing the SWNTs into the metal salt solution, the transition metal was physisorbed onto the surface of the SWNTs at the position defect sites, which may exist as oxygen containing substituent groups or kinks.

Defects are typically predominant at the ends of the nanotubes where the end cap or Ni/Co catalyst particles from the laser synthesis have been removed. However, various other defects can exist along the length of the nanotube, which are introduced either during the laser synthesis of the SWNTs or during their purification (Figure 24). The adsorption onto the surface of the SWNTs allows for the nucleation of the transition metal, and is done prior to adding the $NaBH_4$ reducing solution in order to avoid agglomeration of the metal nanoparticles. After adding the $NaBH_4$, the remaining metal in solution was reduced and the growth of the metal nanoparticle occurred. TEM analysis was again employed to characterize the synthesis of the hybrid materials. This provided a means to assess if the transition metals had in fact been deposited, as well as a tool to determine the size and distribution of the particles throughout the sample. The adsorption technique was found to produce hybrid materials with well dispersed transition metal particles that had diameters between 30 – 50 nm (Figure 25). Additionally, it was important to note that the Fe-, Ni-, Co-, Cr- and Rh-SWNT samples all behaved in similar fashion and TEM images were virtually identical in terms of the size and distribution of the metal particles.

Although metal deposition had been achieved, the metal particle size was considerably large for use as FT catalysts, and the metal particles were not of uniform diameter distribution, having greater than 75% variability. Ideally, the deposited metal particle size would be smaller than 10 nm, as it has been demonstrated that the smaller the catalyst particle size, the greater the catalytic activity in FT synthesis.[18] In an effort to control particle size, the synthesis was carried out over a range of concentrations and temperatures. TEM analysis of these samples demonstrated that no significant difference

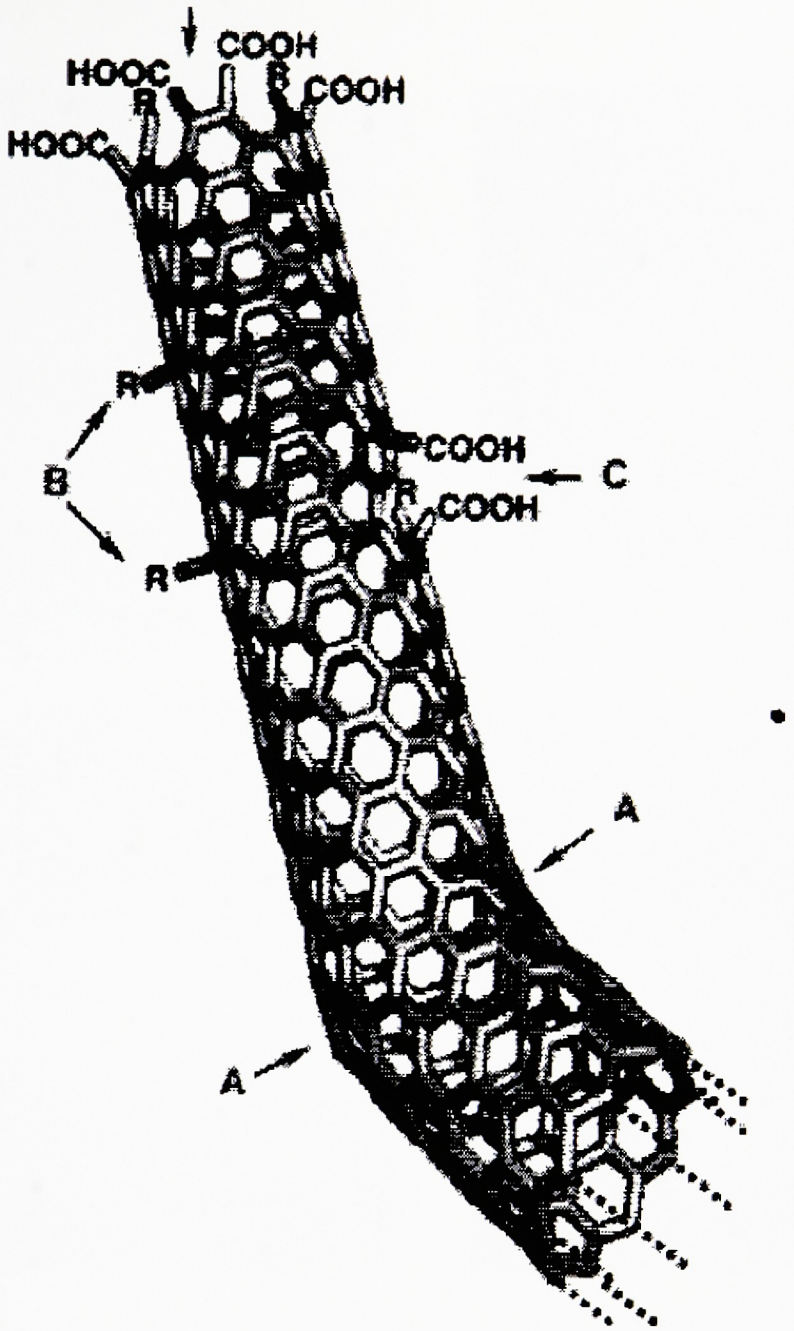

Figure 24: Schematic of an individual SWNT, which shows that the carbonaceous and metal catalyst impurities have been removed, but various defects and kinks remain. In this case carboxylic acid groups are prevalent at the defect sites, however, carbonyl and hydroxyl groups may be present as well. It is at these oxidized defect sites, and possibly kinked sites, that the transition metal adsorption appears to takes place.[59]

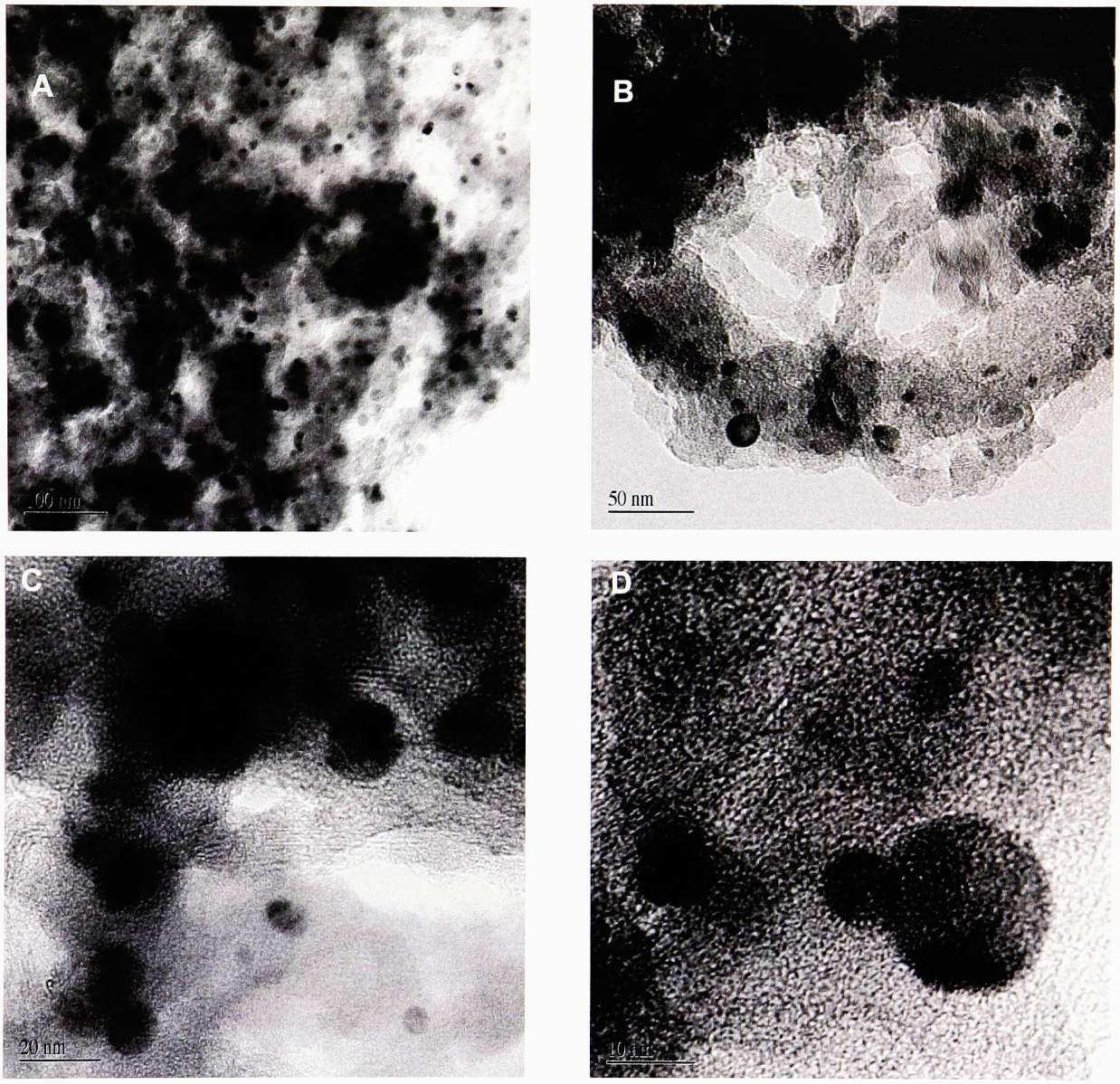

Figure 25: Transmission electron micrographs of a Cr-SWNT sample prepared from Chromium(III) Nitrate just that the final mass of metal would be 15% of the final sample mass. Images are provided in increasing resolution from (A) 100 nm, (B) 50 nm, (C) 20 nm, and (D) 10 nm. As is seen the Cr particle size varies on average between 10 – 50 nm.

in particle size distribution was observed for the various samples. As a result, this synthetic method was not investigated further since it could not be tailored to produce <10 nm metal catalyst nanoparticles for the production of FT catalysts. Additionally, the major disadvantage of the adsorption technique was that reproducible results were difficult to obtain. The variation between SWNT samples and the ability to form defect sites at the surface, may be related to the quality and size of the SWNTs. SWNTs with fewer inherent defects and smaller diameters will likely be more resilient to damage during the relatively harsh treatment during purification, and therefore fewer defects would be expected. Since there is no way to standardize the formation of defects on the SWNTs the adsorption method will not provide a reliable method for depositing transition metals along the surface of the SWNTs.

3.2.2 Metal Deposition via the Direct Reduction Technique

Unlike the adsorption technique, the direct reduction synthesis of transition metal – carbon nanotube hybrid materials was achieved by the spontaneous deposition of the transition metal onto the surface of the SWNTs without the aid of a reducing agent. The spontaneity of these reactions is possible by reducing the purified SWNT material with sodium, potassium, or lithium naphthalate prior to immersion of the reduced SWNTs into the transition metal salt solution. The reduction of the SWNTs changes their E_{red} to values close to those of the alkali metal used, and causes them to be incredibly reactive.[71] As such, the value of E_{red} for the Na-, K-, and Li-reduced SWNTs would be approximately -2.71, -2.93, and -3.04 V vs. NHE, respectively. Upon immersing the reduced SWNTs into the metal salt solution, the transition metals appear to spontaneously nucleate at defect sites and kinks on the surface of the nanotubes, at which

time the autocatalytic growth of larger metal nanoparticles occurs. In this case, TEM analysis was again employed for the characterization of the newly synthesized hybrid materials. A comparison was made between materials synthesized from Na-, K-, and Li-SWNTs, and it was determined that all three reduced species of nanotube produced indistinguishable forms of transition metal – carbon nanotube hybrid materials. These results were independent of the transition metal salt solution used as well (Figure 26).

The synthesis of the hybrid materials by direct reduction with Na-, K-, and Li-reduced SWNTs yielded metal nanoparticles that ranged in size on average between 20 nm upwards of >200 nm, and was independent of the transition metal used in the deposition (Figure 27). Again, the goal of the present study was to control particles size such that particles with diameters smaller than 10 nm could be achieved. The large particles were postulated to be the result of nucleation at low energy defect sites, and particle growth continued where this first precipitation of the metals occurred. In an effort to control particles size, the concentration of metal and reaction time allowed for the transition metal deposition was examined. A series of Rh-SWNT samples were prepared on Na-reduced SWNTs using Chlorotris(triphenylphosphine)rhodium(I), or Wilkinson's Catalyst (WC), as the transition metal source. The reaction between the Na-reduced SWNTs and the WC was carried out for a total of 144 hr., however, aliquots were quenched and prepared for analysis at 1, 16, 24, 48, 72, and 144 hr. As can be seen from the TEM images (Figure 28), after 1 hr. of reaction time, the rhodium particles were between 20 – 50 nm in diameter, but were not very well dispersed and only a few nucleation spots were evident. At 16 hr. into the reaction, it was evident that there was significantly more metal present, which was more uniformly distributed throughout the

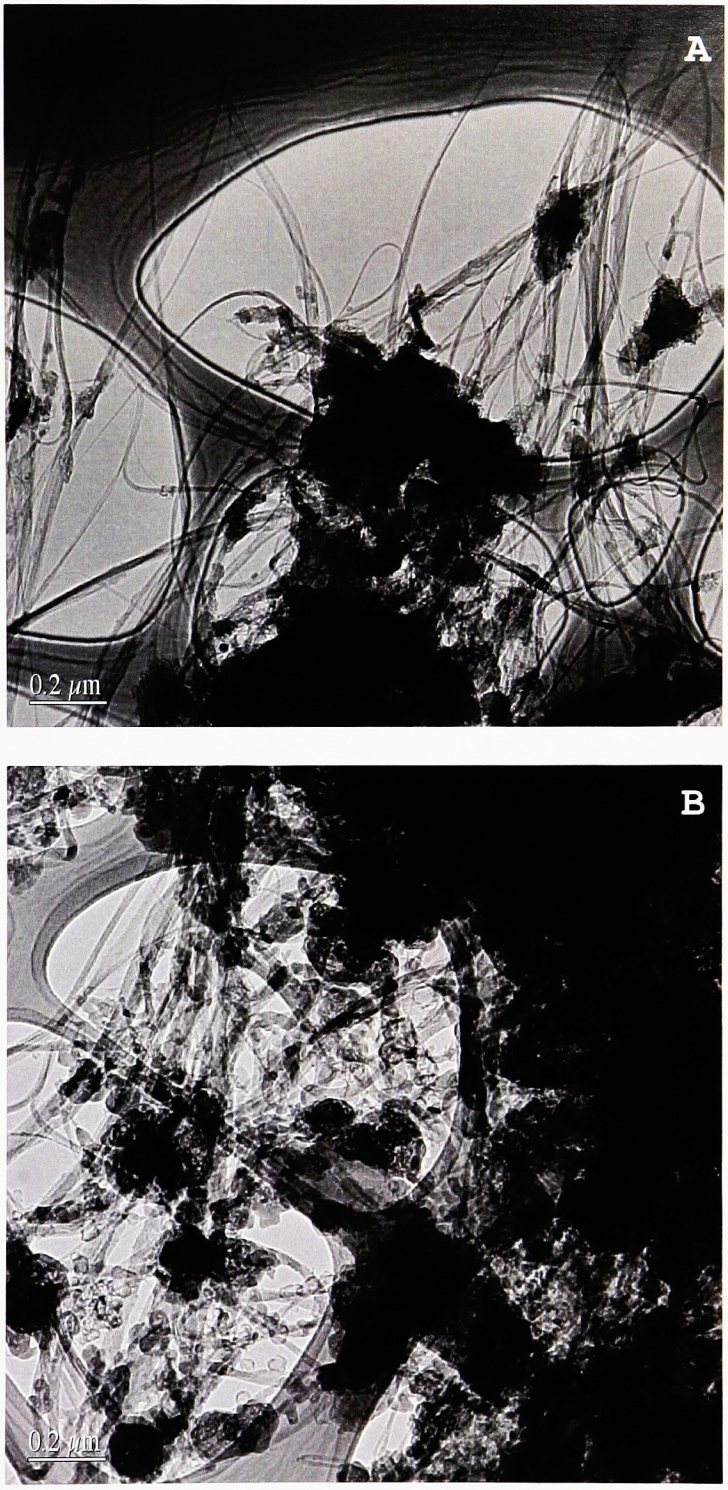

Figure 26: Transmission electron micrographs of Cr-SWNTs prepared from (A) Na-reduced SWNTs and (B) Li-reduced SWNTs. Both images are scaled to 0.2μm. As can be seen, both samples show significant metal deposition with relatively the same particle size distribution.

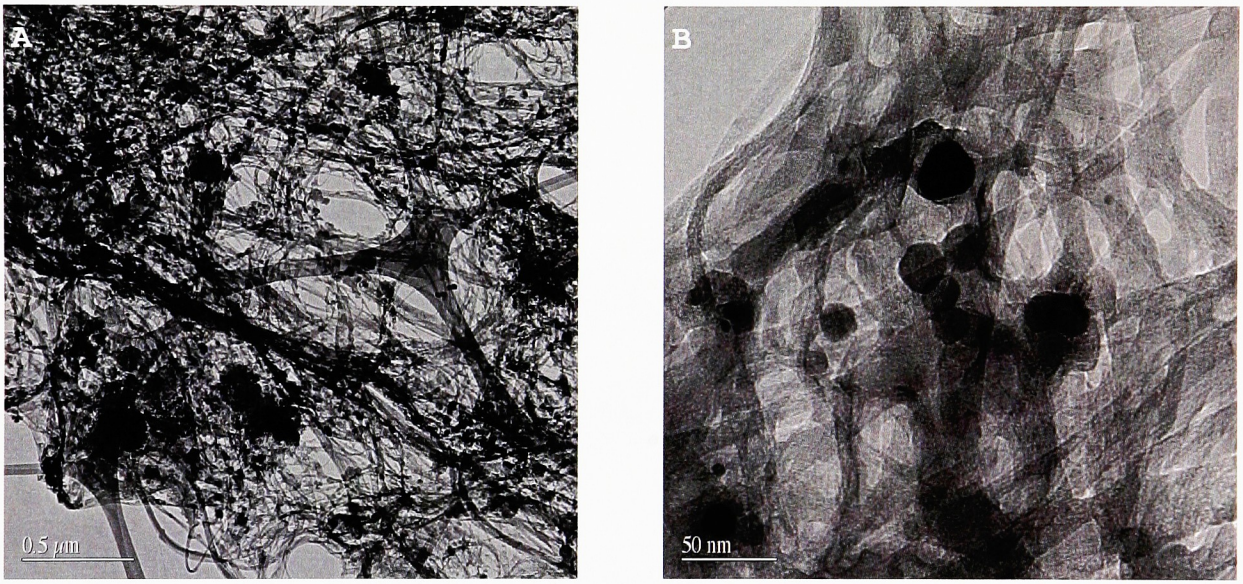

Figure 27: Rh-SWNTs prepared by the direct reduction of Chlorotris(triphenylphosphine)rhodium(I) onto Na-reduced SWNTs. The diameter of the metal particles ranges from approximately 20 nm to 200 nm.

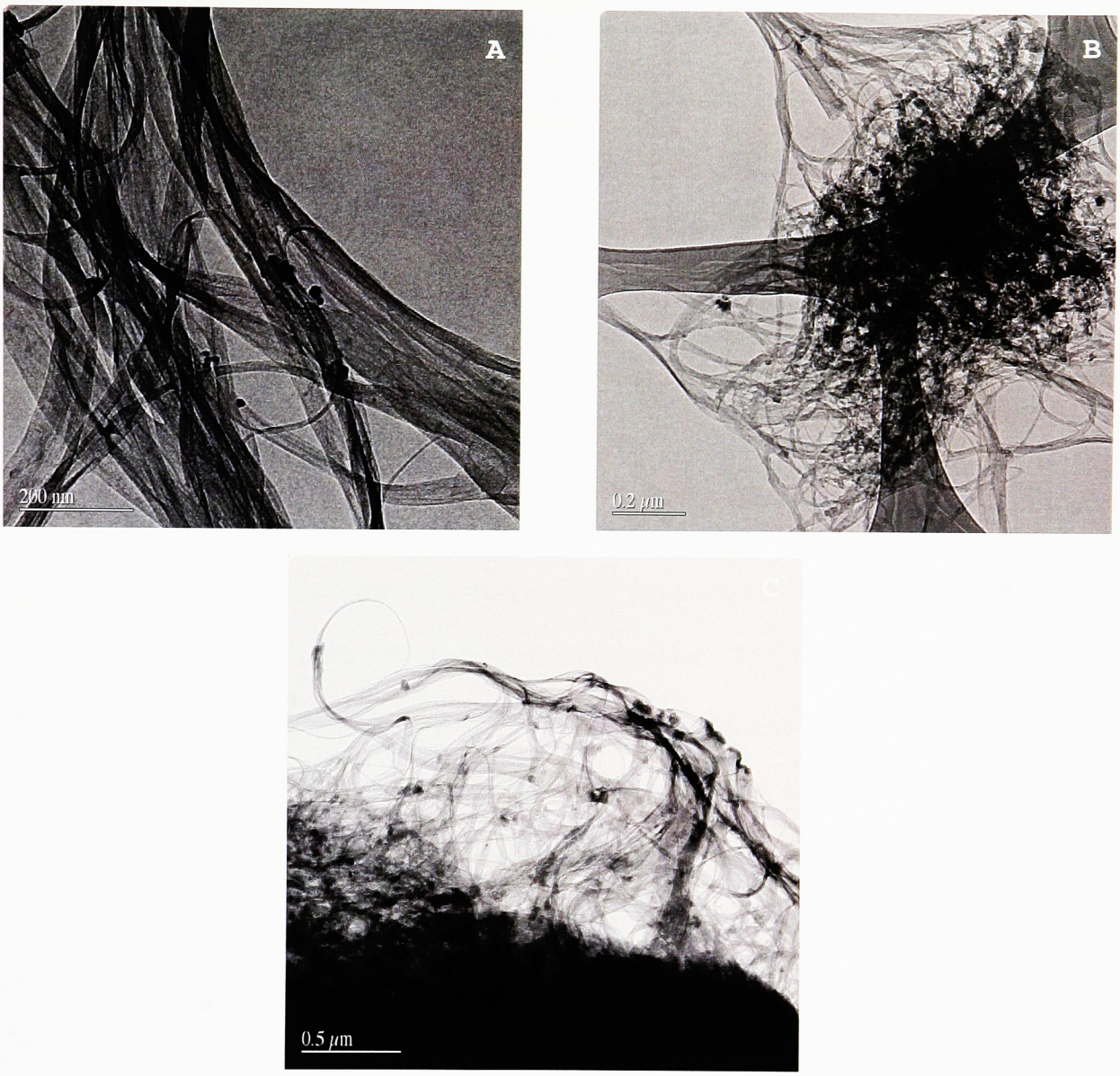

Figure 28: Transmission electron micrographs of Rh-SWNTs prepared by the direct reduction of Chlorotris(triphenylphosphine)rhodium(I) onto Na-reduced SWNTs for (A) 1 hour, (B) 16 hours, and (C) 144 hours.

sample. At this point the rhodium particles seemed to be equally large in size as those observed with the previous sample. The subsequent samples through to the 144 hr. sample were examined and it appeared that no further nucleation had occurred past 16hr., yet the particle sizes were slightly increased. This kinetic study showed that the nucleation of the metal was complete in the first 16 hr. of reaction, and at reaction times longer than 16hr. no new nucleation occurred and the metal particles only continued to grow.

3.2.3 Metal Deposition via Pre-reduction of the SWNT Surface

In this third synthesis technique, aspects of both the adsorption and direct reduction techniques were combined in order to achieve the deposition of various transition metals onto the surface of the SWNTs. The purified SWNT material was first pretreated with a $NaBH_4$ reducing solution, but in the absence of a transition metal salt solution. This pretreatment was expected to remove most oxidative groups, such as –COOH, -CO, or –OH groups, present on the SWNTs that may have been introduced during the purification process from the HNO_3 reflux. The resultant material was expected to be closer to oxygen-free, pristine-like SWNTs, which were depicted previously in the schematic provided in Figure 20. After obtaining the oxygen-free, pristine-like SWNT sample, a slightly different direct reduction technique was employed for the deposition of the transition metal. The SWNTs were further reduced to a negatively charged free-radical system (Figure 29) with sodium naphthalate, isolated, and then immersed into the metal salt solution. The use of pristine-like SWNTs eliminated the reliance on defect sites and kinks for the nucleation and growth of transition metal particles. Instead, the deposition on pristine-like SWNTs is believed to occur via

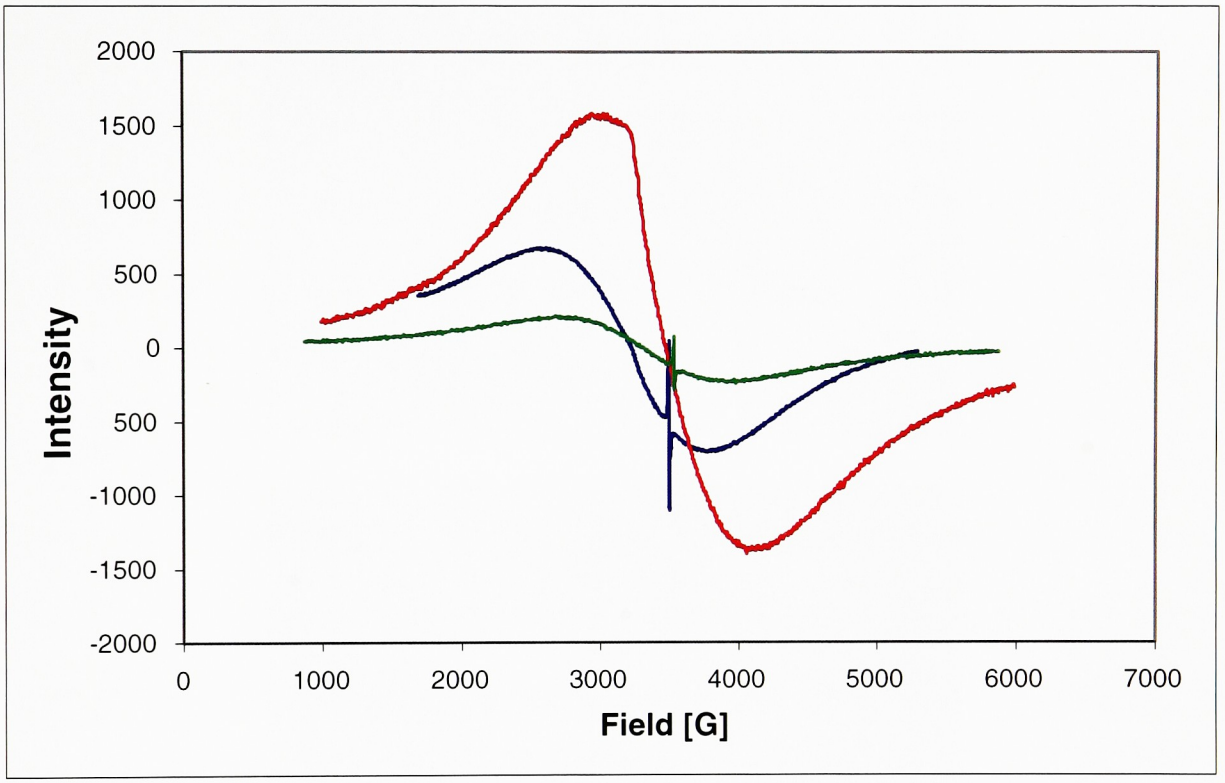

Figure 29: EPR spectrum that demonstrates the free-radical behavior of the Na-SWNTs. The sharp peak is most likely an organic radical, namely Na-Naphthalate.

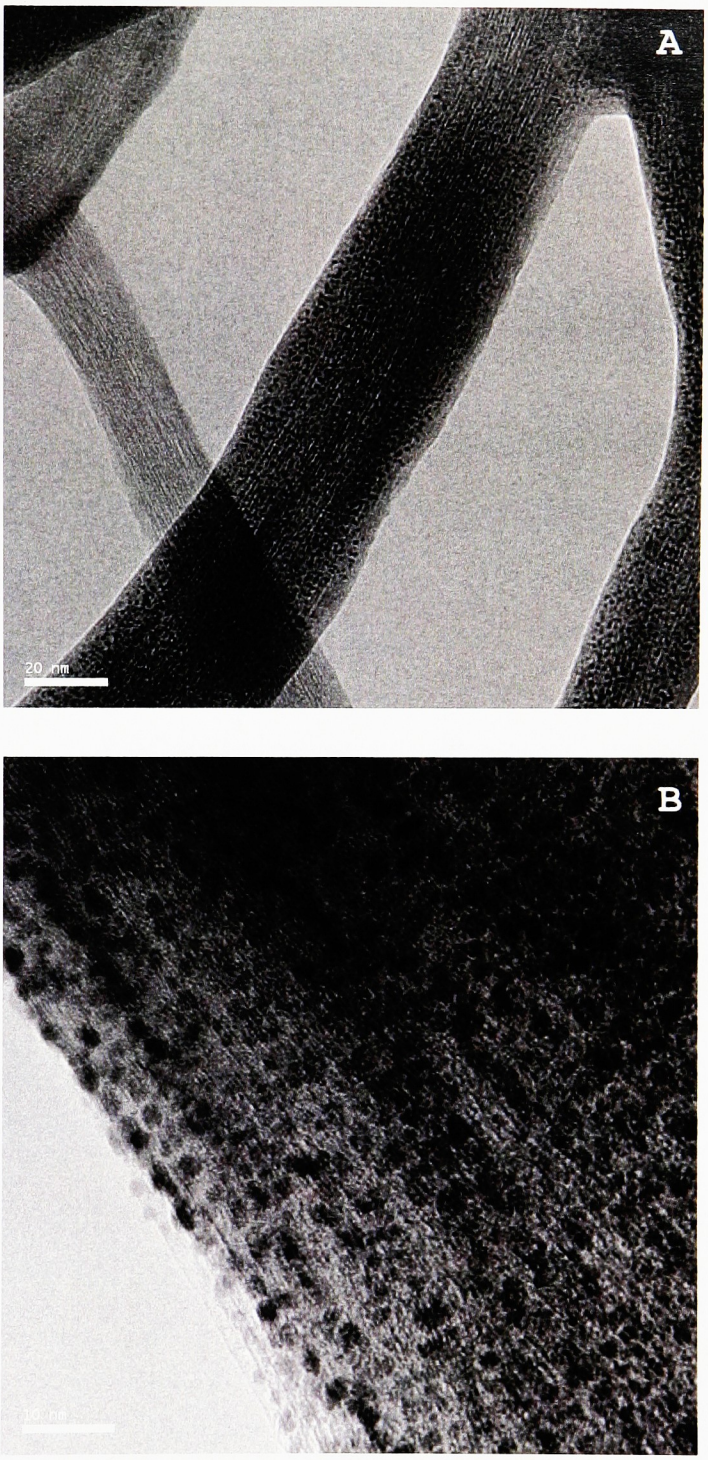

Figure 30: Transmission electron micrograph of Rh-SWNTs prepared by prereducing the purified SWNTs with $NaBH_4$ to yield pristine SWNTs, followed by the direct reduction of the metal onto Na-reduced SWNTs from a Rhodium(III) 2,4-Pentanedionate salt solution. (A) is scaled to 20nm whereas (B) is a higher resolution images scaled to 10nm.

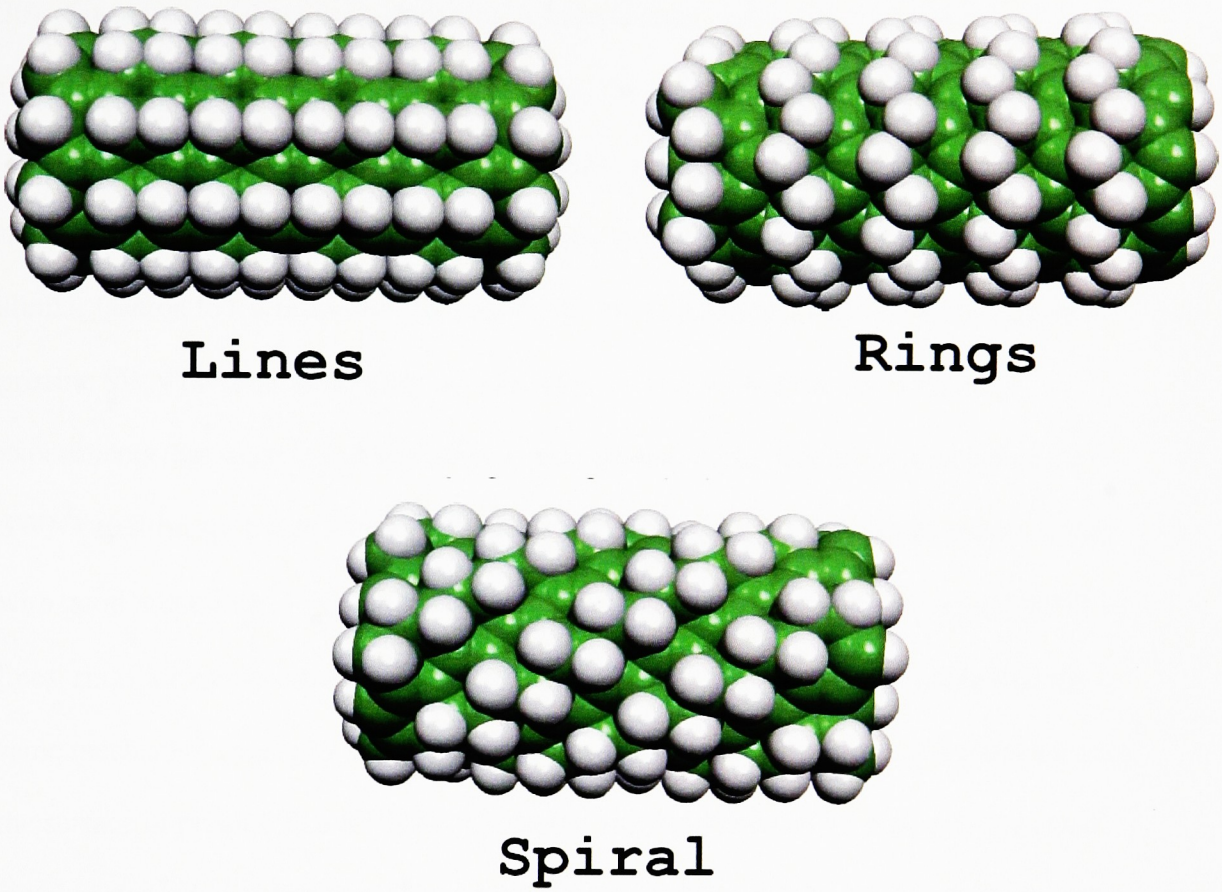

Figure 31: Various models for 50% H_2 coverage on SWNTs, including lines, rings, and spiral.[72]

chemical precipitation upon exposure of the Na-reduced SWNTs to the metal salt solution. TEM analysis demonstrated that evenly dispersed rhodium nanoparticles with <2 nm diameters could reproducibly be deposited using this synthetic technique (Figure 30). Since the metal catalyst deposition is independent of the defect chemistry utilized in the adsorption and direct reduction techniques, the metal particles can be deposited without the restriction of needing to produce multiple nucleation sites. It is believed that the point attachment of the Rh catalyst particles using this technique may proceed in similar fashion to the proposed mechanism for the attachment of atomic hydrogen on pristine SWNTs. Bauschlicher et al conducted a series of AM1 level of theory experiments that suggest that with 50% coverage, half of the C atoms bulge out of the SWNT to form sp^3 hybridized C-H bonds, while the remaining C-C bonds remain intact with good π bonding.[72] Here it was shown that the hydrogen may attach to the SWNT in lines, rings, or spirals around the nanotube (Figure 31). As such, it is possible that the same mechanistic pathway is employed for the attachment of metal catalyst particles onto the surface of pristine-like SWNTs. Currently, the deposition of <2 nm, well dispersed metal particles has only been achieved for the Rh-SWNT sample. TEM data showed that attempts to synthesize Fe- and Cr-SWNTs using this technique only yielded large metal particles as were observed with both the adsorption and direct reduction techniques, however further work in this area is underway.

3.3 Hydrogen Storage in the Transition Metal – Carbon Nanotube Hybrid Materials

All newly synthesized hybrid materials were examined through a series of TPD experiments for H_2 storage. This was done by loading a 1 mg portion of each sample into a quartz tube and affixing it to the external port on the TPD apparatus. The external port

was preferentially used so that the samples could be loaded under inert He atmosphere. Using a series of VCR connections and sample isolation valves, each sample was easily loaded into the quartz tube in the glovebox. After evacuating the sample chamber, the sample was heated to a specified temperature at a constant rate to remove any adsorbed gaseous molecules from the surface of the SWNT samples. The headspace gas, which contained any desorbed molecules, was monitored by mass spectrometry for compounds between 0 – 300 amu, and each compound was tracked in real-time and displayed on a computer display. The sample was then dosed with H_2 to 500 torr by opening the appropriate valve on the gas manifold, and was then allowed to react for 10 min at 25°C. The sample was then heated again to analyze the sample for H_2 storage uptake. The TPD was calibrated to determine the H_2 wt. % desorbed from the sample by integrating the area under the curve. The first materials to be analyzed in this manner were the reduced SWNTs, which were used as precursors in the direct reduction synthesis technique. Given the reactive nature of the Na-, K-, and Li-reduced SWNTs, these materials were expected to be very sensitive to moisture and were therefore loaded onto the TPD apparatus in a glovebox under inert He atmosphere. All three samples were degassed to 700°C over a 20 min period. The mass spectra indicated the presence of a significant amount of water in the K- and Li-reduced SWNT samples (Figures 32 and 33, respectively). This was unexpected due to the fact that these alkali metals should theoretically have decomposed in the

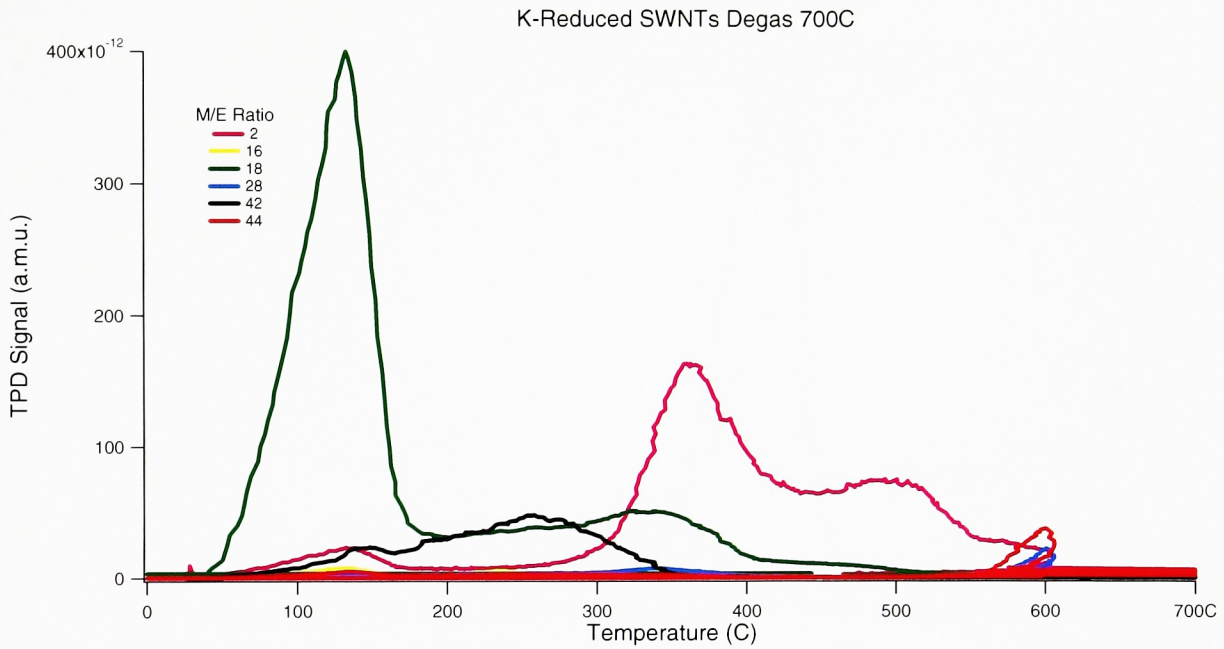

Figure 32: Degas spectrum of the K-reduced SWNTs obtained by TPD. The sample was loaded onto the TPD apparatus under inert He atmosphere, and degassed from 25 – 700°C over the course of 20 min.

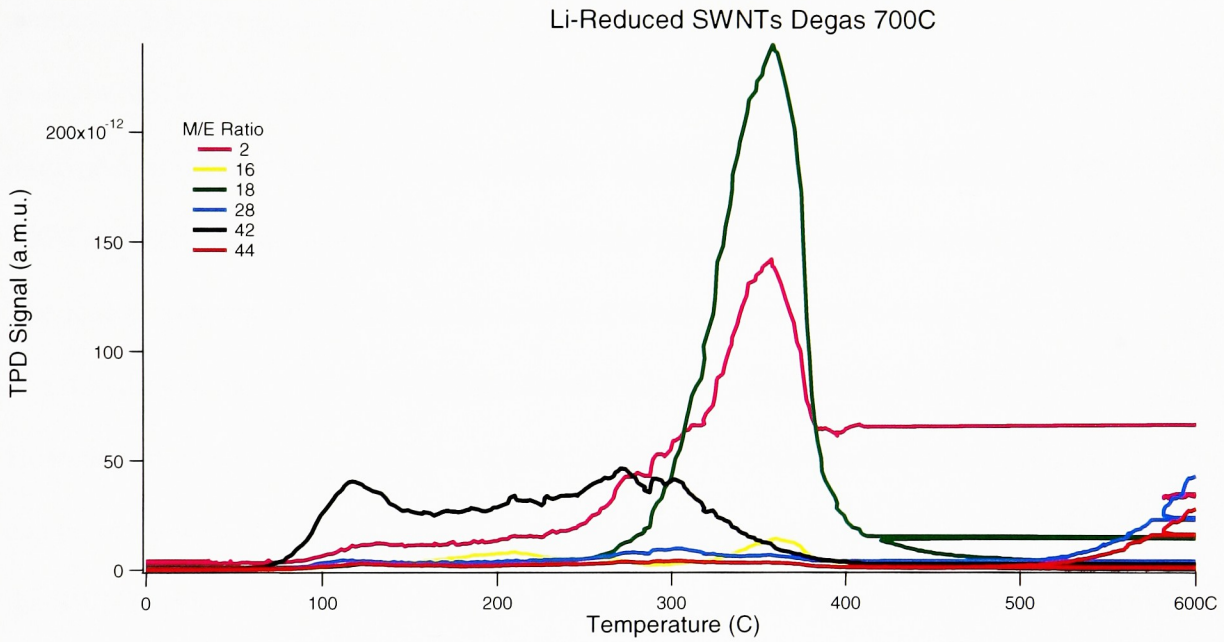

Figure 33: Degas spectrum of the Li-reduced SWNTs obtained by TPD. The sample was loaded onto the TPD apparatus under inert He atmosphere, and degassed from 25 – 700°C over the course of 20 min.

presence of water. It is plausible that the water may have been stored in the interstitial sites in the SWNT bundles, and was only released upon heating during the TPD experiments. Interestingly, this was not observed with the Na-reduced SWNTs, rather the mass spectra of this sample showed approximately 4 wt% H_2 being irreversibly desorbed from the sample between 200 – 600°C. The Na-reduced SWNTs that were synthesized by pre-reducing the SWNT surface with $NaBH_4$, showed two distinct H_2 peaks in the degas spectra (Figure 34). As seen from the mass spectral data, there was a large peak at temperatures greater than 450°C. Additionally, the peak at approximately 300°C is likely due to some type of non-traditional H_2 bonding, such as a Kubas complex. The Kubas complex, which was discovered in 1984 by Kubas, involves the coordination of a dihydrogen molecule to a transition metal while still maintaining the H-H bond.[74] However, more careful examination of these materials is needed before this conclusion can be made with complete certainty. When the oxidative groups are not removed from the SWNTs prior to performing the Na-reduction, then the 300°C peak disappears (Figure 35). This was confirmed using Na-reduced activated carbon, which was prepared using the same protocols as for the SWNTs. When the activated carbon was heated to remove the oxidative groups, the presence of non-traditional H_2 peak were observed, otherwise only the peak at temperatures in excess of 450°C were observed (Figure 36 and 37).

A series of isotope labeling experiments were conducted using deuterium to determine the possible mechanism for the hydrogenation of the Na-SWNTs. It was determined that the Na-SWNTs exist as a radical system that mimics the known butyl-lithium reactions in THF.[73] After reduction with the sodium naphthalate, the SWNTs are basic and this leads to hydrogenation of the Na-SWNTs (Figure 38). Once the SWNTs

are dianions, the adjacent arene rings in the nanotubes appear to react with some of the ethylene (C_2H_4), which was produced during the hydrogenation of the Na-SWNTs.[75] The presence of ethylene was confirmed by mass spectroscopy. Ultimately, the mass spectroscopy data obtained from these deuterium labeling experiments confirmed that the H_2 observed desorbing from the Na-SWNT materials was originating from the THF. (Figure 39). These peaks result from the presence of both SWNT-H and Na-SWNT-$(H)_{n-1}(CH2CH2)_{n-1}$. Additionally, it was deduced that the K- and Li-reduced SWNTs do not behave in similar fashion to the Na-reduced SWNTs due to the fact that they are more highly reactive. As such, the K-SWNTs and Li-SWNTs do not undergo the same type of hydrogenation reactions, and were found to desorb less than 1 wt% H_2 during a typical degas.

After degassing the Na-, K- and Li-SWNTs, they were dosed with H_2 at 25°C for 10 min. The reaction was quenched using N_2 (l), and the excess H_2 was pumped out of the apparatus. The sample was then allowed to warm to 25°C followed by subsequent heating with an external furnace again to 700°C, all the while the headspace gas was being monitored by mass spectrometry.

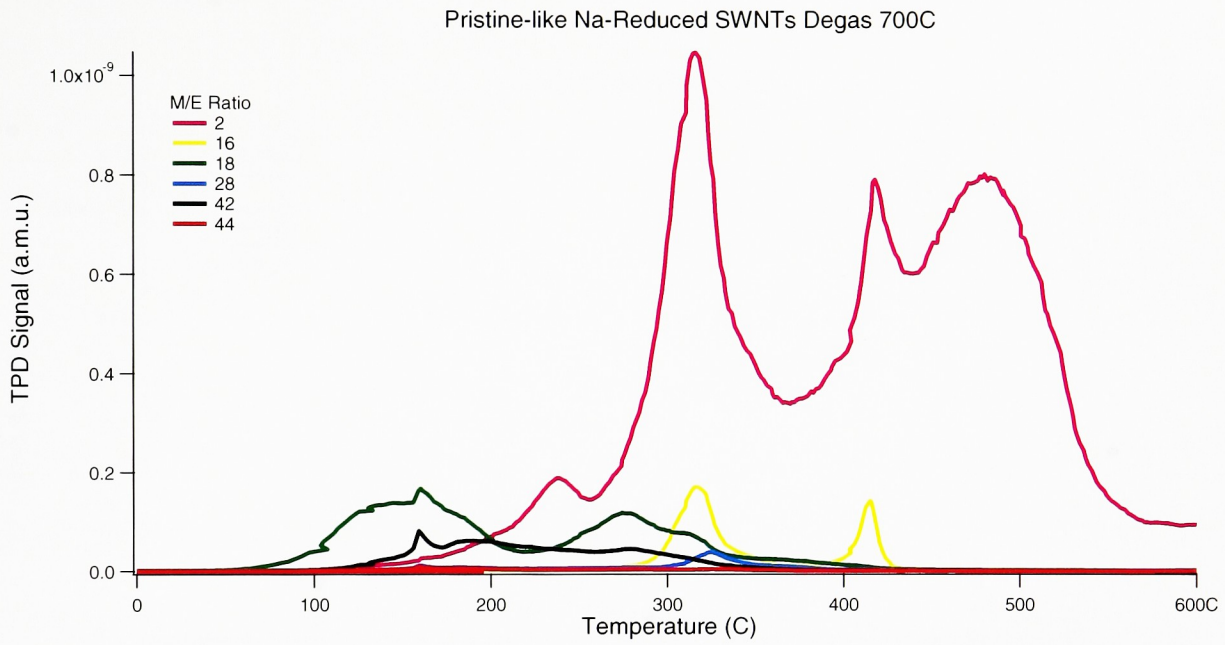

Figure 34: Degas spectrum of the Na-reduced, pristine-like SWNTs obtained by TPD. The sample was loaded onto the TPD apparatus under inert He atmosphere, and degassed from 25 – 700°C over the course of 20 min. Removal of the oxygen-containing defects prior to the Na-reduction of the SWNTs, causes a non-traditional H_2 peak around 300°C, as well as the traditional H_2 peak at approximately 400 – 500°C. This sample demonstrated the desorption of an irreversible 4 wt.% H_2.

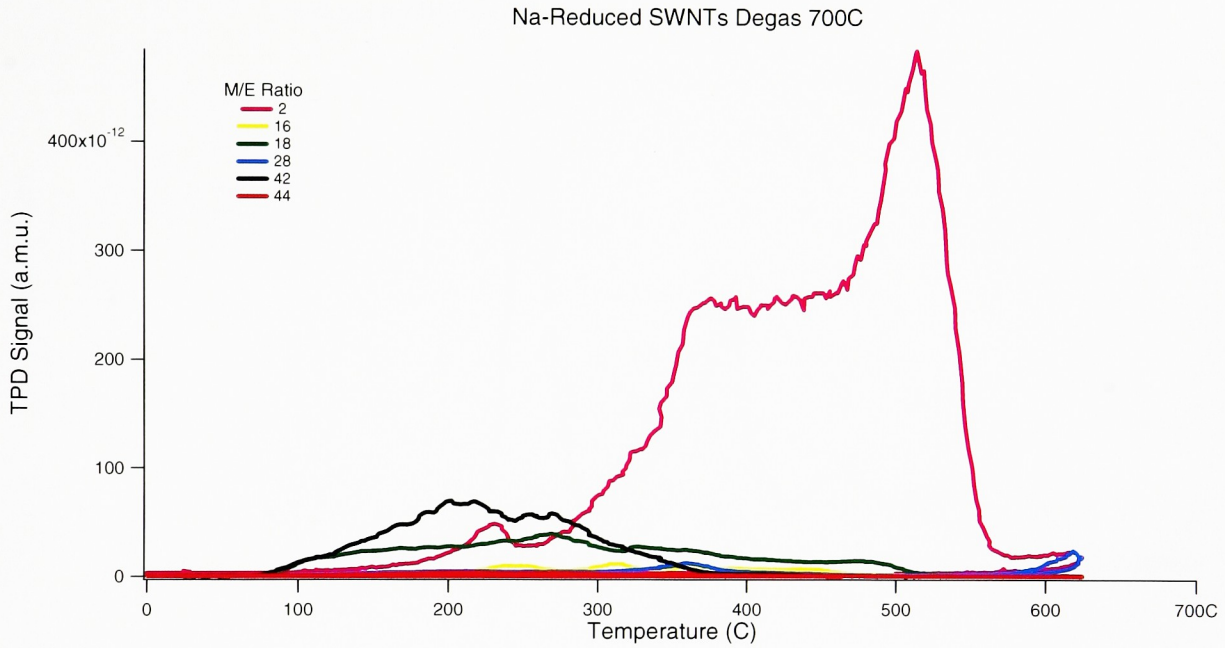

Figure 35: Degas spectrum of the Na-reduced SWNTs obtained by TPD. The sample was loaded onto the TPD apparatus under inert He atmosphere, and degassed from 25 – 700°C over the course of 20 min. In comparison Na-reduced, pristine-like SWNTs, it was demonstrated that the non-traditional H_2 peak disappeared.

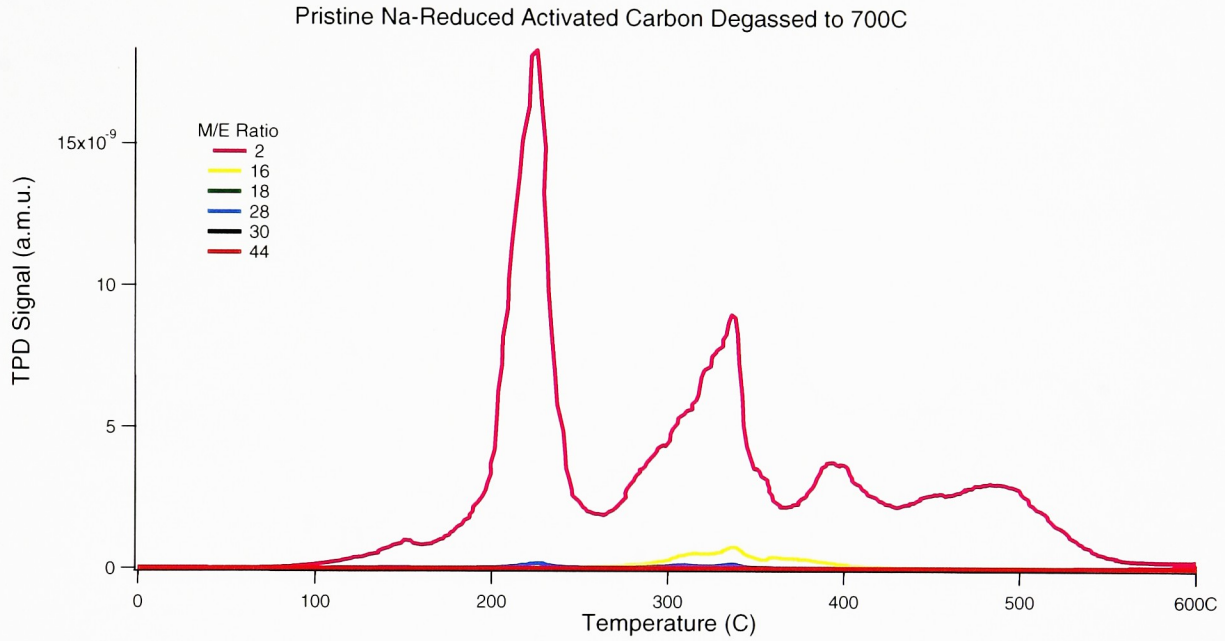

Figure 36: TPD degas spectrum for Na-reduced activated carbon, prepared after removing oxygen-containing defects by heat treatment. The non-traditional H_2 peak at 200°C, as well as the traditional H_2 peak at 350°C confirm the unique character observed with the Na-reduced, pristine-like SWNTs.

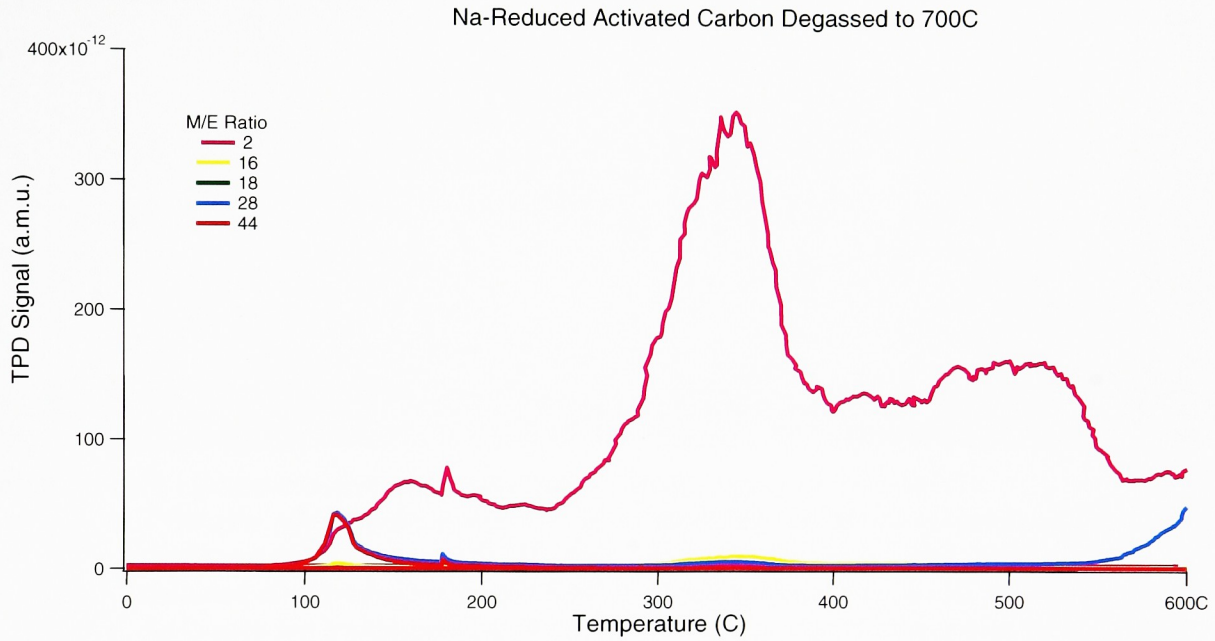

Figure 37: TPD degas spectrum for Na-reduced activated carbon. The non-traditional H_2 peak at 200°C is not observed when the oxygen-containing defects are not removed. The presence of only the traditional H_2 peak exemplifies the results obtained for the Na-reduced SWNTs.

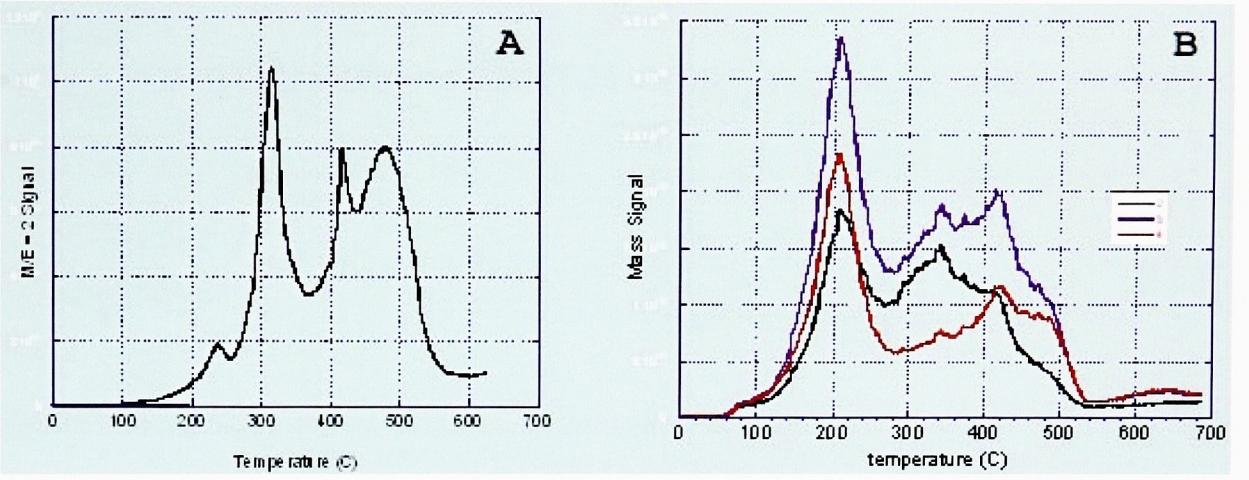

Figure 38: (A) Representative degas spectrum of the H_2 signal on Na-SWNTs. Typically, approximately 4% w/w H_2 is desorbed. (B) Representative degas spectra of the mass signal for H_2, HD, and D_2, respectively. This data was obtained after preparing the Na-SWNTs using naphthalene-d_8 and THF-d_8. As is seen the hydrogenation of the Na-SWNTs is caused by reaction with THF.

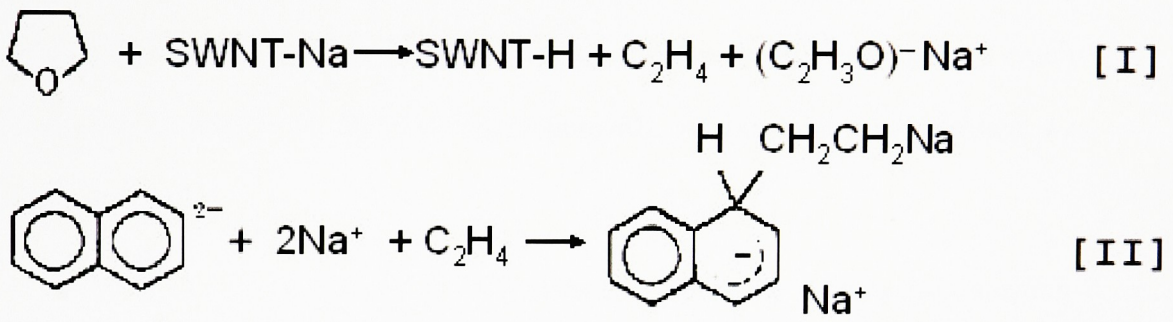

Figure 39: Proposed mechanism by which hydrogenation of Na-SWNTs occurs. In Scheme [I], the SWNT-Na radical system reacts with THF to undergo hydrogenation, forming SWNT-H.[73] Ethylene is formed as a byproduct, which reacts in Scheme [II] with the adjacent arene rings of the nanotubes to form Na-SWNT-$(H)_{n-1}(CH2CH2)_{n-1}$.[75]

The spectra of the Na-, K-, and Li-reduced SWNTs were very similar in that they demonstrated a sharp physisorbed H_2 peak at temperatures less than 0°C, which was observed almost immediately after removing the N_2 (l). As the temperature of the samples was increased above 0°C, no gaseous molecules were observed to be desorbed from the samples. At the very end of the experiments, as the temperature approached 700°C, H_2 and CO were occasionally observed rapidly coming off of the sample, which was indicative of the sample decomposing (Figure 40). At this point the experiment was terminated.

After analyzing the reduced SWNT precursors, the newly synthesized transition metal – carbon nanotube hybrid materials synthesized by the direct reduction technique were analyzed for H_2 storage using the same TPD protocol. The samples were analyzed once by loading them onto the TPD apparatus under inert He atmosphere, and once by exposing them to air. Due to the fact that there was no difference in the mass spectra, it was found that the hybrid materials were not sensitive to air, and could be handled without working in the glovebox. The hybrid samples were again degassed prior to doping them with H_2. The degassing was only run to 500°C because the samples began to decompose at higher temperatures. The degas spectra of these samples demonstrated that the hybrid materials were very much like either the K- or Li-reduced SWNTs or the purified SWNTs that they were synthesized from. An example of this is portrayed in Figure 41, which shows the degas spectra for Co-SWNTs that was prepared on K- and Li-reduced SWNTs, respectively, by the direct reduction of Co onto the surface of the SWNTs from a Cobalt(II) 2,4-Pentanedionate solution. As was explained in previous discussions, the Na-reduced SWNTs exhibited an exceptional amount of H_2 desorption

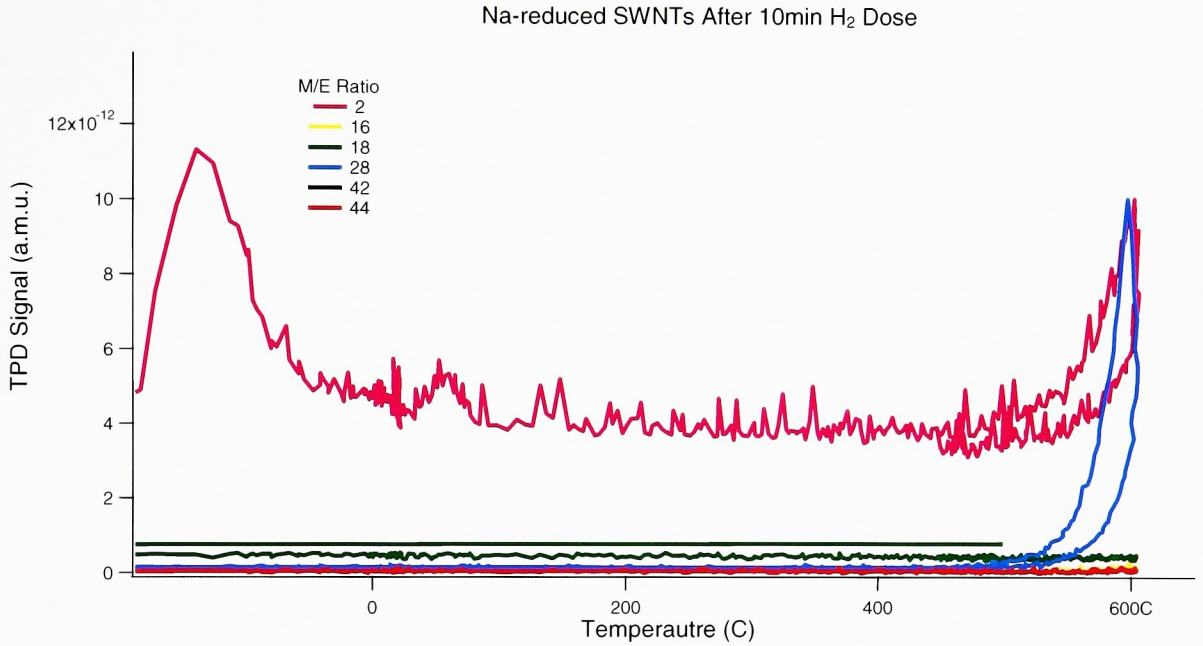

Figure 40: Mass spectrum of the Na-reduced SWNTs after dosing for 10 min with H_2. An initial physisorbed H_2 peak is observed immediately after quenching the reaction and removing the N_2 (l). The spetra for both the K- and Li-reduced SWNTs is very similar to the data obtained for the Na-SWNTs.

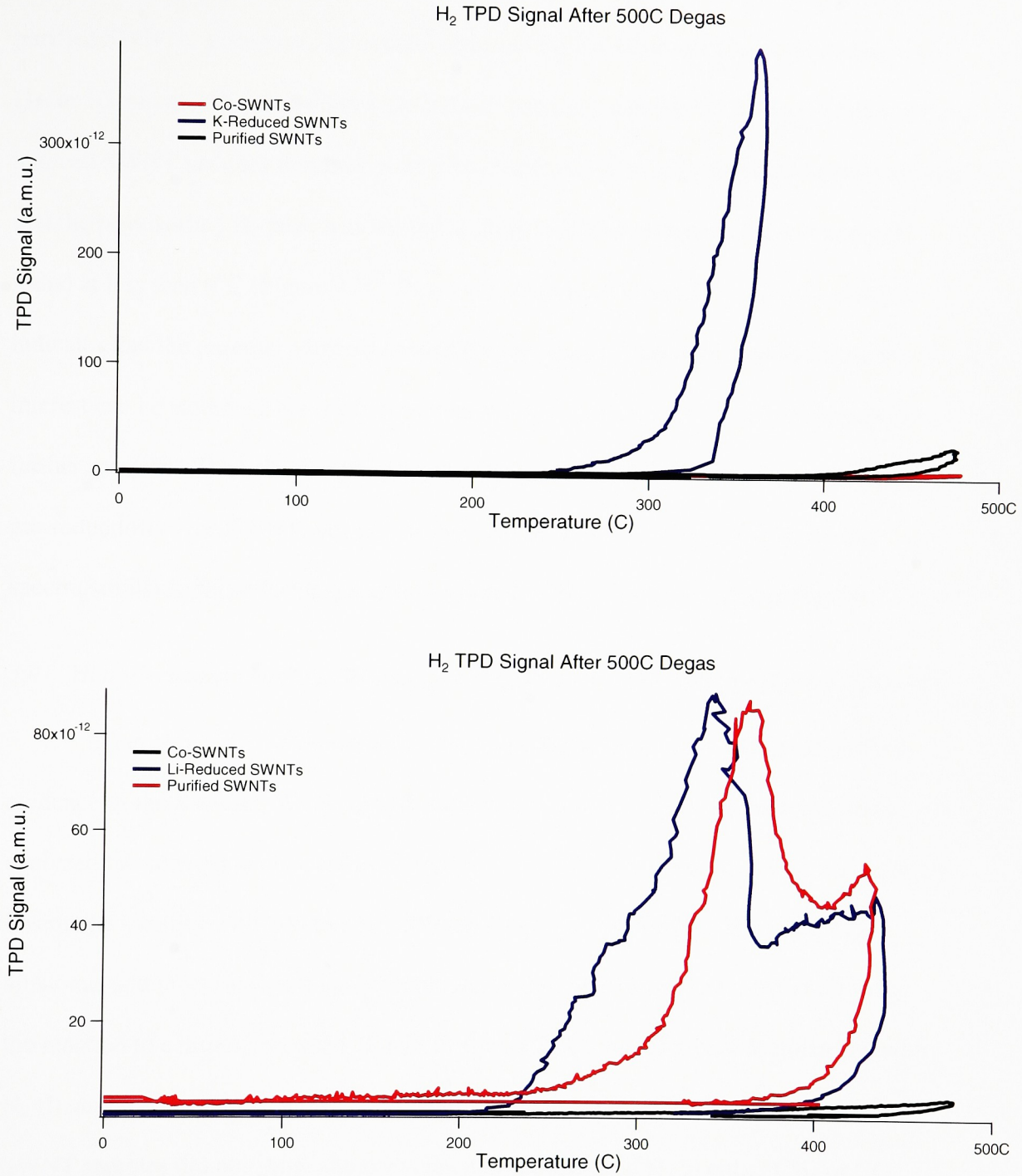

Figure 41: Degas spectra for Co-SWNTs prepared via the direct reduction technique on K- and Li-reduced SWNTs, respectively, from a solution of Cobalt(II) 2,4-Pentanedionate. H_2 desorption from these samples resembles either the reduced SWNTs or purified SWNTs, and does not show increased H_2 desorption. The Fe-, Ni-, and Cr-SWNT samples had similar degas spectra.

during degassing, but none of the hybrid materials resembled this and merely looked like purified SWNTs. Likewise, the spectra obtained for the same samples after dosing with H_2 for 10 min at 25°C showed that the hybrid materials appeared to be very similar to the reduced SWNT samples that they were prepared from. The only difference observed was that the physisorbed H_2 peak was shifted slightly to higher temperatures, but was still found at less than 0°C (Figure 42). This was shown for CO and CO_2 as well, which indicates that the gaseous reagents needed for the various heterogeneous reactions of interest can be stored within the hybrid material and may prove to be advantageous for further reaction. The hybrid materials prepared by the adsorption technique and by the pre-reduction of the SWNT surface, all showed initial degas spectra and H_2 dosing spectra similar to those for the samples prepared by the direct reduction technique.

3.4 Heterogeneous Catalysis Reactions Using the Newly Synthesized Hybrid Materials

Upon obtaining the preliminary TPD data, the samples were then analyzed for evidence of the Sabatier, WGS, and FT synthesis reactions. The samples were first analyzed for heterogeneous catalysis reactions other than FT synthesis. This was done by dosing the samples with 100 torr H_2, 100 torr CO_2, and 400 torrH_2. The same TPD apparatus and protocols were again employed as described previously. After allowing the reaction to continue between 10 min to 1 hr at 25°C, the reaction was quenched with N_2 (l), and the mass spectra obtained while heating to 500°C. The Fe-, Ni-, Co-, and Cr-SWNT samples did not show any conversion of the CO_2 and H_2 to either CH_4 or CO, thereby indicating that neither the Sabatier reaction nor the RWGS reaction had occurred. On the other hand, the Rh-SWNT sample, produced by the adsorption technique from a Rhodium(III) 2,4-Pentanedionate solution, showed evidence that the RWGS, Sabatier,

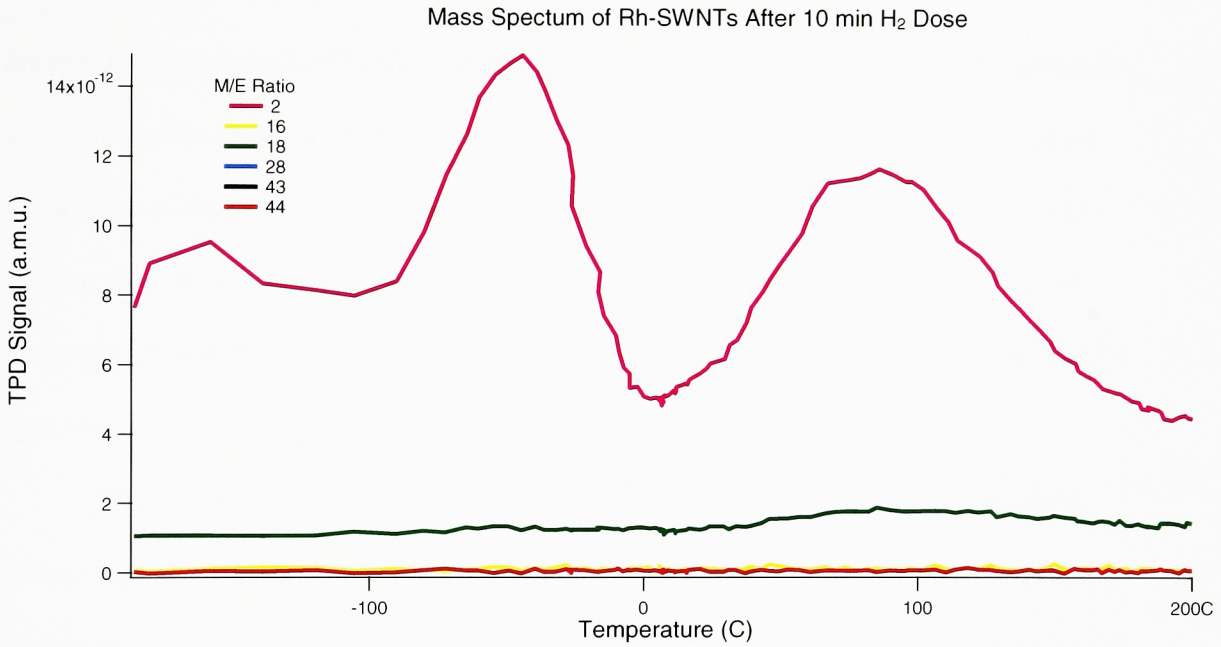

Figure 42: Mass spectrum of Rh-SWNTs produced by the pre-reduction of the nanotubes followed by the direct reduction of the metal particles onto Na-reduced SWNTs from a Rhodium(III) 2,4-Pentanedioante solution. The spectrum shows the potential for this sample to act as a Kubas complex as seen by the H2 peak at 100°C.

and FT reactions had occurred. Initially, H_2, CO_2, and CO were observed coming off of the sample, indicating that the RWGS reaction had taken place. The conversion of CO_2 to CO allowed for further reaction to occur with the H_2, which is evident by the CH_4 and H_2O desorbing from the sample. It is difficult to determine whether the CH_4 was produced solely by FT synthesis or Sabatier reaction, and most likely was from a combination of the two (Figure 43). Additionally, the mass spectra of Rh-SWNTs prepared on pristine-like SWNTs via the direct reduction technique from a Rhodium(III) 2,4-Pentanedionate solution demonstrated evidence that the Sabatier reaction occurred. In this case, CO_2 is observed coming off of the sample, followed by methane and water (Figure 44). With this data, it seems as though the synthesis of the Rh-SWNT hybrid materials are able to act as functioning catalysts for the RWGS, Sabatier reaction, and FT synthesis.

While it has been demonstrated previously that the Rh-SWNTs are efficient at catalyzing the FT synthesis, the remaining Fe-, Ni-, Co-, and Cr-SWNT samples were finally examined for their use as catalysts in FT synthesis. As with previous experiments, the samples were dosed with 100 torr H_2, 100 torr CO, and 400 torr with H_2. The reactions were quenched with N_2 (l) after 10min to 1 hr, and were heated to 500°C while continually monitoring the headspace gas via mass spectrometry for evidence that the FT reaction had occurred. The Co-, Cr-, and Fe-SWNT samples all show evidence that the FT reaction had occurred, which is demonstrated in the mass spectral data by the significant amounts of methane and water observed (Figures 45, 46, and 47, respectively). The Co-SWNTs appear to be the most efficient of the hybrid materials synthesized at catalyzing the FT synthesis, which is evident by the presence of only CH_4

and H_2O in the mass spectrum. The Fe- and Cr-SWNT hybrid materials showed some unreacted H_2 coming off the sample, indicating that the reaction had not been driven to completion. As such, representative data for the Co-SWNT hybrid material is provided, which demonstrates the ability of the newly synthesized hybrid materials to produce higher molecular weight hydrocarbons, such as ethane and propane (Figure 48). Not enough information has been gathered to assess the ability of the Ni-SWNTs to be used as FT catalysts. Preliminary data obtained in this thesis research shows that transition metal – carbon nanotube hybrid materials synthesized by the various methodologies proposed are effective in their use as FT catalysts. A concise summary of the aforementioned results is given in Table 5.

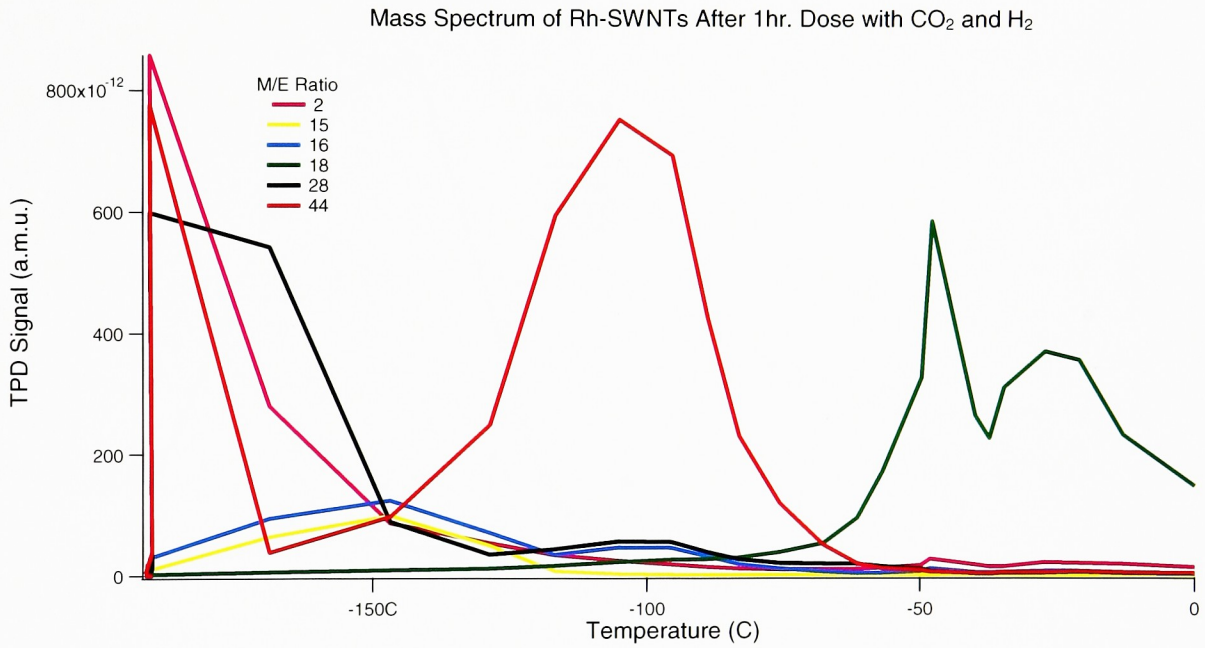

Figure 43: Mass spectrum of Rh-SWNTs produced by the adsorption technique from a Rhodium(III) 2,4-Pentanedioante solution. The spectrum demonstrates the conversion of CO2 and H2 to CO as well as CH4. This indicates that both the RWGS and Sabatier reactions have occurred.

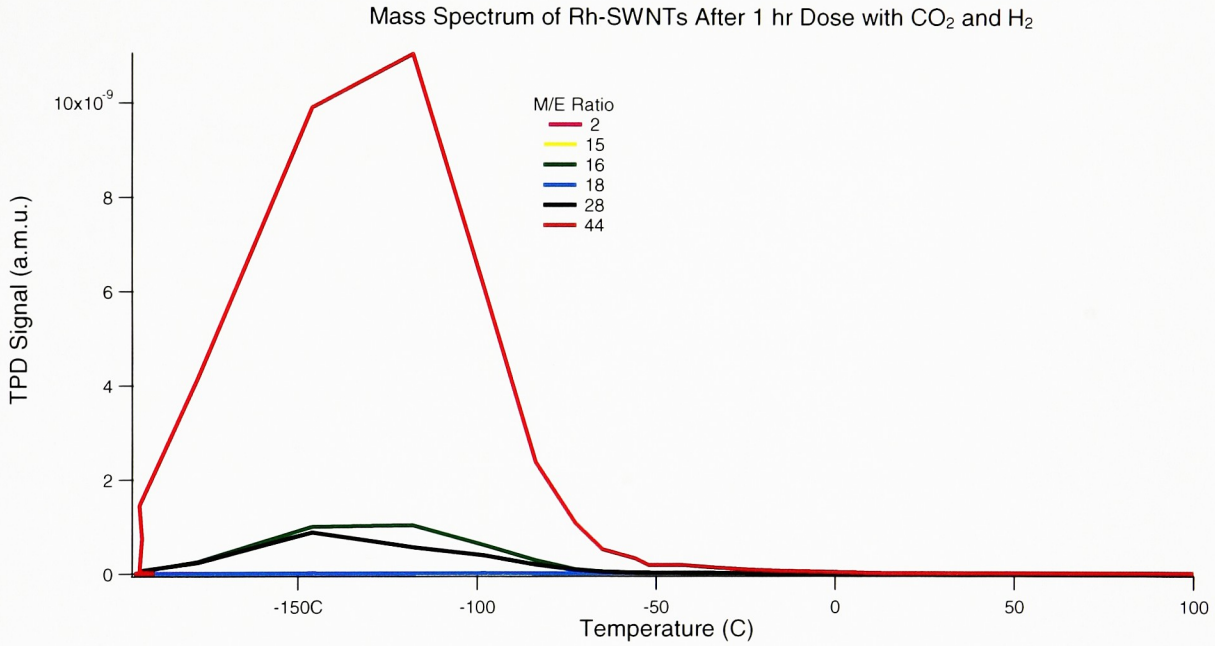

Figure 44: Mass spectrum of Rh-SWNTs produced by the pre-reduction of the nanotubes followed by the direct reduction of the metal particles onto Na-reduced SWNTs from a Rhodium(III) 2,4-Pentanedioante solution. As can be seen from the mass spectrum, the Sabatier reaction has taken place, which is evident by the production of CO and H2O.

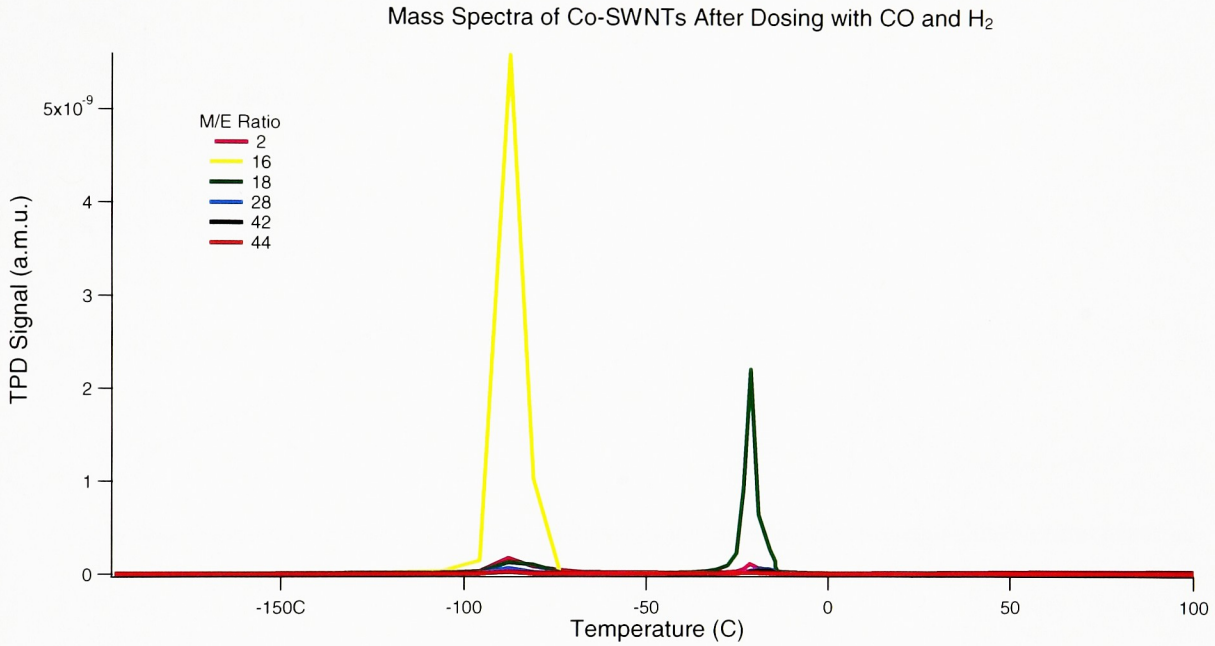

Figure 45: Mass spectrum of Co-SWNTs after dosing with CO to 100 torr and H_2 to 500 torr. Upon heating, methane and water are observed desorbing from the sample, indicating that the FT reaction has occurred.

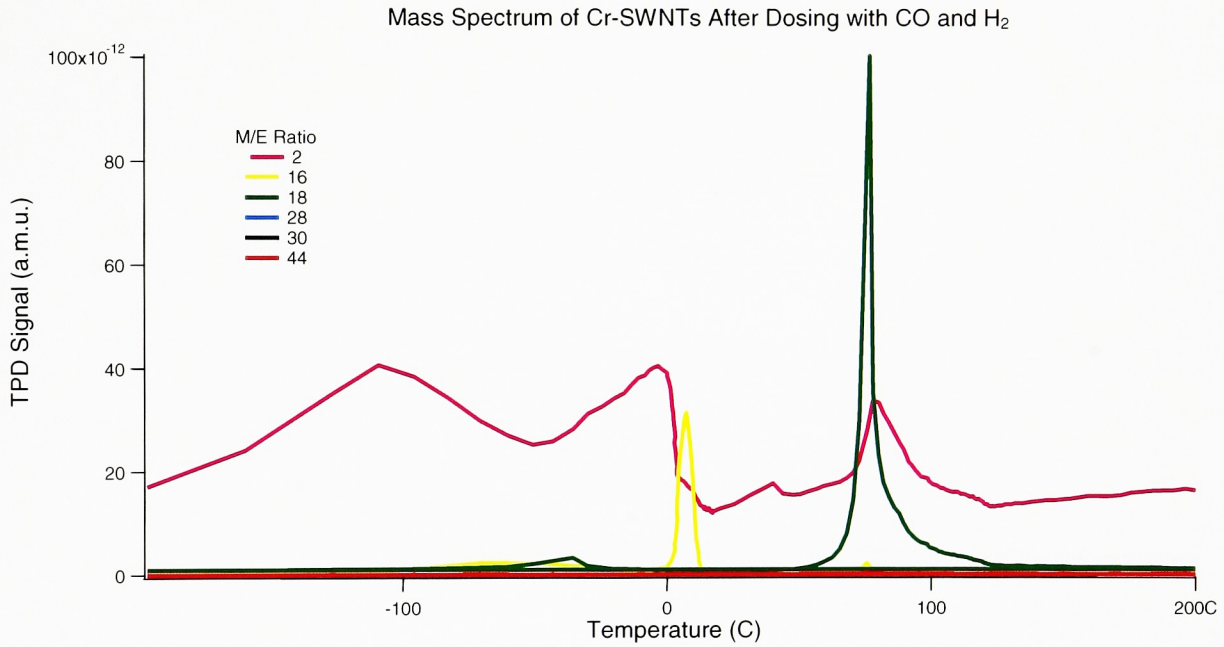

Figure 46: Mass spectrum of Cr-SWNTs after dosing with CO to 100 torr and H_2 to 500 torr. Upon heating, methane and water are observed desorbing from the sample, indicating that the FT reaction has occurred.

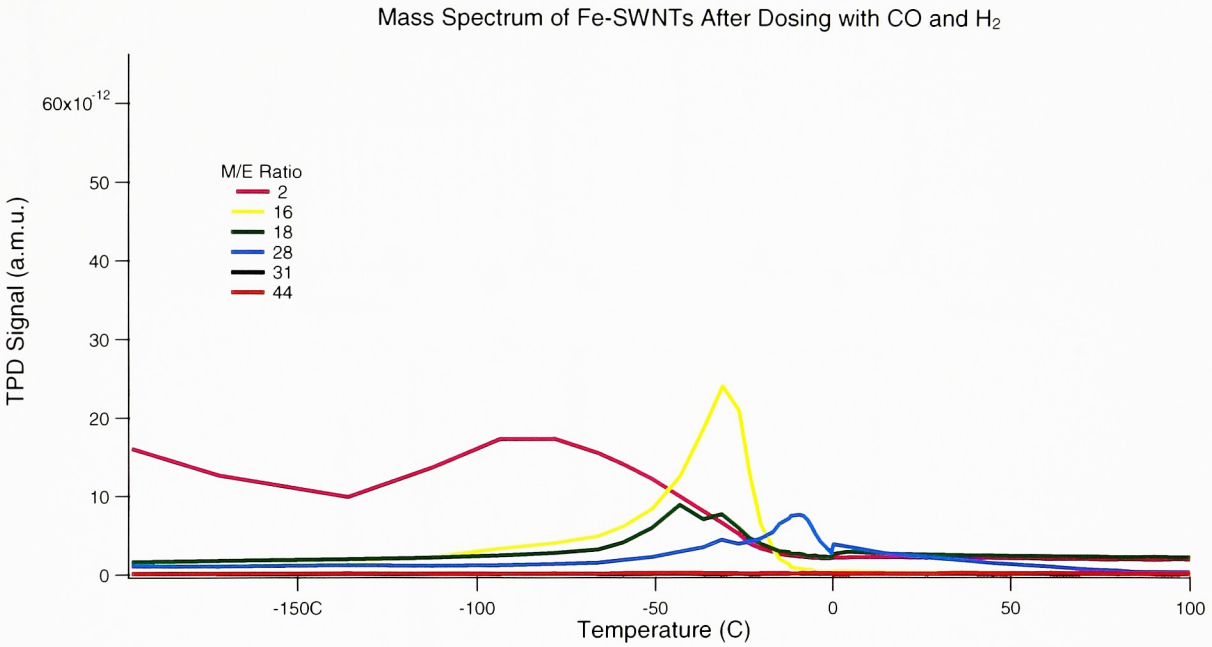

Figure 47: Mass spectrum of Fe-SWNTs after dosing with CO to 100 torr and H_2 to 500 torr. Upon heating, methane and water are observed desorbing from the sample, indicating that the FT reaction has occurred.

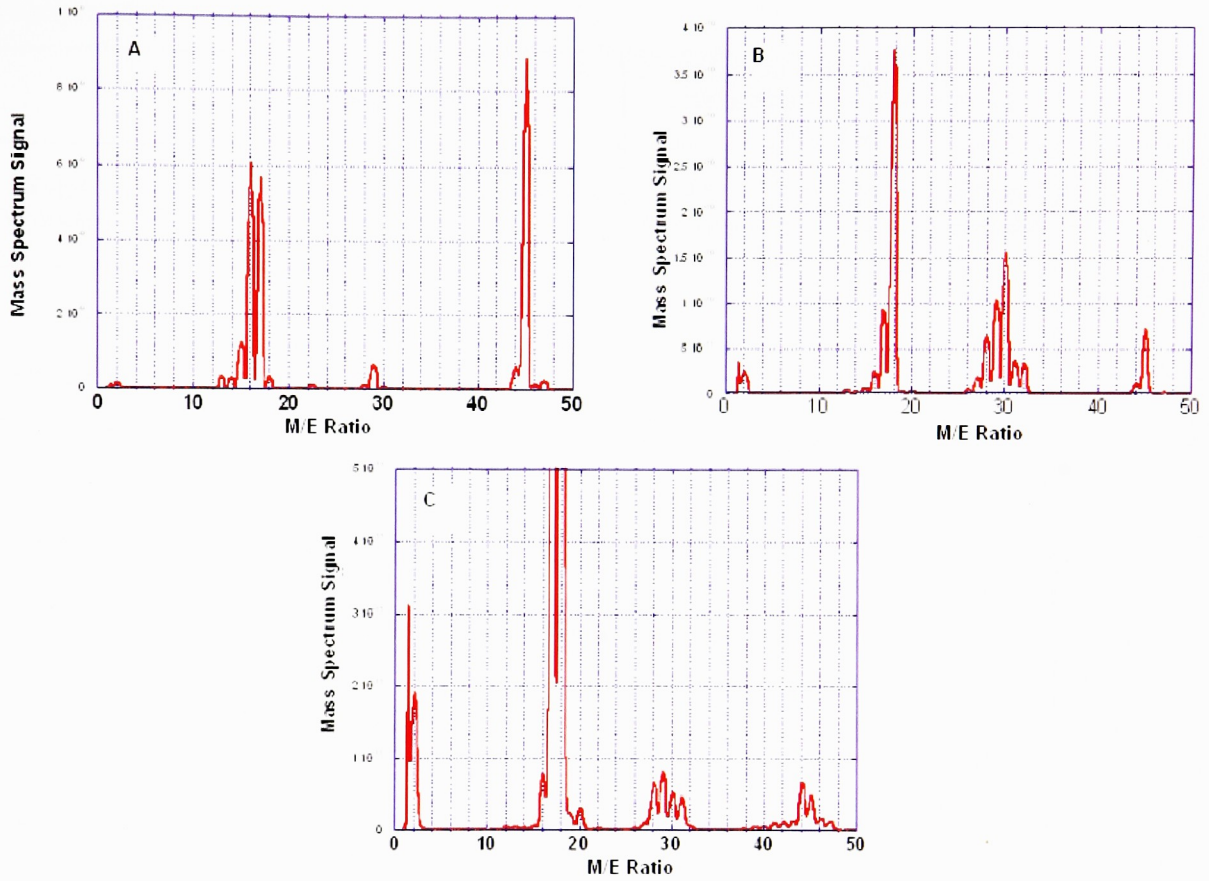

Figure 48: Representative data for Co-SWNT hybrid materials. The TPD data shows the presence of methane, ethane and propane at increasing degas temperatures (A: -50°C, B: -15°C, C: 0°C) in the mass spectrum.

Table 5: Project summary.

	Synthetic Method			Ability to Catalyze Various Heterogeneous Catalysis Reactions		
Metal Deposited	**Adsorption**	**Direct Reduction**	**Pre-reduction of SWNT Surface**	**FT Synthesis**	**Sabatier Reaction**	**RWGS Reaction**
Cobalt	20 - 50 nm particles with non-uniform diameter distribution	20-200nm particles with non-uniform diameter distribution		✓		
Chromium			20-200nm particles with non-uniform diameter distribution	✓		
Iron				✓		
Nickel				Not Enough Information		
Rhodium			**<2 nm evenly distributed particles**	✓	✓	✓

4.0 Conclusions and Future Work

4.1 Conclusions

In this thesis research, three novel techniques were described for the synthesis of transition metal – carbon nanotube hybrid materials to be used as catalysts in various heterogeneous catalysis reactions, with an emphasis on FT synthesis. FT synthesis is a process that involves the hydrogenation of CO over a transition metal catalyst to produce varying length hydrocarbons and olefins. The ultimate goal of the present study was to achieve smaller than 10 nm catalyst particles that were evenly dispersed over the surface of the SWNT material, as it has been demonstrated that small-sizedd catalyst particles with large surface areas produce the greatest amount of catalytic activity in the FT reaction scheme. The synthesis of these hybrid materials was successfully achieved using a series of transition metals, including Fe, Ni, Co, Cr, and Rh, which were deposited onto the surface of purified and pristine-like SWNTs. The purity of the SWNT material was confirmed by TEM and TGA analysis, and demonstrated that the purification process was efficient in removing the metal catalyst particles and carbonaceous impurities that were introduced during the laser vaporization synthesis of the SWNTs.

The hybrid materials were first synthesized using an adsorption technique that involved the nucleation and growth of the catalyst particles on the surface of the SWNTs via the aid of a $NaBH_4$ reducing agent. In this process, metal catalyst particles ranging in size from 30 – 50 nm were achieved, however, it was difficult to gain control over the particle size using this technique. The main disadvantage of the adsorption technique was that this process did not consistently yield reproducible results, which was mainly

due to the variability in the number of defects produced on the surface of the SWNTs. Next, the hybrid materials were synthesized using the direct reduction technique, which involved the pre-reduction of the SWNTs with Na-, K-, or Li-naphthalate. Theoretically, the pre-reduction of the SWNTs in this manner would change the E_{red} of the SWNTs to be close to that of the alkali metal that they were reduced with, potentially allowing for the spontaneous deposition of the transition metal at the position of a defect site. Again this technique relied on the ability to reproducibly create defect sites along the surface of the SWNTs to achieve an evenly dispersed catalyst deposition. The size of the catalyst particles in the hybrid materials synthesized using the direct reduction technique ranged in size between 20 – 200 nm. Finally, the synthesis of small, well dispersed Rh catalyst particles was achieved by prereducing the surface of the SWNTs to remove any oxidative groups, followed by the catalyst deposition via direct reduction. In this case, <2 nm metal catalyst particles were reproducibly deposited onto the SWNTs. The ability to obtain these small, evenly dispersed particles was most likely the result of performing the deposition on pristine-like SWNTs, which do not have oxygen-containing defect sites for the nucleation of the catalyst particles. Instead, the particles are believed to be precipitated onto the surface of the SWNT.

While the catalyst particle size varied considerable depending on the synthesis technique employed for the production of the hybrid materials, it was determined that the Fe-, Co-, Cr-, and Rh-SWNT samples were all successful at catalyzing FT synthesis. After doping these samples with CO and H_2, the presence of methane, ethane, propane, and water were observed in the data obtained via mass spectrometry. Additionally, the Rh-SWNT samples demonstrated the ability to catalyze the Sabatier and RWGS reactions

as well. Essentially, this thesis research has been successful in demonstrating the ability to synthesize transition metal – carbon nanotube hybrid materials for their use as catalysts in the FT synthesis, and have additionally shown limited catalytic activity in both the Sabatier and RWGS reactions.

4.2 Future Work

Future investigations will continue to focus on the incorporation of transition metals with SWNTs via novel methodologies. Currently, two such techniques are being investigated. The first involves a series of photolysis reactions in which various metal-carbonyl compounds are UV irradiated and the deposition of the transition metal onto the surface of the SWNT achieved. The second technique currently being examined involves burning the purified SWNT *papers* in CO_2 thereby creating more active sites on the surface of the nanotubes. The SWNT material is then be dipped into a metal salt solution and the metals reduced using a high temperature Sieverts apparatus to reduce the metals to the elemental state using flowing H_2. These two techniques may provide greater control over the catalyst particle size and may simplify the synthesis process.

In addition to examining various other novel techniques for the incorporation of transition metals with SWNTS, more thorough characterization of these newly synthesized hybrid materials must be conducted. For instance, through the utilization of the Brunauer, Emmett, and Teller (BET) method, it will be possible to determine how the surface area and pore size distributions of the SWNTs are affected by the deposition of the various transition metals. Additionally, X-ray Diffraction will be used to determine the structure of the metal catalyst particles deposited on the SWNTs, as well as to determine how the transition metals interact with the nanotube material. Most

importantly, the catalytic activity of the hybrid materials in the FT synthesis will be compared to more traditional metal catalysts prepared on various oxide supports and activated carbon.

5.0 List of Terms

- **Arc Discharge:** Technique used in the synthesis of CNTs. An electric current is generated between two graphitic carbon electrodes; the anode is consumed and the resulting plasma condenses on the cathode causing the growth of the CNTs.
- **Brunauer, Emmett, and Teller Method (BET):** Used to analyze surface area and pore size distributions based on the volumetric adsorption of gas molecules onto a particular sample.
- **Carbon Nanotube (CNT):** Graphite sheet rolled into an elongated cylinder and terminated with an hemispherical endcap. (See also SWNT and MWNT)
- **Cetane:** Also known as hexadecane, this is an alkane hydrocarbon with the chemical formula $C_{16}H_{34}$. Cetane ignites very easily under pressure, and is typically found in diesel fuel.
- **Chemical Vapor Deposition (CVD):** Technique used in the synthesis of CNTs. A gaseous carbon feed stock is passed over or through a substrate containing a transition metal catalyst. Upon applying thermal energy, the carbon feedstock cracks and the CNTs are grown on the substrate surface.
- **Chiral Vector (C_h):** Also known as the roll-up vector. Describes the general structure of a SWNT. The Chiral Vector is defined as: $C_h=na_1+ma_2$.
- **Circulating Fluidized Bed Reactor (CFB):** A second generation HTFT reactor bed that contains two phases of fluidized catalyst.
- **Dangling Bond:** Occurs in SWNTs as a defect; exits when a carbon atom is missing in the CNT hexagonal network.
- **Euler's Theorem:** States that there must be twelve pentagons in a hexagonal network in order to obtain a closed cage structure.
- **Fischer-Tropsch Synthesis (FT):** A catalyzed chemical reaction in which carbon monoxide and hydrogen are converted into liquid hydrocarbons of various forms.
- **Fixed Fluidised Bed Reactor (FFB):** The first HTFT reactor bed.
- **Heterogeneous Catalysis:** Describes a catalysis reaction in which the catalyst is present in a different phase than the reactants thus providing a surface for the reaction to take place upon.
- **High Pressure Carbon Monoxide Synthesis (HiPco):** Technique used in the mass production of SWNTs.
- **High Temperature Fischer Tropsch Synthesis (HTFT):** Operate at 2 MPa and between 300-350°C. (See also CFB and FFB)
- **Homogeneous Catalysis:** Describes a catalysis reaction in which the catalyst is present in the same phase as the reactants.
- **Hydrocarbon:** Organic compound consisting entirely of hydrogen and carbon.
- **Isolated Pentagon Rule:** States that the amount of local surface stress induced by curvature must be minimized by maximizing the distance between the twelve pentagons in the end cap of a SWNT by surrounding each with five hexagons.
- **Laser Vaporization:** Technique used in the synthesis of CNTs. Carbon is vaporized within a quartz reaction chamber by rastering a laser beam over the

surface of a graphitic target. The vaporized material is cooled causing the condensation and growth of the CNTs.

- **Low Temperature Fischer Tropsch Synthesis (LTFT):** Operate at 2 MPa and between 200-250°C. In contrast to HTFT synthesis, LTFT synthesis creates significant amounts of wax.
- **Multiwalled Carbon Nanotube (MWNT):** First form of tubular carbon to be discovered; consist of concentric layers or shells of graphene rolled in cylindrical fashion one inside the other.
- **Olefin:** An unsaturated chemical compound containing at least one carbon-to-carbon double bond.
- **Paraffin:** A common name for a group of alkane hydrocarbons with the general formula C_nH_{2n+2}, where n is the number of carbon atoms.
- **Reverse Water Gas Shift Reaction (RWGS):** A catalyzed reaction in which carbon dioxide and hydrogen form carbon monoxide and water.
- **Sabatier Reaction:** A catalyzed reaction in which carbon monoxide and hydrogen form methane and water.
- **Scanning Electron Microscopy (SEM):** A type of electron microscopy capable of producing high-resolution images of a sample surface
- **Single Walled Carbon Nanotube (SWNT):** A single graphene sheet rolled seamlessly into an elongated cylinder.
- **Standard Cubic Centimeters Per Minute (sccm):** Unit of measurement for the quantification of flow of bulk liquid or gas.
- **Stone Wales Defects:** A type of defect that occurs in SWNTs; a disruption in the ordering of the carbon atoms within a hexagonal carbon network (ie. atoms are arranged in an adjacent heptagon-pentagon pairs rather than the two hexagons as would otherwise be expected).
- **Synthesis Gas (Syngas):** A mixture of H_2 and CO.
- **Temperature Programmed Desorption (TPD):** The method of observing desorbed molecules from a surface when the surface temperature is increased
- **Tensile Strength:** The maximum amount of stress that a material can be subjected to before failure.
- **Thermogravimetric Analysis (TGA):** Analysis performed on samples to determine changes in weight in relation to change in temperature.
- **Transmission Electron Microscopy (TEM):** An imaging technique whereby a beam of electrons is transmitted through a sample forming an image which is then magnified and displayed.
- **X-Ray Diffraction (XRD):** A non-destructive analytical technique which reveals information about the crystallographic structure, chemical composition, and physical properties of a sample.
- **Young's Modulus:** A measure of the stiffness of a given material.

6.0 References

1. Iijima, S. *Nature,* **1991,** 354, 56-58.
2. Iijima, S.; Ichihashi, T. *Nature,* **1993,** 363, 603-605.
3. Bethune, D.S.; Kiang, C.H.; de Vries, M.S.; Gorman, G.; Savoy, R.;Vazquez, J.; Beyers, R. *Nature,* **1993,** 363, 605-607.
4. Guo, T.; Nikolaev, P.; Thess, A.; Colbert, D.T.; Smalley, R.E. *Chem. Phys. Lett.,* **1995,** 243, 49-54.
5. Dai, H.; Rinzler, A.G.; Nikoleav, P.; Thess, A.; Colbert, D.T.; Smalley, R.E. *Chem. Phys. Lett.,* **1996,** 260, 471-475.
6. Duesberg, G.S.; Blau, W.; Byrne, H.J.; Muster, J.; Burghard, M.; Roth, S. *Synth. Met.,* **1999,** 103, 2484-2485.
7. Harutyunyan, A.R.; Pradhan, B.K.; Chang, J.; Chen, G.; Eklund, P.C. *J. Phys. Chem. B,* **2002,** 106, 8671-8675.
8. Kajiura, H.; Tsutsui, S.; Huang, H.; Murakami, Y. *Chem. Phys. Lett.,* **2002,** 364, 586-592.
9. Chiang, I.W.; Brinson, B.E.; Huang, A.Y.; Willis, P.A.; Bronikowski, M.J.; Margrave, J.L.; Smalley, R.E.; Hauge, R.H. *J. Phys. Chem. B,* **2001,** 105, 8297-8301.
10. Dillion, A.C.; Gennett, T.; Jones, K.M.; Alleman, J.L.; Parilla, P.A.; Heben, M.J. *Adv. Mater.,* **1999,** 11, 1354-1358.
11. Chiang, I.W.; Brinson, B.E.; Margrave, J.L.; Smalley, R.E.; Hauge, R.H. *J. Phys. Chem. B,* **2001,** 105, 1157-1161.
12. Skoog, D.A.; Holler, F.J.; Nieman, T.A. *Principles of Instrumental Analysis,* 5th ed.; Saunders College Publishing, 1998.
13. Landi, B.J.; Cress, C.D.; Evans, C.M.; Raffaelle, R.P. *Chem. Mater.,* **2005,** 17, 6819-6834.
14. Lambin, Ph.; Loiseau, A.; Culot, C.; Biro, L.P. *Carbon,* **2002,** 40, 1635-1648.
15. Baughman, R.H.; Zakhidov, A.A.; de Heer, W.A. *Science,* **2002,** 297, 787-792.
16. Overett, M.J.; Hill, R.O.; Moss, J.R. *Coord. Chem. Rev.,* **2000,** 206-207, 581-605.
17. Liu, Z.P.; Hu, P. *J. Am. Chem. Soc.,* **2002,** 124, 11568-11569.
18. Dry, M.E. *Catal. Today,* **2002,** 71, 227-241.
19. Ngwenya, T.; Glasser, D.; Hildebrandt, D.; Coville, N.; Mukoma, P. *Ind. Eng. Chem. Res.,* **2005,** 44, 5987-5994.
20. Bezemer, G.L.; Radstake, P.B.; Koot, V.; van Dillen, A.J.; Geus, J.w.; de Jong, K.P. *J. Catal.,* **2006,** 237, 291-302.
21. Giordano, R.; Serp, P.; Kalck, P.; Kihn, Y.; Schreiber, J.; Marhic, C.; Duvail, J.L. *Eur. J. Inorg. Chem.,* **2003,** 610-617.
22. Yu, Z.; Borg, O.; Chen, D.; Enger, B.C.; Froseth, V.; Rytter, E.; Wigum, H.; Holman, A. *Catal. Lett.,* **2006,** 109, 43-47.
23. van Steen, E.; Prinsloo, F.F. *Catal. Today,* **2002,** 71, 327-334.
24. Bahome, M.C.; Jewell, L.L.; Hildebrandt, D.; Glasser, D.; Coville, N.J. *Appl. Catal. A,* **2005,** 287, 60-67.

25. Bezemer, G.L.; Bitter, J.H.; Kuipers, H.P.C.E.; Oosterbeek, H.; Holewijn, J.E.; Xu, X.; Kapteijn, F.; van Dillen, A.J.; de Jong, K.P. *J. Am. Chem. Soc.,* **2006,** 128, 3956-3964.
26. Serp, P.; Corrias, M.; Kalck, P. *Appl. Catal.,* **2003,** 253, 337-358.
27. Bell, A.T. *Science,* **2003,** 299, 1688-1690.
28. Kroto, H.W.; Heath, J.R.; O'Brian, S.C.; Curl, R.F.; Smalley, R.E. *Nature,* **1985,** 318, 162-163.
29. (a) Lu, X.; Chen, Z. *Chem.Rev.,* **2005,** A-BB.
30. Hamada, N.; Sawada, S.; Oshiyama, S. *Phys. Rev. Lett.,* **1992,** 68, 1579-1581.
31. Minmire, J.W.; Dunlap, B.I.; White, C.T. *Phys. Rev. Lett.,* **1992,** 68, 631-634.
32. Saito, R.; Fujita, F.; Dresselhaus, G.; Dresselhaus, M.S. *Phys. Rev. B,* **1992,** 46, 1804-1811.
33. Robertson, D.H.; Brenner, D.W.; Mintmire, J.W. *Phys. Rev. B,* **1992,** 45, 12592-12595.
34. Smalley, R.E.; Nalwa, H.S. *Encyclopedia of Nanoscience and Nanotechnology;* American Scientific Publisters, 2004.
35. Daenen, M.; de Fouw, R.D.; Hamers, B.; Janssen, P.G.A.; Schouteden, K.; Veld, M.A.J. *The Wonderous World of Carbon Nanotubes: A Review of Current Carbon Nanotube Technologies,* 2003.
36. Dresselhaus, M.S.; Dresselhaus, G.; Eklund, P.C. *Science of Fullerenes and Carbon Nanotubes,* Academic Press, 1996.
37. Li, F.; Cheng, H.M.; Bai, S.; Su, G.; Dresselhaus, M.S. *Appl. Phys. Lett.,* **2000,** 77, 3161-3163.
38. Salvetat, J.P.; Bonard, J.M.; Thomson, N.H.; Kulik, A.J.; Forro, L.; Benoit, W.; Zuppiroli, L. *Appl. Phys. A,* **1999,** 69, 255-260.
39. Salvetat-Delmotte, J.P., Rubio, A. *Carbon,* **2002,** 40, 1729-1734.
40. Thostenson, E.T.; Ren, Z.; Chou, T. *Composites Science and Technology,* **2001,** 61, 1899-1912.
41. Journet, C.; Maser, W.R.; Bernler, P.; Loiseau, A.; de la Chapelle, L.; Lefrant, S.; Deniard, P.; Lee, R.; Fischer, J.E. *Nature,* **1997,** 388, 756-758.
42. Krupke, R.; Hennrich, F.; Lohneysen, H.; Kappes, M.M. *Science,* **2003,** 301, 344-347.
43. Kim, Y.; Hong, S.; Jung, S.; Strano, M.; Choi, J.; Baik, S. *J. Phys. Chem. B,* **2006,** 110, 1541-1545.
44. Collins, P.G.; Zettl, A.; Bando, H.; Thess, A.; Smalley, R.E. *Science,* **1997,** 278, 100-103.
45. Ebbesen, T.W.; Ajayan, P.M. *Nature,* **1992,** 358, 220-222.
46. Kiang, C.H.; *J. Phys. Chem. A,* **2000,** 104, 2454-2456.
47. Qin, L.C.; Zhao, X.; Hirahara, K.; Miyamoto, Y.; Ando, Y.; Iijima, S. *Nature,* **2000,** 408, 50-50.
48. Yudasaka, M.; Kokai, F.; Takahashi, K.; Yamada, R.; Sensui, N.; Ichihashi, T.; Iijima, S. *J. Phys. Chem. B,* **1999,** 103, 3576-3581.
49. Yudasaka, M.; Yamada, R.; Sensui, N.; Ichihashi, T.; Iijima, S. *J. Phys. Chem. B,* **1999,** 103, 6224-6229.
50. Eklund, P.C.; Pradhan, B.K.; Kim, U.J.; Xiong, K. *Nano Lett.,* **2002,** 2, 561-566.

51. Puretzky, A.A.; Schittenhelm, H.; Fan, X.; Lance, M.J.; Allard, L.F.; Geohegan, D.B. *Phys. Rev. B,* **2002,** 245425.
52. Ren, H.F.; Huang, H.P.; Xu, J.W.; Wang, J.H.; Bush, P.; Siegal, M.P.; Provencio, P.N. *Science,* **1998,** 282, 1105-1107.
53. Yudasaka, M.; Kikuchi, R.; Matsui, T.; Ohki, Y.; Yoshimura, S.; Ota, E. *Appl. Phys. Lett.,* **1995,** 67, 2477-2479.
54. Yudasaka, M.; Kikuchi, R.; Ohki, Y.; Ota, E.; Yoshimura, S. *Appl. Phys. Lett.,* **1997,** 70, 1817-1818.
55. Cassell, A.M.; Raymakers, J.A.; Kong, J.; Dai, H. *J. Phys. Chem. B,* **1999,** 103, 6484-6492.
56. Nikolaev, P.; Bronikowski, M.J.; Bradley, R.K.; Rohmund, F.; Colbert, D.T.; Smith, K.A.; Smalley, R.E. *Chem. Phys. Lett.,* **1999,** 313, 91-97.
57. Lewis, L.N. *Chem. Rev.,* **1993,** 93, 2693-2730.
58. Subramaniam, B. Fischer-Tropsch Synthesis In Supercritical Reaction Mediua. US Patent PC92532, 1995.
59. Anson, A.; Jagiello, J.; Parra, J.B.; Sanjuan, M.L.; Benito, A.M.; Maser, W.K.; Martinez, M.T. *J. Phys. Chem.,* **2004,** 108, 15820-15826.
60. Banerjee, S.; Hemraj-Benny, T.; Wong, S.S. *Adv. Mater.,* **2005,** 17, 17-29.
61. Tasis, D.; Tagmatarchis, N.; Bianco, A.; Prato, M. *Chem. Rev.,* **2005,** A-AF.
62. Che, G.; Lakshmi, B.B.; Martin, C.R.; Fisher, E.R. *Langmuir,* **1999,** 15, 750-758.
63. Choi, H.C.; Shim, M.; Bangsaruntip, S.; Dai, H. *J. Am. Chem. Soc.,* **2002,** 124, 9058-9059.
64. Banjerjee, S.; Wong, S.S. *Nano Lett.,* **2002,** 2, 49-53.
65. Quinn, B.M.; Dekker, C.; Lemay, S.G. *J. Am. Chem. Soc.,* **2005,** 127, 6146-6147.
66. Wildgoose, G.G.; Banks, C.E.; Compton, R.G. *Small,* **2006,** 2, 182-193.
67. Li, J.; Moskovits, M.; Haslett, T.L. *Chem. Mater.,* **1998,** 10, 1963-1967.
68. Zhao, Q.; Buongiorno Nardelli, M.; Lu, W.; Bernholc, J. *Nano Lett.,* **2005,** A-E.
69. Yang, S.H.; Shin, W.H.; Lee, J.W.; Kim, S.Y.; Woo, S.I.; Kang, J.K. *J. Phys. Chem. B,* **2006,** 110, 13941-13946.
70. Tzitzios, V.; Georgakilas, V.; Oikonomou, E.; Karakassides, M.; Petridis, D. *Carbon,* **2006,** 44, 848-853.
71. Tarabek, J.; Kavan, L.; Kalbac, M.; Rapta, P.; Marketa, Z.; Dunseh, L. *Carbon,* **2006,** 44, 2147-2154.
72. Bauschlicher, C.W. *Nano Lett.,* **2001,** 1, 223-226.
73. Bates, R.B.; Kroposki, L.A.; Potter, D.E. *J. Org. Chem.,* **1972,** 37, 560-562.
74. Carnahan, J.C.; Colsson, W.D. *J. Org. Chem.,* **1972,** 37, 4469-4471.
75. Tomas, J.; Lledos, A. *Organometallics,* **1998,** 17, 190-195.

Submitted For Publication

Hydrogenation Mechanism for the Reaction of Single Wall Carbon Nanotubes Carbanions with Tetrahydrofuran.

National Renewable Energy Laboratory, 1617 Cole Blvd, Golden, CO 80401; #Chemistry Department, Rochester Institute of Technology, Rochester, NY 14623

RECEIVED DATE (automatically inserted by publisher); txgsch@rit.edu

Improved understanding of the chemistry of single walled carbon nanotubes (SWNTs) is of significant importance. With the development of novel nanostructured carbon materials for the molecular adsorption and covalent interaction of hydrogen, a new genre of interesting and sometimes unexpected chemistry for the intermediate species has evolved.

Carbon nanotubes have historically been reduced by two distinct metal reduction methods: modified birch reductions in liquid ammonia[1-5] and via reactions with alkali metal naphthalenides in tetrahydrofuran (THF).[4-6] Typically these reduced nanotubes are then functionalized via either alkylation or arylation reactions.[2,7-15] This work summarizes a systematic investigation of the reactions of sodium-naphthalenide reduced laser generated-SWNT materials with tetrahydrofuran that leads to an efficient hydrogenation of the nanotube backbone. We have found that upon reduction laser-SWNTs, unlike arc and Hipco materials[2-6,9,10], form insoluble, highly reactive, paramagnetic carbanions. Through a series of isotope labeling experiments we were able to ascertain that the NaSWNT radical system mimics known butyl-lithium reactions with THF.[16-18]

The single wall carbon nanotubes used in this investigation were produced via laser vaporization utilizing a well developed process described elsewhere.[19,20] The laser-nanotubes were then purified with a modification of our previously reported process which is described in supplemental information.[19] Subsequently, the purified laser SWNTs were hydrogenated through a modification of the procedures recently published in the literature.[4-6] The experimental protocol for the generation of the carbanion NaSWNT materials is included in supplemental information. The samples were quantitatively analyzed for hydrogen content utilizing our in-house Temperature Programmed Desorption, (TPD) apparatus. This TPD has been independently certified for evaluation of hydrogen gravimetric content (%w/w). Specifically, in these experiments approximately 2 mg samples were evacuated to 10^{-8} torr at 90K and then were heated at 1°C/sec to 700 °C while constantly monitoring via mass spectroscopy the species evolved from the sample.

Figure 1 illustrates the typical hydrogen degas TPD spectrum observed for the NaSWNT materials. The samples exhibited an unexpected high hydrogen content that typically averaged 3.9% w/w hydrogen as compared to the 0.64 – 1.5% w/w reported in the literature for other reduced nanotube materials.[1-3,21-25] Theoretical predications of the coverage of the nanotube backbone with atomic based hydrogen does predict a thermodynamically stable coverage of ~4.5% w/w, so our value is within reasonable agreement.[14,22,26,27] For reduction experiments

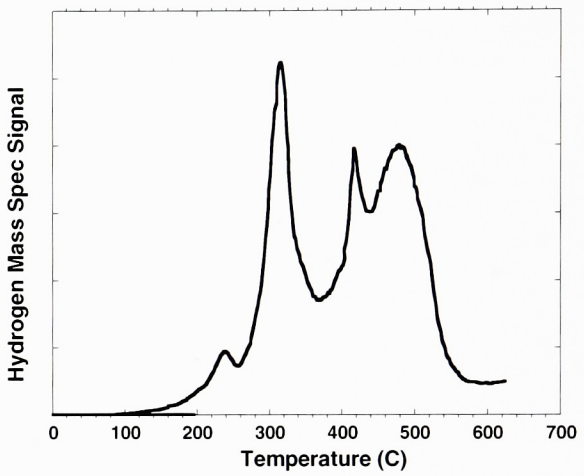

on the laser-SWNTs utilizing lithium or potassium naphthalenide, the amount of hydrogenation observed was much lower on average 1.1% w/w, with two desorption peaks at 350 and 500 °C.

Intercalation of graphite and nanotubes[28] with alkali metals typically yield LiC_6 and KC_8, while sodium invariably leads to a much poorer, NaC_{64}.[29-31] Since sodium is the least effective alkali metal for graphite intercalation,[30,31] our results reflect a limited intercalation of the sodium into the nanotube matrix which effectively leaves more uncoordinated reduced sites open for hydrogenation. This correlation to graphite can be drawn because of the highly crystalline (graphitic) nature of the laser generated nanotubes a direct result of their minimal disorder as compared to other SWNT samples.[32]

Figure 1: TPD spectrum of an NaSWNT sample degassed at heating rate of 1°C/sec. Hydrogen evolved at a series of temperatures; 225, 305, 420 and 490 °C. The total hydrogen content of the samples averaged 3.9% w/w. No solvent or naphthalene mass spec peaks were observed.

In Figure 1 several distinct hydrogen desorption peaks in the NaSWNT samples at 225, 305, 420 and 490 °C are observed. The considerable amount of hydrogen that is desorbed below 400 °C suggests some of the hydrogen is not bound to the sample by a true C-H sp^3 type bond.[2,3,26,27] When the NaSWNT material was reacted with methanol, the lower temperature peaks markedly decreased in intensity, and an additional dehydrogenation peak at 600 °C, similar to that seen with Birch reduction materials,[1-5] was observed. After the reaction with methanol, the total hydrogen content decreased to < 2% w/w.

The Raman spectroscopy results with a 488 nm incident excitation wavelength of the NaSWNT samples were very similar to those previously reported.[2] After sodium reduction and hydrogenation, the ratio between the integrated area of tangential mode G band (~1590 cm^{-1}) and the disorder peak D band (~1350 cm^{-1}), i.e. the G/D ratio, decreases by about 50%. As suggested, this ratio change is expected as the hydrogenation causes some sp3 C-Hx formation which introduces disorder on SWNT sidewalls thereby increasing the D band intensity.[2] In conjunction, the reduction of the nanotubes may alter the resonance frequency of the G-band, reducing its intensity as well.[32] After the hydrogen is desorbed from the samples by heating to 700 °C, the G/D ratio recovers to almost its original value.

Next we carried out a series of experiments to evaluate the possibility that the hydrogen on the sample is stored in the form of sodium hydride. Sodium hydride contains 4.2% w/w hydrogen by mass and the hydrogen desorbs via a thermal decomposition reaction at 425 °C, as confirmed in our TPD system.[33] The reduced NaSWNT sample was analyzed for sodium content at it was found to contain approximately 1 sodium per ~60-70 carbons, similar to NaC_{64} reported in the literature for graphite[29,30]. If all of this sodium was in the form of sodium hydride it would only contribute approximately 0.1% w/w of the hydrogen found on the NaSWNT materials. While others have found up to1 sodium per 10 carbons for HipCo and arc generated reduced nanotubes,[5,6] this would still only contribute 0.6% w/w hydrogen to the 3.9% we have observed. Clearly, while we do not know the specific role the sodium may have in facilitating the hydrogenation of the nanotubes, by itself it cannot be responsible for the large amount of hydrogen thermally evolved from the reduced laser NaSWNT samples.

In order to determine the source of hydrogen that is attached to the NaSWNT materials, a series of isotope labeling experiments were performed. In these experiments we utilized naphthalene-d_8, THF-d_8 and SWNT samples purified with all deuterated reagents. Via mass spectroscopy, the various m/e signals for H_2, HD, and D_2 were monitored during the thermally initiated desorption of the hydrogen/deuterium moieties. As shown in Figure 2 it was observed that only the reactions carried out in THF-d_8 led to the evolution of HD and D_2. When only naphthalene-d_8 was used, the dehydrogenation spectrum was similar to that shown in Figure 1, i.e. no deuterium incorporation. When the total area under the curve for each individual mass was integrated and normalized to m/e = 2, the total hydrogen content was found to be 3.8% w/w, in direct agreement with the non-deuterated sample.

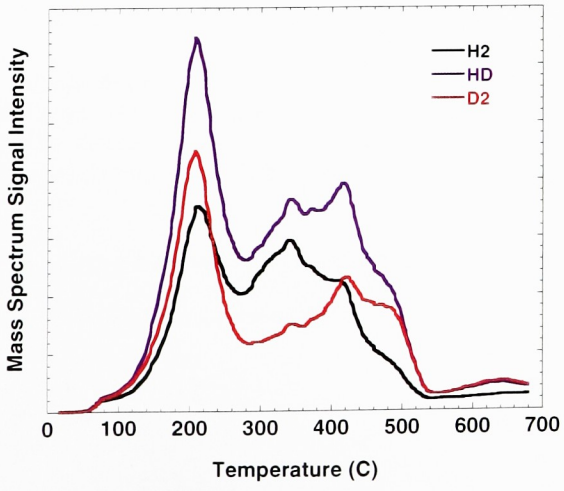

Figure 2: Dehydrogenation TPD spectrum for a NaSWNT sample prepared in d^8-THF. Black-H_2 signal, m/e = 2; Blue-HD signal, m/e = 3; Red-D_2 signal m/e = 4. When corrected for mass, the total amount of adsorbed hydrogen isotopes equals the amounts observed for non-deuterium experiments.

This reaction behavior of the NaSWNT carbanions which involves abstraction of hydrogen from THF is similar to that observed for butyl lithium salts.[16-18] It is well established that butyl lithium cleaves THF to yield butane (hydrogenated alkane), ethylene and lithium enolate. As illustrated in the reaction scheme below, the NaSWNT carbanion also can cleave the THF to give hydrogenated SWNTs, ethylene, and sodium enolates.

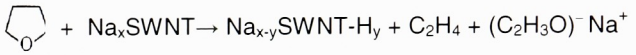

Scheme 1. Proposed reaction mechanism for the hydrogenation of SWNT carbanions through cleavage of the THF heterocyclic ring. The resultant air sensitive, hydrogenated nanotubes are paramagnetic as evidenced by existence of an ESR signal.

To confirm this mechanism, the reduction reaction was conducted in-vacuo instead of under a nitrogen atmosphere. The increase in pressure over the reaction mixture was then measured after the reaction had gone to completion. The headspace gas was sampled via mass spectroscopy and found to consist of a mixture of ethylene and THF. After correcting for the vapor pressure of THF, the amount of hydrogenation predicted from the molar amount of ethylene produced was approximately 5% w/w on that particular SWNT sample. When totally degassed under the conditions described previously, we observed 3.9% w/w hydrogen for that specific NaSWNT material. These experiments are direct confirmation that the SWNT carbanion is a very strong, reactive base that can cleave THF under ambient conditions resulting in the hydrogenation of the SWNT material.

In summary, we have found a marked improvement of the solution phase hydrogenation of SWNT materials utilizing sodium-naphthalenide in THF. The hydrogen appears to be bound both by sp^3 C-H interactions and by another not yet determined weaker interaction. We expect that the residual sodium on the sample has played a role in the hydrogenation of the SWNTs, possibly via a spillover type mechanism[34,35] and it has been proven not to be the major hydrogen sorbent. The fact that sodium is the least effective graphite intercalant of the alkali metals,[29-31] may also contribute to the increased hydrogenation level of NaSWNT as compared to lithium and potassium derivatives. This work is basic in nature and expected to have implications for hydrogen storage and catalysis applications of functionalized carbon nanotubes. Finally, the results further illustrate the differences in reactivity and behavior of SWNTs based upon their synthetic route and chemical history.

Supporting Information available:

SWNT Purification Procedure: After a 16 hour reflux in 2M nitric acid, the solution was filtered on 5micron xxx 47 mm filters, washed with a sequence of water, 3M NaOH, water, acetone solutions until the filtrate was clear. To maximize the yields of SWNTs the buckypapers of refluxed material were all kept below a mass of <10mg. The refluxed nanotubes were dried at 70 °C for 10 minutes. The resultant buckypapers were then burned in air at 525 °C, 760 torr for 30 seconds, at which time an approximate 50% loss in mass was typically observed. The air oxidized SWNTs were then immersed in conc-HCl for 5 minutes to remove residual metal impurities, the papers were then immersed in 6M NaOH, and subsequently allowed to soak in 3 separate water washes. This purified-SWNT material was then heated to 800 °C for 5 minutes in 100 sccm flowing carbon dioxide after which the hydrochloric acid cycle was repeated until no further metal was removed in the acid soak. After removal of the residual metals, a final purification vacuum anneal to 600 °C at 10^{-7} torr was conducted to degas a significant portion of the oxygen moieties attached to the nanotubes after the purification process. In the end about 30% of the original mass was recovered and contained less than 1% metal impurities as determined by thermogravimetric analysis.

Reduction Reaction Specifics: Under an inert helium atmosphere, 5 mg of purified SWNTs, 100 mg of naphthalene, and 100 mg of sodium metal were added to a round bottom flask with a magnetic stir bar. The excess of the naphthalene and sodium were necessary to minimize side reactions from any residual water or oxygen in the reaction vessel. On a Schlenk line, the reaction flask was backfilled with N_2, and 100 mL of distilled THF was added. The mixture was sonicated for 30 min and then allowed to stir for 12 hours in order to ensure the complete reduction of the SWNTs. The suspension of reduced SWNTs (Na-SWNTs) was transferred via the Schenk line into a centrifuge tube. The NaSWNT-THF suspension was centrifuged at 20000 rpm for 20 minutes, the THF was removed, and the pellet was washed with new 100 ml of THF. This procedure was performed until the solution was clear. At this point solid NaSWNT material was transferred to a vacuum line inside and dried for 12 hours at approximately 10^{-5} torr to remove residual solvent. Utilizing the sample pretreatment, only trace amounts of solvent and reagents were observed during the sample degas. The NaSWNT powder was then transferred to a quartz TPD sample holder inside of a helium filled inert gas chamber. Small variations in thermal transport properties of the sample can lead to variations in observed hydrogen degas temperatures in the TPD.

ACKNOWLEDGMENT : Funding from the U.S. Department of Energy, Office of Energy Efficiency and Renewable Energy, and the Office of Science, Basic Energy Sciences, Division of Materials Science under Grant No. DE-AC36-99GO10337

Supporting Information Available: Purification procedure for the generation of highly pure SWNT samples and the experimental protocol for the reduction of the SWNTs

REFERENCES

(1) Pekker, S.; Salvetat, J.-P.; Jakab, E.; Bonard, J.-M.; Forro, L. *J. Phys. Chem. B* **2001**, *105*, 7938-7943.

(2) Zhang, G.; Qi, P.; Wang, X.; Lu, Y.; Mann, D.; Li, X.; Dai, H. *J. Am. Chem. Soc.* **2006**, *128*, 6026-6027.

(3) Zhang, X.; Cao, D.; Chen, J. *J. Phys. Chem. B* **2003**, *107*, 4942-4950.

(4) Borondics, F.; Bokor, M.; Matus, P.; Tompa, K.; Pekker, S. *Fullerenes, Nanotubes, and Carbon Nanostruct.*, **2005**, *13*, 375-382.

(5) Borondics, F.; Jakab, E.; Pekker, S. *J. Nanosci. Nanotech.* **2007**, *7*, 1551-1559.

(6) Penicaud, A.; Poulin, P.; Derre, A.; Anglaret, E.; Petit, P. *J. Am. Chem. Soc.* **2004**, *127*, 8-9.

(7) Bahr, J. L.; Tour, J. M. *J. Mater. Chem.* **2002**, *12*, 1952-1958.

(8) Banerjee, S.; Hemraj-Benny, T.; Wong, S. S. *Adv. Mater.* **2005**, *17*, 17-29.

(9) Chattopadhyay, J.; Cortez, F. d. J.; Chakraborty, S.; Slater, N. K. H.; Billups, W. E. *Chem. Mater.* **2006**, *18*, 5864-5868.

(10) Chattopadhyay, J.; Sadana, A. K.; Liang, F.; Beach, J. M.; Xiao, Y.; Hauge, R. H.; Billups, W. E. *Org. Lett.* **2005**, *7*, 4067-4069.

(11) Liang, F.; Beach, J. M.; Kobashi, K.; Sadana, A. K.; Vega-Cantu, Y. I.; Tour, J. M.; Billups, W. E. *Chem. Mater.* **2006**, *18*, 4764-4767.

(12) Lu, X.; Chen, Z. *Chem. Rev.* **2005**, *105*, 3643-3696.

(13) Ormsby, J. L.; King, B. T. *J. Org. Chem.* **2007**, *72*, 4035-4038.

(14) Tasis, D.; Tagmatarchis, N.; Bianco, A.; Prato, M. *Chem. Rev.* **2006**, *106*, 1105-1136.

(15) Liang, F.; Alemany, L. B.; Beach, J. M.; Billups, W. E. *Journal of the American Chemical Society* **2005**, *127*, 13941-13948.

(16) Bates, R. B.; Kropskai, L. M.; Potter, D. E. *J. Org. Chem.* **1972**, *37*, 560-564.

(17) Carnahan, J.; Closson, W. D. *J. Org. Chem.* **1972**, *37*, 4469-4471.

(18) Clayden, J.; Yasin, S. A. *New J. Chem* **2002**, *26*, 191-192.

(19) Dillon, A. C.; Gennett, T.; Jones, K. M.; Alleman, J. L.; Parilla, P. A.; Heben, M. J. *Adv. Mater.* **1999**, *11*, 1354-1358.

(20) Gennett, T.; Dillon, A. C.; Alleman, J. L.; Jones, K. M.; Hasoon, F. S.; Heben, M. J. *Chem. Mater.* **2000**, *12*, 599-601.

(21) Callejas, M. A.; Ansóna, A.; Benito, A. M.; Maser, W.; Fierro, J. L. G.; Sanjuán, M. L.; Martınez, M. T. *Mater. Sci. Eng. B* **2004**, *108*, 120-123.

(22) Nikitin, A.; Ogasawara, H.; Mann, D.; Denecke, R.; Zhang, Z.; Dai, H.; Cho, K.; Nilsson, A. *Phys. Rev. Lett.* **2005**, *95*, 225507.

(23) Park, K. A.; Seo, K.; Lee, Y. H. *J. Phys. Chem. B* **2005**, *109*, 8967-8972.

(24) Seifert, G. *Solid State Ionics* **2004**, *168*, 265-269.

(25) Yoo, E.; Gao, L.; Komatsu, T.; Yagai, N.; Arai, K.; Yamazaki, T.; Matsuishi, K.; Matsumoto, T.; Nakamura, J. *J. Phys. Chem. B* **2004**, *108*, 18903-18907.

(26) Bauschlicher, C. W. *Nanolett.* **2001**, *1*, 223-226.

(27) Barnard, A. S.; Terranova, M. L.; Rossi, M. *Chem. Mater.* **2005**, *17*, 527-535.

(28) Fischer, J. E. *Acc. Chem. Res.* **2002**, *35*, 1079-1086.

(29) Edmana, L.; Herold, A.; Jacobsson, P.; Lelaurain, M.; McRaeb, E.; Sundqvista, B. *J. Phys. Chem. Solids* **1999**, *60*, 475-482.

(30) Metrot, A.; Guerard, D.; Billaud, D.; Herold, A. *Syn. Metals* **1980**, *1*, 363-369.

(31) Pruvost, S.; Herold, C.; Herold, A.; Lagrange, P. *Carbon* **2004**, *42*, 1825-1831.

(32) Dillon, A. C.; Parilla, P. A.; Alleman, J. L.; Gennett, T.; Jones, K. M.; Heben, M. J. *Chem. Phys. Lett.* **2005**, *401*, 522-528.

(33) Grochala, W.; Edwards, P. P. *Chem. Rev.* **2004**, *104*, 1283-1315.

(34) Yang, F. H.; Lachawiec, A. J.; Yang*, R. T. *J. Phys. Chem. B* **2006**, *110*, 6236-6244.

(35) Yang, H.; Chen, H.; Chen, J.; Omotoso, O.; Ring, Z. *J. Catalysis* **2006**, *243*, 36-42.